Study of bismuth complexation with amino acids and biologically active molecules

Dhuneshan Govender

A Dissertation submitted to the Faculty of Science, University of the Witwatersrand, Johannesburg, in fulfilment of the requirements for the degree of Master of Science
March 2015

DECLARATION

I declare that this Dissertation is my own, unaided work. It is being submitted for the Degree of Master of Science at the University of the Witwatersrand, Johannesburg. It has not been submitted before for any degree or examination at any other University.

_____

(Signature of candidate)

_____day of _____20_____in_____

Abstract

Bismuth(III) has been used in the medicinal industry for many years, but its mechanism of action is not fully understood and there is very little information on thermodynamic and kinetic parameters for complex formation. Amino acids are the building blocks of life and so, by initially simply determining the complexing ability of various amino acids with bismuth, an indication of how bismuth could interact in the body can slowly be developed and could assist in the eventual development and design of more effective bismuth containing drugs.

Bi^{3+} has the ability to form insoluble hydrolysis products which precipitate around pH 2 in the presence of a background electrolyte and therefore studies need to be conducted from low pH where it is still soluble. In this study, stability constants have been determined using polarographic-pH titrations. The sudden drop in current was used to identify the approximate pH of precipitation of Bi^{3+} species and the shift in potentials as pH increased were used to evaluate stability constants. One of the major issues with employing polarography in low pH regions (below pH 2) is the presence of the diffusion junction potential which contributes large errors to the measured potentials and therefore needs to be corrected for. Since KNO_3 was used as the supporting electrolyte, and Bi^{3+} forms complexes with nitrate as well as hydrolyses at these low pHs, determination of the free Bi^{3+} potential (needed to calculate the stability constants) also had to be determined indirectly.

In order to run the multi-hour polarographic-pH titrations, automated procedures using NOVA software were developed and validated. Automation of these experiments was key to ensuring reproducibility of the procedure and all the measurements.

Complex formation studies between Bi^{3+} and the three amino acids, namely glutamic acid (Glu), histidine (His) and glutamine (Gln) were conducted in 0.5 M KNO_3 solutions at 25^{o}C. It was demonstrated that a very large excess of ligand was required in order for complex formation to take place. Studies with Glu and His produced fully reversible reduction waves as required, but that with Gln produced quasi-reversible reduction waves and this also needed to be accounted for.

Acknowledgments

I thank my supervisor, Dr Caren Billing, for her endless support during my experimental work and for her help during this dissertation.

I thank the School of Chemistry for allowing me to complete my M.Sc. and for the willingness of all colleagues to assist in times of need.

I thank the NRF for their financial support and allowing me to attend the IC2013 Conference to present part of the work in this study.

I thank my Mother, Sister and Brother who stood by me during the pursuit my M.Sc.

Table of Contents

List of Figures

List of Tables

Chapter 1: Introduction

1.1. Properties and Industrial Uses of Bismuth

Bismuth is the heaviest of the Group 15 elements with an ionic and covalent radius of 1.08 Å (for Bi^{3+}) and 1.52 Å, respectively.[1] Bismuth forms the least stable 5^{+} oxidation state within the group, with its most stable form being Bi^{3+}.[1] Due to the high reactivity of bismuth in nature, it is almost never found in its pure state, but rather occurs as an oxide or sulphide. The bismuth crystals found in nature are often very aesthetically pleasing due to the unique patterns associated with the different types of crystals. This causes different wavelengths of light to be seen, thus displaying a rainbow of colours, however, the bismuth crystal is generally found with a white, silver-pink hue.[2]

Elemental bismuth is one of very few substances where the liquid phase is more dense than its solid phase (such as antimony and water).[2] The property of expanding (by approximately 3%) when cooling is responsible for much of bismuth's commercial uses such as low-melting typesetting alloys and in soldering or plumbing (for joining pipes), where it compensates for the contraction of the other alloying components.[2-3] Bismuth alloys have been known to have varying melting points[3-4] with some comparable to that of ice, hence a bismuth-alloy casting can be covered by plastic or other material to form intricate machine parts. The bismuth-alloy core is simply removed by melting it in hot water and pouring it out. The use of low-melting bismuth alloys is widespread in fire fighting sprinkler systems in buildings where the bismuth alloy trigger system melts when heat is applied to it, causing the seal to break and the water to extinguish the fire.

More recently, there have been studies focused on bismuth in its nanoparticle state. Bismuth nanoparticles (BNPs) have been of great interest due to their use in a variety of fields, from catalysis to biosensing.[5] Due to the high surface area of BNPs, they have also been extensively studied for their use in determining the concentrations of trace elements found in the environment and hence the extent to which metals have contaminated a certain area.[6]

1.2. Bismuth-Medicinal Uses

Bismuth and its respective compounds have been used in the medicinal field for over 200 years in many countries.[4] It was a major component used to combat syphilis and other bacterial infections such as peptic ulcers. The toxic effects which arose due to the overdose of bismuth compounds have been reported wherein patients were diagnosed with reversible bismuth-induced neurotoxicity. The effects suffered by the numerous patients arose due to the heavy-handed and careless use of medication containing bismuth (>10 g per day). Kidney failure, gingivitis and stomatitis (irritation of the inner lining of the mouth) have all been associated with an overdose of bismuth containing drugs. The kidney is the organ shown to contain the highest concentration of bismuth after its intake into the body, followed by the liver.

The unfortunate cases of overdosing and illnesses due to the bismuth containing medication did not completely eradicate the use of bismuth in the medicinal field and it still remains as an important component for stomach ulcer remedies, which include Pepto-Bismol[7] (bismuth subsalicylate – see Figure 1.1a) and De Nol (colloidal bismuth subcitrate (CBS) – see Figure 1.1b), where the latter is also used in the treatment of many cancer types, particularly for stomach cancer strains.[8]

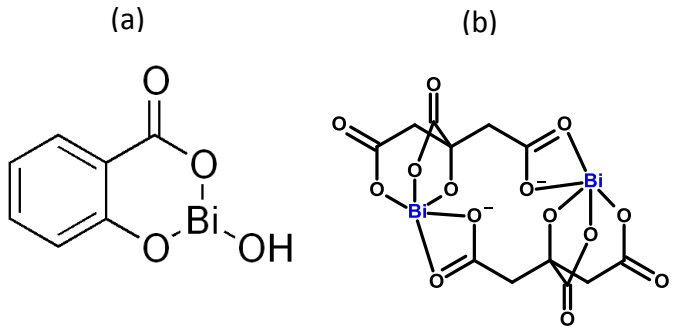

Figure 1.1: The structures of (a) bismuth subsalicylate[7a, 7c] and (b) colloidal bismuth subcitrate (CBS).[8a, 9]

The mechanism by which the substances shown in Figure 1.1 act in gastric and duodenal ulcer therapy[7b, 9-10] and the eradication of Helicobacter pylori (H. pylori), a bacterium associated with the pathogenesis of gastroduodenal ulcers,[8] is not fully understood. The

standard pH of the stomach is approximately pH 1.3-3.5.[11] It has been suggested[10c] that bismuth's ease in hydrolyzing (as will be discussed in detail in section 1.3) and precipitating plays an important role in the mechanism. The precipitated bismuth-hydroxy products and the antimicrobial active, such as salicylate, attach to the surface of the ulcer or affected area.[10c] Alternatively, the longer remission times achieved with bismuth therapies are probably due to eradication of the organism by bismuth. Clinical studies with colloidal bismuth subcitrate and bismuth subsalisylate have shown that patients treated with bismuth alone experience a slower relapse than patients treated with other ulcer-healing agents[12] possibly due to the bactericidal action of these complexes against H. pylori.

Rantidine bismuth citrate (RBC) is another type of medicinal complex which has been used extensively in the treatment of stomach ulcers and the structure may be closely related to that of $Na_2[Bi_2(citrate)].7H_2O$, which contains highly stable dimeric units of $[Bi(cit)_2Bi]_2$.[13] It is the potential action of these bismuth citrate units to inhibit the uptake of Fe(III) into some bacteria, thereby allowing the eradication of the bacteria. It is also possible to envisage dimeric bismuth citrate units inhibiting the uptake of Fe(II) into some types of bacteria, since Fe(II) also forms a dimeric citrate complex.[14]

There have also been reports of organic bismuth thiolates having anti-tumour capabilities and reducing the toxicity of some platinum-based anti-cancer agents.[15] Recent in-vitro studies have shown bismuth to be an active HIV-I inhibitor[16], from chronically infected H9 cells.[17] Although an interesting observation, the research with bismuth containing drugs against HIV is at a very premature stage, however, the proven medicinal characteristics of bismuth cannot be ignored and therefore could result in an effective HIV drug in due time.

Due to the formation of radioactive isotopes, bismuth can also be used in radioactive therapy. ^{212}Bi is known to be a strong alpha-particle emitter with a short half-life of one hour.[18] The isotope has been extensively used in targeted radioactive therapy against cancer once it has been complexed to ligands such as diethylene-triaminepentaacetate

(DTPA) and 1,4,7,10-tetra-azacyclododecane-1,4,7,10-tetraacetate (DOTA) and then further complexed with monoclonal antibodies.[19]

1.3. Bismuth complex formation

Pearson's hard soft acid base (HSAB) theory[20] has been widely used to classify elements according to characteristics relating to their atomic centres radii, charge, number of empty orbitals in the valence shell, electronegativity, solvation ability and whether they possess high or low energy HOMOs or LUMOs. According to Pearson's theory,[20] soft metal ions prefer ligands with soft donor atoms and hard metal ions prefer HSAB ligands with hard donor atoms. Bi^{3+} is thus classified as borderline[20-21] and illustrates that it is able to form many different complexes with different ligands.[4, 22] These complexes show many varying characteristics and impart stability onto the metal ion or in some cases result in it becoming more reactive, depending on the type of ligand which complexes.

Bismuth is able to complex with glutathione (GSH) forming the complex [Bi(H-GSH)3]. Binding/Formation constants have been reported from studies[23] of competition reactions between EDTA (logK 29.6) and GSH(log 31.4)[4] for the ML_3 species. Other types of ligands studied[4] which have been shown to exhibit complexing behaviour with bismuth include allyls, alkoxides, hydroxides and thiol containing compounds.

The table below indicates formation constants of other types of ligands which have been studied for the formation of ML species, and report their respective log *K*1 values.

Table 1.1: Table showing different ligands attached to the Bismuth metal ions with their respective log K values.[4]

Ligand	log K_1
hydroxide	12.49
ammonia	5.1
dein	17.4
trien	21.9
oxalate	7.7
L-malate	9.9
citrate	13.5
ascorbate	25.3
succinate	8.8
fumarate	6.9
glycine	10
aspartate	10.5
glutamate	10.5

Since bismuth has the ability to form complexes with ligands containing oxygen, nitrogen and sulphur, it would be expected to provide a foundation on which the complexation of bismuth to amino acids would take place. It is already known that heavy metals in living organisms form complexes with sulfur containing molecules like cysteine and glutathione.[22d] Polarographic studies[23-24] have shown that the Bi^{3+} ion, like Cu^{2+} and Hg^{2+} ions, has a high affinity for nitrogen-donor ligands.

Due to its large atomic radius (1.08Å), Bi^{3+} also favours the formation of five-membered ring complexes. Bi^{3+} also has a highly variable coordination number, ranging between 3 and 10, and frequently has irregular coordination geometry. Strong intermolecular interactions could result in polymeric structure formation. The kinetics of complex formation has also been described as generally fast or at least within minutes. Solid state structures of some bismuth complexes with oxygen containing bio molecules crystallized at acidic pH values have been solved by Herrmann[22] and some of these include lactate, L-(-)-malate, oxalate and L-(+)- tartrate complexes. In these complexes, bismuth exhibits a high coordination number, as high as eight or nine[23], and all the complexes are polymeric via carboxylate oxygen bridging. In the bismuth oxalate complex, the bismuth is also bridged by chloride ions. Five-membered chelate rings are preferentially formed in the complexes, and this is attributed to the large atomic radius of Bi^{3+}.

In aqueous solutions Bi^{3+} readily hydrolyses, thus the formation of Bi^{3+}-hydroxide complexes are particularly difficult to avoid, even in very acidic solutions. To increase the complexity of the system, it has been found that some of the Bi-OH complexes formed are insoluble and precipitate at pH >2. Early work by Granier and Sillen[25] laid the foundation for the studies of bismuth hydrolysis. Initially the studies showed that not only complexes of the form $Bi\text{-}OH_n$ occurred in solution, but it was suggested that polynuclear species such as Bi_2O^{4+}, $Bi_3O_2^{5+}$ and $Bi_4O_3^{6+}$ also existed. Although a breakthrough at the time, improvements in analytical methods and minimizations in errors of the electrodes used showed that the main polynuclear species formed under the conditions used was $Bi_6(OH)_{12}^{6+}$.[26] In recent times the acceptance of the $Bi_9(OH)_n$, where n =20, 21 and 22 are formed in aqueous solutions. As with all chemical reactions the ability for a complex to form depends on the reaction conditions. Studies by Olin[27], Bidleman[28] and later by Hataye[29] were able to show that in very dilute solutions of the hexamer was not present in solution, but rather the mononuclear $Bi(OH)^{2+}$ species was present. Since Bi^{3+} hydrolysis will always be a factor in aqueous solutions, methods used to determine Bi^{3+}-ligand formation constants must take these bismuth hydroxide complexes into account. The methodology used in this work will be discussed in Chapter 4.

The background or supporting electrolyte used in metal-ligand studies is of relatively great importance when determining stability constants as they are used in high concentrations to maintain ionic strengths of solutions. Sodium or potassium perchlorates and nitrates are the most commonly used background electrolytes.[30] These are used as they are weakly complexing and so should not have a significant affect in metal-ligand complexation. Studies by Maroni and Spiro[31] and Hataye *et al*.[29] all agreed that perchlorate is not bound strongly enough to the hydrolysed bismuth complex and as such allowed close examination of the bismuth-hydroxide products formed. Nitrate backgrounds were also studied by Maroni and Spiro[31] who concluded that the major complexes formed were $Bi(NO_3)_n^{3-n}$, $Bi(OH)(NO_3)_n^{2-n}$, $Bi(OH)_2(NO_3)_n^{1-n}$ and $Bi(OH)_3(NO_3)_n^{-n}$. At pH greater than 2, bismuth tends to become highly insoluble due to the formation of Bi-hydroxy-nitrate species or Bi^{3+} hexamers. The formation of these species at such a low pH limits the window in which solution based studies can be conducted as significant

complexation must occur at pH less than 2, making it susceptible to many errors which will be discussed later.

1.4. Amino Acids

Amino acids are the building blocks of life as they make up all proteins and exist in organs which are important for humans and animals to survive. α-amino acids are naturally occurring and are made up of an amine group which is located on the carbon atom immediately adjacent to the carboxylic acid group and a sidechain denoted by R in Figure 1.2 (Table 1.2) indicates the structure of R-sidechain. Humans are able to synthesize approximately ten of these amino acids in amounts which are vital for survival. The other ten, which must be supplemented via ingestion, are described as essential amino acids because they are considered necessary components in our diet for energy production. All proteins contain one or more of the essential amino acids. During the formation of proteins and enzymes, the amino acids are joined together via peptide bonds to form polypeptide chains. The grouping together of polypeptide chains by sulfide bridges then allows the formation of the specific protein.

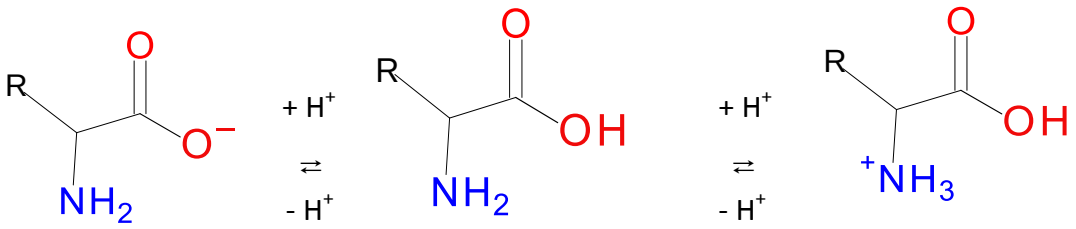

Figure 1.2: General formula for α-amino acids, showing the deprotonated and protonated forms. The sidechain R varies depending on the amino acid type and these are given in Table 1.2.

Table 1.2: The twenty common amino acids with the structural representations of their respective sidechains.[32]

Amino Acid	Sidechain		Amino Acid	Sidechain
Glycine	H		Threonine	$HC(OH)-CH_3$
Alanine	CH_3		Asparagine	$CH_2-C(O)-NH_2$
Valine	$CH-(CH_3)_2$		Glutamine	$CH_2-CH_2-C(O)-NH_2$
Leucine	$CH_2-CH-(CH_3)_2$		Tyrosine	
Isoleucine	$C(CH_3)CH_2CH_3$		Cysteine	CH_2-SH
Methionine	$CH_2-CH_2-S-CH_3$		Lysine	$(CH_2)_4-NH_3+$
Proline			Arginine	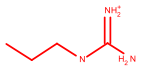
Phenylalanine			Histidine	
Tryptophan			Aspartic Acid	CH_2-COOH
Serine	CH_2-OH		Glutamic Acid	CH_2-CH_2-COOH

As can be seen in Figure 1.2, the amino acid skeleton has a central carbon atom, surrounded by 4 different sidechains (except in the case of glycine) which makes the amino acid chiral. A chiral molecule has no plane of symmetry and is therefore not superimposable on its mirror image. It can exist in two forms, right-handed or left-handed, defined by the term enantiomer. The chiral character of an amino acid allows it to be utilized in a large number of important chemical reactions in the human body. Proteins and enzymes are highly selective molecules. The chirality of the amino acid constituents thus allows their selectivity to be tailor made only for the substance they are interacting with, ensuring the reactions which are taking place are both optimal and correct. The different sidechain moieties occurring in amino acids allow them to perform a multitude of functions, hence their biological importance.

From Figure 1.2 it is noted that the amino acids contain at least two sites available for complexation. The amino acid skeleton has both O and N donor ligands and, depending on the R-sidechain, an additional donor atom could be present. The pK_a of the donor atoms are dependent on the type of sidechain present on the amino acid which contain the electron donating or withdrawing groups. The complexation of Bi^{3+} with amino acids has been reported, firstly for the use of biosensing and secondly as more efficient drug carrying molecules.[4, 22a, 33] Although some studies on complex formation between Bi^{3+} and amino acids have been looked at before, very few formation constants have been published. Singh and Srivastava[34] conducted studies where metal ions, including Bi^{3+}, have been investigated in perchlorate solutions using the Calvin-Bjerrum's pH titration method. Singh and Srivastava's[34] studies included the use of aspartic and glutamic acids and suggest their formation constants with beryllium(III), aluminium(III), palladium (III), gold(III) and platinum (IV) in perchlorate solutions (see Table 1.3). From these results it appears that metal ion with the most similar formation constants to Bi^{3+} is Au^{3+}.

Table 1.3: Log βvalues for various metal ions with aspartic and glutamic acids at 25°C and in 0.1 M $NaClO_4$ solutions. [34]

Metal Ion	Aspartic Acid			Glutamic Acid		
	Log β_1	Log β_2	Log β_3	Log β_1	Log β_2	Log β_3
Aluminium(III)	16.29	36.69	42.19	15.12	29.40	38.60
Beryllium(II)	12.26	20.99	-	12.04	20.02	-
Palladium(II)	10.44	18.14	-	10.38	17.84	-
Gold (III)	9.63	18.23	24.93	9.56	17.58	23.83
Platinum(IV)	9.56	13.49	-	8.99	12.68	-
Bismuth (III)	10.47	19.12	22.79	10.47	18.75	22.25

1.5. Polarography

Polarography is an electroanalytical technique invented by Jaroslav Heyrovsky in 1929.[35] It allows the analysis of the effect that an applied potential at a dropping mercury electrode (DME) in an electrolytic cell has on the current flowing in the cell. Varying the potential at the electrode results in the oxidation or reduction of the electro-active species in solution provided it occurs in the potential region of interest; this results in an increase in current and hence a peak or wave on the polarogram (depending on which electrochemical technique is used). Different electro-active species have characteristic reduction potentials and thus polarography also gives an indication as to what electro-active species is present in solution. Due to the fact that the transfer of electrons results in an increase in current, the higher the concentration of the electro-active species present in solution (and hence at the electrode surface) the greater the current.

There are three electrodes in a polarographic cell, namely the reference electrode, counter electrode and working electrode. The reference electrode facilitates measurement of the potential at the working electrode. The counter electrode acts as either the anode or cathode (the opposite of the working electrode) to complete the circuit and allow electron flow to counteract the charge experienced by the working electrode. In polarography, the working electrode used is a DME. The DME provides a fresh mercury drop, and thus a new surface for the electrode reaction to occur, at each potential step. This ensures that there are no remnants from previous reactions which may be left on it.

A direct current (DC) polarogram has an S-shaped curve as can be seen in Figure 1.3 At low overpotentials, a non-faradaic current is present, but as the applied potential increases there is a sharp increase in the current which indicates the oxidation or reduction of an electro-active species depending whether the potential is moving in a positive or negative direction, respectively. The diffusion limited current, I_d, is the difference between the current at the plateau of the wave and the residual or non-faradaic current. The half-wave potential, $E_{1/2}$, is the potential midway up the wave and this value indicates the type of electro-active species being oxidized or reduced under specific reaction conditions. DC polarography is defined as the physico-chemical technique based on the recording of current vs voltage curves.[36] A current-voltage curve

is constructed by applying a constant potential for each respective potential step. Each step is synchronized with the drop life of the DME. The current measurement is taken at the end of the DME drop life. The potential is then increased or decreased by a small amount and the process is repeated. The resulting potential-time profile is thus a staircase. Differential pulse polarography (DPP) is an alternative polarographic measurement. In this case a potential pulse is introduced at the end of the drop life and superimposed on the staircase profile applied in DC polarography. The current is measured immediately before the pulse and then again just before the end of the pulse (and hence the drop lifetime). The plotted current in this case is the difference between the current at the end of the step and the current before the step (the differential current) and produces a peak shaped polarogram, where the concentration of electro-active species is proportional to the height of the peak.

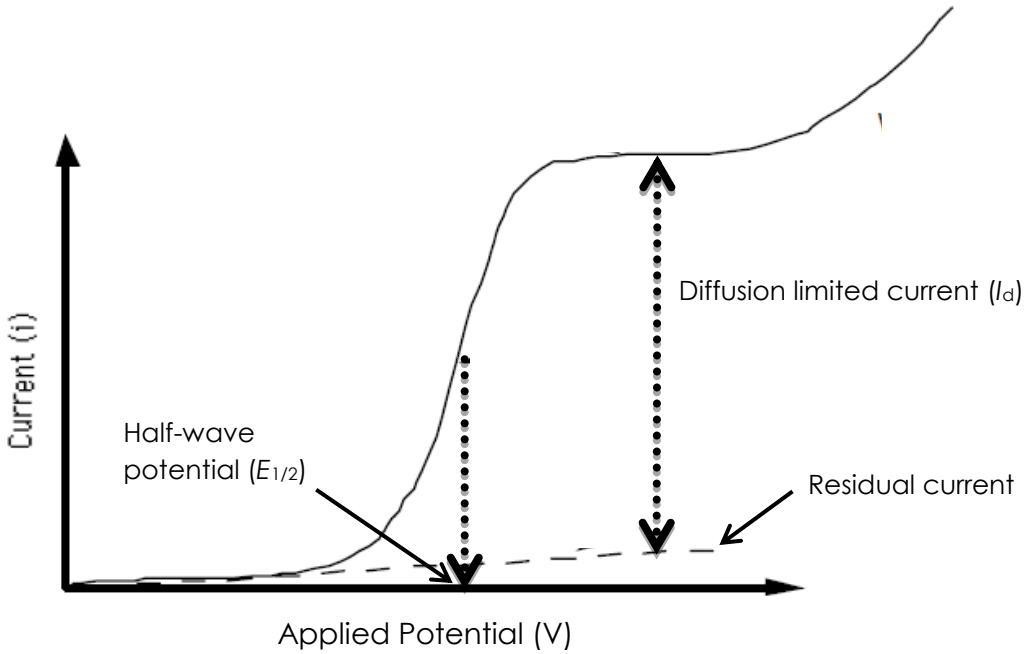

Figure 1.3: A typical direct current polarogram indicating the wave produced, the diffusion limited current, I_d, the half wave potential, $E_{1/2}$, and the residual current.

As described in section 1.3, analysis of the complexation of Bi^{3+} needs to start at pH <2. The problem which occurs in the analysis of metal-ligand complexes using polarography at this low pH is the formation of a large diffusion junction potential (E_j). The E_j is defined as the voltage difference which develops at the interface of two dissimilar electrolyte solutions in contact. This phenomenon arises in the cell when the diffusion of ions occurs

across the aqueous contacting layer between the sample solution and salt bridge solution in which the reference electrode sits. When the sample solution is very acidic (as it would initially be in this study), the large E_j is due to the extremely high mobility of the hydrogen ions (36.30 x 10^{-8} $m^2 s^{-1} V^{-1}$ at 25 °C)[37] as compared to that for any of the other cations present, K^+ (7.62 x 10^8 $m^2 s^{-1} V^{-1}$ at 25 °C)[37] for this study. This concept is illustrated in Figure 1.4. The overall measured potential is therefore a combination mainly of the reduction potential of the metal ion (with respect to the reference electrode potential) and the E_j. The E_j is also a source of error in pH measurements. It develops at the reference junction separating the filling solution of the reference electrode from sample solutions.

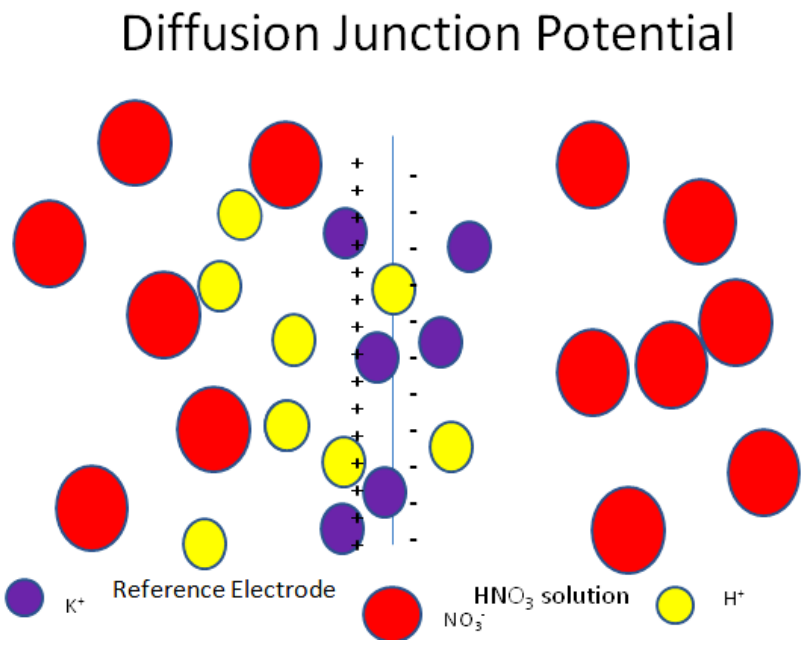

Figure 1.4: An illustration of E_j whereby the hydrogen ions move much faster across the reference electrode frit due to its high mobility compared to the K^+ ions. The result is a surplus of positive charge at the inner face of the reference electrode and negative charge on the outer face of the reference electrode.

During pH titrations the pH is changed throughout the experiment and hence the junction potential changes drastically, especially below pH 2. It has been shown that a witness ion provides the most suitable method for the determination of E_j.[38] This is achieved by monitoring the difference between the measured reduction potential and the expected potential (as determined at higher pH where E_j is insignificant) for the uncomplexed

witness ion. This process will be fully discussed in Chapter 4. The witness ion which will be used is thallium(I) because it forms very weak complexes and hence is not expected to coordinate with the ligands to be studied, especially in acidic solutions. The thallium data must be taken very accurately to ensure no unwanted processes are occurring which will influence the value of the calculated E_j at each respective pH.

The analysis of the Bi^{3+}-ligand complexation will be done by polarography employing pH titrations, starting with solutions containing Bi^{3+} and the ligand at low pH (about pH 0.3–1) and then titrating by a base solution. A negative shift in the reduction potential of bismuth will occur as bismuth is complexed by the ligand as pH of the solution is increased. As Bi^{3+} complexes with ligand, it becomes more difficult to reduce the metal ion centre and thus more energy is required to enable the electron transfer, and more negative reduction potentials have to be applied. A requirement which must be used in order to allow satisfactory analysis of the metal-ligand complexation is that the concentration of the ligand must be at least about 100 times greater than that of the metal studied.

1.6. Aims

The main aim of this work is to learn about the interaction between Bi^{3+} and amino acids. Polarographic methods will be used to determine which complexes are formed between Bi^{3+} and the amino acid ligands and their respective formation constants will be evaluated. A greater understanding of this chemistry will shed some light on the behaviour of Bi^{3+} once placed inside the body and be a step closer to potentially develop and design more effective Bi^{3+} containing drugs.

Additionally, it is intended to get a new polarographic-potentiometric autotitration system fully functioning. This would include developing and testing procedures using NOVA[39] software which is supplied with the newer Autolab potentiostats.

1.7 References

[1] F. A. Cotton and W. G., *Advanced Inorganic Chemistry - A Comprehensive Text*, John Wiley and Sons Inc., New York, **1980**.

[2] Lenntech-Elements-Bismuth, http://www.lenntech.com/periodic/elements/bi.htm, (Date Accessed: 30-08-2011)

[3] Bismuth Compunds and Materials of High Purity and Reactivity, http://www.solid.nsc.ru/eng/develop/bismuth_eng.htm, (Date Accessed: 28-08-2011)

[4] H. Sun, H. Li and P. J. Sadler, *Chem. Ber. Recueil.*,**1997**, *130*, 669.

[5] C. C. Mayorga-Martinez, M. Cadevall, M. Guix, J. Ros and A. Merkoçi, *Biosensors and Bioelectronics*,**2013**, *40*, 57.

[6] S. Caudle, W. Steven, R. Spidle and A. Wanyeka, *Abstracts of Papers, 245th ACS National Meeting & Exposition, New Orleans, LA, United States, April 7-11, 2013*,**2013**, 859.

[7] a) E. Asato, *Chem. Lett.*,**1992**, 1967; b) U. Dittes, B. K. Keppler and B. Nuber, *Angew.Chem. Int. Ed.(English)*,**1996**, *35*, 67; c) M. Abrams and B. Murrer, *Science*,**1993**, *261*, 725.

[8] a) A. K. Jha and R. G. Mendiratta, *J. Mater. Sci.*,**1996**, *31*, 1735; b) N. Burford, M. D. Eelman and T. S. Cameron, *Chemical Communications*,**2002**, 1402.

[9] E. Asato, K. Katsura, M. Mikuriya, U. Turpeinen, I. Mutikainen and J. Reedijk, *Inorg. Chem.*,**1995**, *34*, 2447.

[10] a) E. Asato, C. M. Hol, F. B. Hulsbergen, N. T. M. Klooster and J. Reedijk, *Inorg. Chim. Acta*,**1993**, *214*, 159; b) J. R. Partington, *History of Chemistry*, Macmillian, London, **1961**. 1; c) T. E. Sox and C. A. Olson, *Antimicrob. Agents.Chemother.*,**1989**, *33*, 2075.

[11] E. N. Marieb and K. Hoehn in *Human Anatomy and Physiology*, *1* Benjamin Cummings, San Francisco, **2010**.

[12] a) B. J. Marshall, C. S. Goodwin and R. J. Warren, *Lancet*,**1988**, *2*, 1437; b) A. J. Wagstaff, P. Benfield and J. P. Monk, *Drugs*,**1988**, *36*, 132.

[13] a) P. J. Barrie, M. I. Djuran, M. A. Mazid, M. Mcpartlin, P. J. Sadler, J. I. Scowcn and H. Sun, *J. Chem. Soc. Dalton Trans.*,**1996**, 2417; b) H. Sun, Ph.D, Universitv of London, **1996**

[14] I. Shweky, A. Bino, D. P. Goldberg and S. J. Lippard, *Inorg. Chem.*,**1994**, *33*, 5161.

[15] P. Köpf-Maier and T. Klapötke, *Inorg.Chim. Acta.*,**1988**, *152*, 49.

[16] N. Yang, J. A. Tanner, Z. Wang, J. D. Huang, B.-J. Zheng, N. Zhu and H. Sun, *Chem. Commun.*,**2007**, 4413.

[17] N. Mahmood, A. Burke, R. M. Anner and B. M. Anner, *Antiviral. Chem. Chemother.*,**1995**, *6*, 187.

[18] R. W. Kozak, R. Waldman, W. Atcher and A. Gansow, *Triends Biotech*,**1986**, *4*, 259.

[19] R. W. Kozak, W. Atcher, A. Gansow, M. Friedman, J. J. Hines and T. A. Waldman, *Proc. Natl. Acad. Sci. U.S.A.*,**1986**, *83*, 474.

[20] A. E. Martell and R. D. Hancock, *Metal Complexes in Aqueous Solutions*, Plenum Press, New York, **1996**. 46.

[21] S. Ahrland, *Inorg. Chim. Acta.*,**1983**, 154.

[22] a) J. Reglinkski, *Chemistry of Arsenic, Antimony and Bismuth*, Blackie Academic & Professional, London **1998**; b) R. D. Hancock, I. Cukrowski, I. Antunes, E. Cukrowska, J. Mashishi and K. Brown, *Polyhedron*,**1995**, *14*, 1699; c) R. D. Hancock, I. Cukrowski, J. Baloyi and J. Mashishi, *J. Chem. Soc., Dalton Trans.*,**1993**, 2895; d) J. R. Frausto and R. J. P. Williams in *The Biological Chemistry of the Elements*, *Vol. 3* Clarendon Press, Oxford, **1991**, 538.

[23] L. J. Farrugia, F. J. Lawlor and N. C. Norman, *J. Chem. Soc. Dalton Trans.*,**1995**, 1163.

[24] a) P. Kiprof, W. Scherer, L. Pajdla, E. Herdtweck and W. A. Herrmann in *Metals in Biology and Medicine. Part 3. Bismuth Lactate: Synthesis and Structure of a Hydroxycarboxylate Complex*, *23* WILEY-VCH Verlag, **1992**; b) H. Sun, H. Li, I. Harvey and P. J. Sadler, *J. Biol.l Chem.*,**1999**, *274*, 29094.

[25] F. Graner and L. G. Sillén, *Acta. Chem. Scand.*,**1947**, *1*, 631.

[26] F. Graner, Olin A. and L. G. Sillén, *Acta. Chem. Scand.*,**1956**, *10*, 476.

[27] A. Olin, *Acta Chem. Scand.*,**1957**, *11*, 1445.

[28] T. F. Bidleman, *Anal. Chim. Acta.*,**1971**, *56*, 221.

[29] I. Hataye, H. Suganuma, Ikegami H. and T. Kuchiki, *Bull. Chem. Soc. Japan*,**1982**, *55*, 1475.

[30] a) G. Sposito and K. M. Holtzclaw, *Soil Sci. Soc. Am. J.*,**1979**, 47; b) P. M. May and R. A. Bulman, The Present Status of Chelating Agents in Medicine, Progress in Medicinal Chemistry, *20*, Elsevier, **1983**, 225

[31] M. V.A. and T. G. Spiro, *J. Am. Chem. Soc.*,**1966**, *88*, 1410.

[32] D. Voet and J. G. Voet in *Biochemistry*, *Vol. 3* Wiley, United States of America, **2004**, 736.

[33] a) R. Chen, C. Gao, Y. Wu, H. Wang, H. Zhou, Y. Liu, P. Sun, X. Feng and T. Chen, *Chem. Comm.*,**2011**, *47*, 8136; b) P. J. Sadler, H. Li and H. Sun, *Coord. Chem. Rev.*,**1999**, *185–186*, 689.

[34] M. K. Singh and M. N. Srivastava, *J. Inorg. Nucl. Chem.*,**1972**, *34*, 2067.

[35] Jaroslav Heyrovski, http://en.wikipedia.org/wiki/Jaroslav-Heyrovsk%C3%BD, (Date Accessed: 2013-07-31)

[36] P. Zuman, *Acta Chim. Slov.*,**2009**, *56*, 18.

[37] R. A. Robinson, R. H. Stokes and *Electrolyte Solutions – The Measurement and Interpretation of Conductance, Chemical Potential and Diffusion in Solutions of Simple Electrolytes*, Butterworth and Co, London, **1959**.

[38] C. Billing, I. Cukrowski and B. Jordan, *Electroanal.*,**2013**, *25*, 2221.

[39] Metrohm-Autolab, NOVA, **2012**, (Utrecht, Netherlands)

Chapter 2: The development of automated procedures using NOVA software to study metal-ligand complexation

2.1 Introduction

The study of metal ligand complexation using polarography has, in recent times been heavily dependent on computer process power, computer software and auxiliary instruments which are able to collect the copious amounts of data generated during an experimental run. Previous studies[1] have shown that the use of powerful computer hardware and software have aided in many breakthroughs regarding the understanding of polarography. Computer simulations have helped understand the double layer effect and its effect on the background of DPP polarograms as described by Josephine and Christie[1] and therefore illustrate that in order to generate the most compelling electro-analytical data, the main foundation on which to build upon is the use of hardware and software capable of matching the stringent experimental needs.

Previous work[2] in the University of Witwatersrand electrochemistry laboratory developed a virtual system for the collection of raw data for metal-ligand equilibria studies, glass electrode potentiometric studies and sampled direct current polarographic studies. Although the development of technology had made great strides at the time of the work,[2] no single instrument was available which could fully automate all the components needed to complete a voltammetric titration experiment. What transpired was the development of a dedicated computer controlled instrumental setup capable of automated titration and pH-polarographic titrations. The automated system was made up of a Bioanalytical Systems (BAS) CV27 potentiostat and a Metrohm VA stand, automated burette (a Dosimat), pH meter and stirrer. All components were connected to an interface built in-house capable of linking to a computer central processing unit (CPU). The software used to develop the system was LABVIEW,[3] an acronym for Laboratory Virtual Instrument Engineering Workbench, and is a general purpose programming environment designed as a complete set of applications for instrumental and process control for a variety of experiments. The LABVIEW[3] software was used to develop an

automated process specific for the application of metal-ligand studies. Functions, user interface and overall look of the automation programme were tailor made to suit the needs of the experiment and therefore an extremely useful tool at the time. The experiments run could also be subjected to subtle changes with current integration time on the mercury electrode which is able to minimize noise, a useful characteristic in times when noise could make data collection impossible. The LABVIEW[3] automated experimental system afforded efficient and reproducible experiments and was successfully utilised in metal-ligand studies thereafter.[2]

Although the LABVIEW[3] system worked well for many years, the system did have some disadvantages which became more apparent as technology was being developed in both hardware and software. LABVIEW[3] was chosen for the automation of instruments since it was powerful and flexible in its application, but the licence to use these developmental features is very costly and training had to be done before the development work could be started. As it stood, the LABVIEW[3] system was also only set up to for a single electroanalytical technique, direct current polarography. As described earlier, the interface between the instruments and computer had to be developed solely for this automation development, which meant that if a component failed it would be difficult to troubleshoot as the people involved in the development were no longer there and no schematics of the system were available. Finally, the BAS CV27 potentiostat used in this setup was more than 30 years old and almost impossible to replace if it had failed. Continuity plans for the experimental work needed to be put in place should certain components stop working.

Fairly recently, Eco Chemie (a member of the Metrohm group) developed the Autolab 302N potentiostat controlled by NOVA[4] software. Through various interfaces it was able to connect to the VA stand, a magnetic stirrer and a Dosino (an automated burette), and a pH module (pX1000) was installed to enable pH and temperature measurements. In turn, all of these instruments would be able to be controlled by the computer using the [4] software. Initially this setup seemed an excellent contingency plan in case of failure of the LABVIEW[3] system, however, the NOVA[4] software would allow for the development of a brand new automated system not only capable of performing all the functions utilised in

the LABVIEW[3] system, but also utilising all other electroanalytical techniques provided by NOVA. [4]

It was therefore one of the aims of this project to develop a new automated system to run the pH-polarographic titrations. Not only would a new system contribute to greater stability, it would also afford us more flexibility and the option to other electroanalytical techniques if required.

2.2 Instrumental Setup

Figure 2.1 shows a schematic diagram of the instrumental setup used throughout this work where all components were supplied by Metrohm. The Autolab 302N potentiostat/galvanostat (designed by Eco Chemie and supplied by Metrohm) was used and a pH (pX1000) module was installed in the potentiostat which allows both a glass electrode and thermocouple to be connected. A low current (ECD) module was also installed for other applications which allows for measurements down to 100 pA, but this was not need for this work as the potentiostat has a default current range of 10 nA to 1 A which was sufficient. The 663 VA stand houses the electrochemical cell (although the polarographic cell was connected directly to the potentiostat leads) and the valves used to control the nitrogen purge gas, as well as the flow of gas to the mercury drop electrode and the drop knocker. These valves are controlled via the IME663 interface. The 800 Dosino with a 20 mL burette (an automated burette used for dispensing the titrant) and magnetic stirrer were connected to the 846 Dosing Interface which was directly connected to the PC via USB. As can be seen in Figure 2.1, the desktop PC running NOVA[4] software controls all components attached to it including the potentiostat, which in turn controls the components it communicates to. Stability and formation constants for Metal-ligand studies are dependent on the temperature at which the respective studies are completed. Temperature plays an important role as it is able to affect the rates and stability of reactions occurring thus it was important for temperature to be monitored during the entirety of our experiments. A Metrohm homemade water bath containing a thermostat was used connected to the jacketed cell in order for the temperature to be regulated strictly to 25 ± 0.1^{o}C.

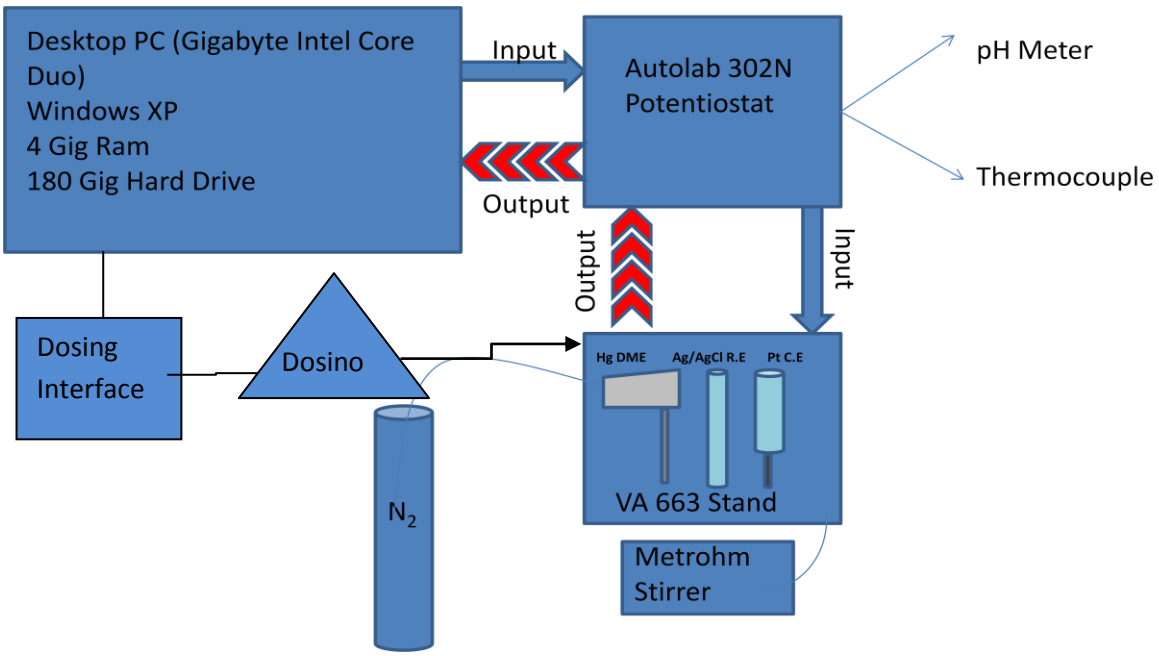

Figure 2.1: Schematic of the general instrumental setup.

Electrochemical measurements using the Autolab 302N potentiostat can be made using either GPES or NOVA[4] software. GPES is easier to use when running once off measurements, but NOVA[4] is required for automating measurements and controlling various hardware components as used in our setup. NOVA[4] is operated by dragging pre-programmed instrument commands into a procedure, which then allows the procedure to become functional provided the correct sequence and commands required are in place. The measurements from an experiment conducted are displayed on screen in real time and the data files saved.

Although the NOVA[4] software controls all the components associated with the experimental setup, it requires a vast amount of procedure design and code in order to run an automated experiment as required and to obtain the data needed for our investigations. The following aspects needed to be considered when developing such a procedure: what measurements need to be made, how and when do these measurements need to be made, what components in the setup need to be activated and what function needs to be performed, what sequence of events need to be followed, how are loops in the procedure dealt with and so on.

Three main NOVA[4] procedures were developed, one for each experimental procedure required to in the investigation of the complexation of bismuth with biologically active molecules. These were (i) the glass electrode calibration, (ii) the polarographic-pH titration starting in solutions containing metal ions (Bi^{3+} and Tl^{+}) (i.e. ligand-free polarographic-pH titrations) and (iii) the polarographic-pH titration where the solutions contain the metal ions and ligand of choice (i.e. metal-ligand complexation studies by polarographic-pH titrations).

2.3 Glass Electrode Calibration Procedure

The instrumental setup for the glass electrode calibration is illustrated in Figure 2.2 and the method used is fully described in Chapter 3, section 3.2. Briefly, this involved beginning with a 0.1 M HNO_3 solution (containing 0.4 M KNO_3) and adding a 0.1 M KOH solution (also containing 0.4 M KNO_3) in 0.500 ml increments until a basic pH (about pH 12) was reached. After each addition of KOH, the potential difference at the glass electrode was recorded. The potential difference is then plotted against the calculated pH after each addition of hydroxide (based on volumes and concentrations of the two solutions), and a relationship between the potential difference and pH is found.

Setting up the NOVA[4] procedure started with setting the initial entries (see Figure 2.3) which indicates the type of instrument present for the experiment. In this case it is the Autolab 302N potentiostat containing the additional pX1000 module. The signal sampler indicates which signals will be sampled in the measurement. For the glass electrode calibration, the signals sampled were the voltage (pX(1).Voltage) and pH (pX(1).pH) at the glass electrode, temperature (pX(1).Temp) and time. The pH sampled was based on the calculation using an ideal calibration, so this was simply an indication of the approximate pH of the solution. It was the voltage readings at the glass electrode that were used in the actual calibration plot.

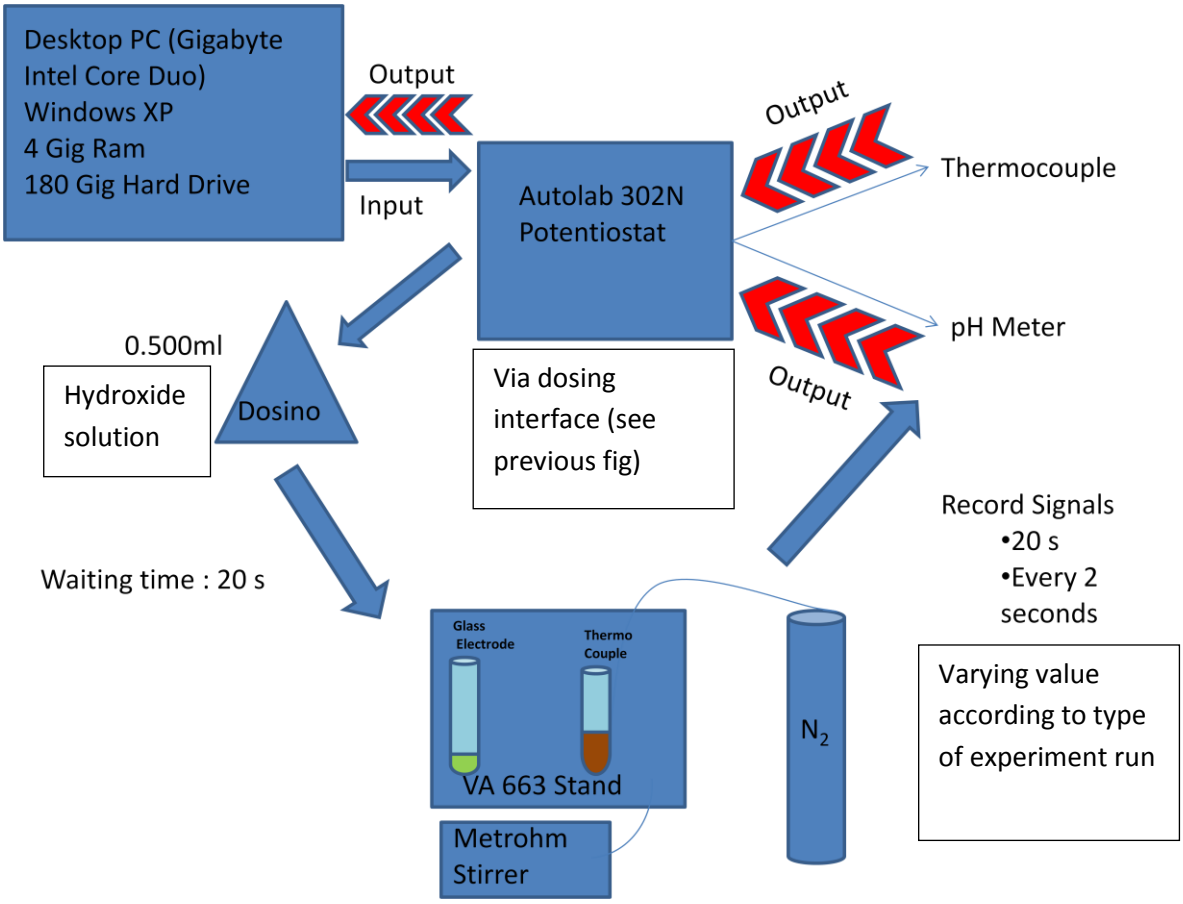

Figure 2.2: Schematic of the instrumental setup during the glass electrode calibration procedure.

Commands	Parameters	Links
GE Calibration test-Final		
Remarks		
End status Autolab		
Signal sampler	Time, pX(1).Voltage, pX(1).pH, pX(1)....	
Options	No Options	
Instrument		
Instrument description		

Figure 2.3: Initial lines of NOVA[4] code showing instrumentation and signals to be measured during the glass electrode calibration procedure.

For a procedure to be valid there must be a logical order of commands. For instruments such as the Metrohm Dosino and Stirrer, the *initialize* command must first be given in order for them to become operable (see Figure 2.4) and the *closed* command must be

given once their function is complete in order for a procedure to be valid. Thus the *Dosino initialize* command must be dragged into the procedure window and within the settings tab, the serial number of the Dosino in use must be entered. The Metrohm magnetic stirrer must also be initialised in the same way and its respective serial number must also be entered in the *stirrer initialize* tab. The stirrer speed can be set in the command tab (between values of 1 and 10) and in order to stop the stirrer, the stirrer speed must be set to *0*.

The *Autolab control* (see Figure 2.4) is a major component of the experiment. This command activates the potentiostat, which then allows it to control commands sent to the VA stand, and in this case activates the N_2 purger. The NOVA[4] software ensures its reproducibility and accuracy by making time a major component of the experiment. Time is constantly measured in order to optimize the procedures and so any command which entails the measurement of a certain signal or the timing of a command, must be placed within a *timed procedure* command.

The cell was set up by adding 25.00 mL of the HNO_3 solution using a Dosimat and placing the glass electrode and thermocouple in the cell. Before any measurement of signals or addition of base, the glass electrode calibration requires that all carbon dioxide (and oxygen for the polarographic experiments) be removed from the cell. This is done by purging with N_2 for approximately 1 min/ml of solution and stirring throughout. In Figure 2.4 it can be seen that the *stirrer speed* was set to 3 and stirring continued throughout the procedure until the *stirrer speed* was set to 0 to stop it. Stirring allowed the titrant to always be uniformly dispersed once added to the cell. The *purge* command is placed within a *timed procedure* so the solution was initially purged for 1800 s, after which the purging was stopped. During the measurement of signals and addition of base, the purger was kept on to remove carbon dioxide and oxygen introduced into the system due the addition of the base. This command is not a timed procedure as it must be done throughout the whole experiment. In order to run the purger constantly throughout the experiment, the *autolab control* command was used and purging was turned on in the *MDE(1)* tab as shown in Figure 2.5.

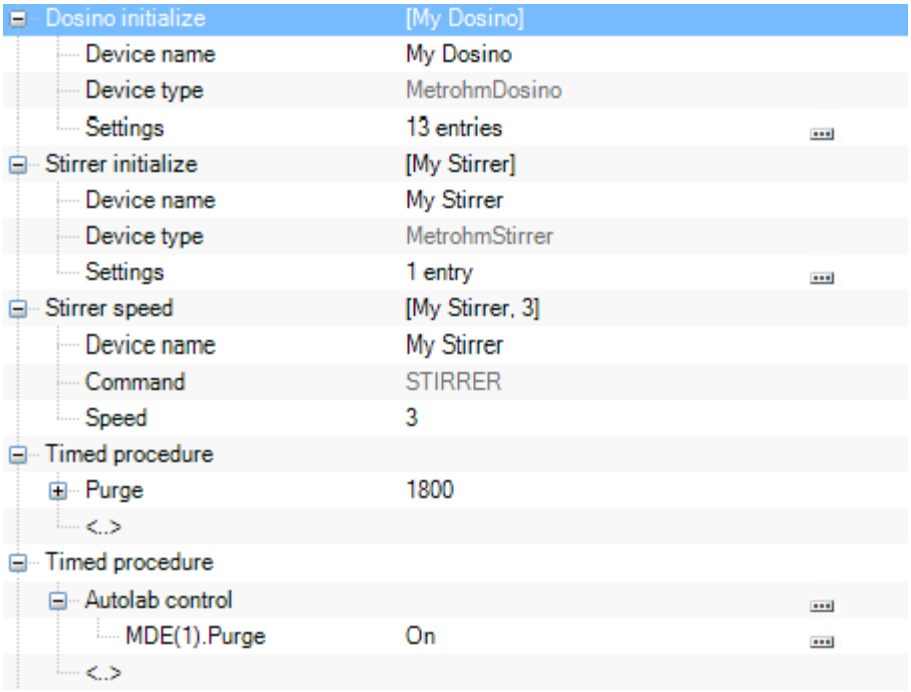

Figure 2.4: Commands for initialising devices and controlling the stirring and purging.

In Figure 2.5 there is also an option to turn a stirrer on, however, this option does not refer to the magnetic stirrer, but rather the rotating stirrer controlled by the VA stand via the IME663 interface. All other options in this Autolab control command tree did not need to be changed as the glass electrode experiment does not require any measurement of current or applied voltage via working, reference or counter electrodes.

The glass electrode calibration experiment was conducted by adding 0.500 ml increments of KOH solution while purging and stirring. The system was then allowed to equilibrate before the voltage at the glass electrode and temperature at the thermocouple were recorded. Since the experiment required multiple additions of base, a *repeat for each value* command was utilized (see Figure 2.6). This loop repeats the commands which are placed within it for each value of a specified parameter. The parameter of importance in this experiment was the 0.500 ml of base which was added multiple times in order for the titration to be done. As can be seen in Figure 2.6, within the *Dosino dose* command, the *volume (ml)* sub command is linked to the *parameter link* command for the repeat loop. This is indicated by the square bracket shown on the right of the commands. The loop is

thus repeated for each value specified in the *repeat for each value* command (i.e. the addition of 0.500 ml as many times as stipulated).

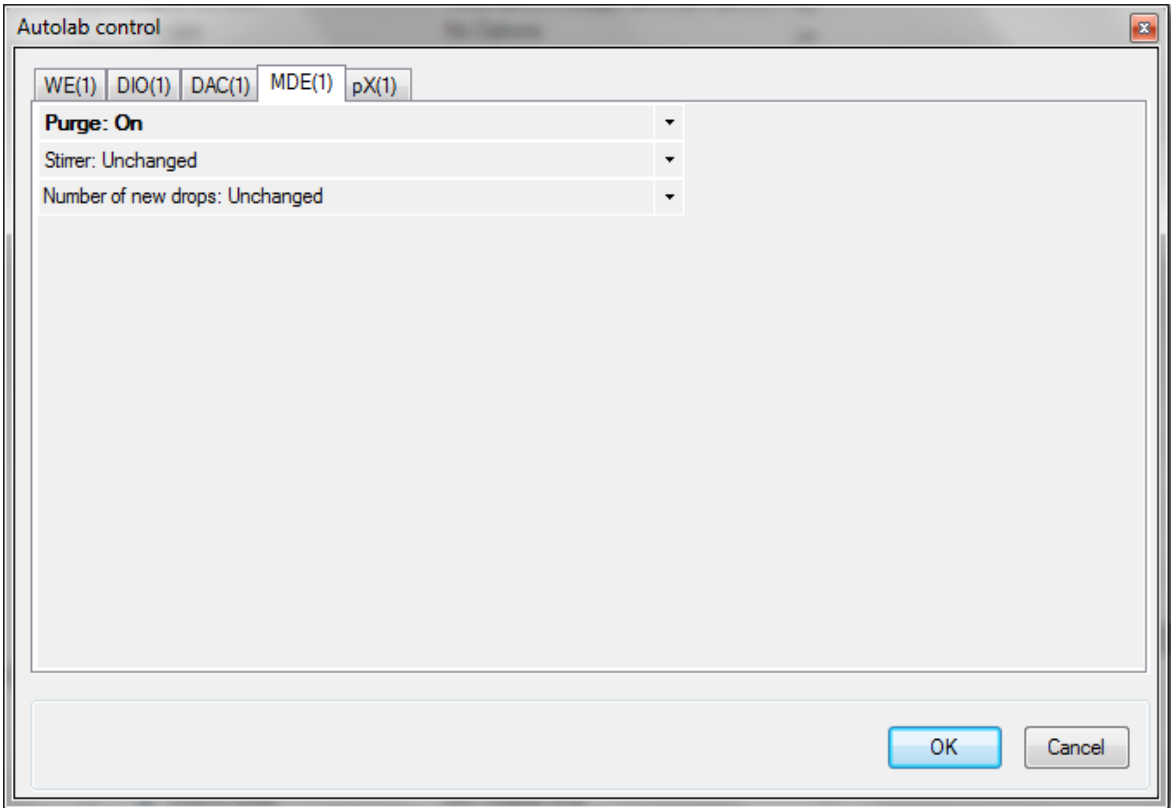

Figure 2.5: *Autolab Control* tab showing the method by which the purger is turned on and allowed to continuously purge throughout the experiment.

The repeat loop is the primary command, with the subsequent commands indicated in Figure 2.6 all placed within the repeat loop. The *timed procedure* command allows the measurement of signals. After the addition of base, a 30 s *wait time* is implemented for equilibration to occur. The signals are then recorded every 2 s for a duration of 30 s. The *signal sampler* once again shows what signals will be measured next, namely, corrected time, voltage at the glass electrode, pH and temperature, and the values are all put into arrays for each type of signal measured. The colour-coding of the signals (found under the *signal sampler* command in Figure 2.6) is important to note. The red signal arrays correspond to the data which was directly measured. The blue signal arrays are due to the addition of calculations on the recorded data which allow further information to be directly obtained from the experiment. In this case the means and standard deviations of

the set of data points collected after each addition of base were calculated for the voltage, pH and temperature. This was done via the *calculate signal* commands indicated in Fugure 2.7. These calculated signals are also put into arrays. The mean voltage values at each step in the titration were used in the calibration plot and the standard deviations were calculated to indicate whether the measurements were stable throughout the 30 s measurement duration. Any errors or fluctuating values may have a detrimental effect on our final results, as our experiments on metal-ligand systems are heavily dependent on the accuracy of the pH-voltage calibration.

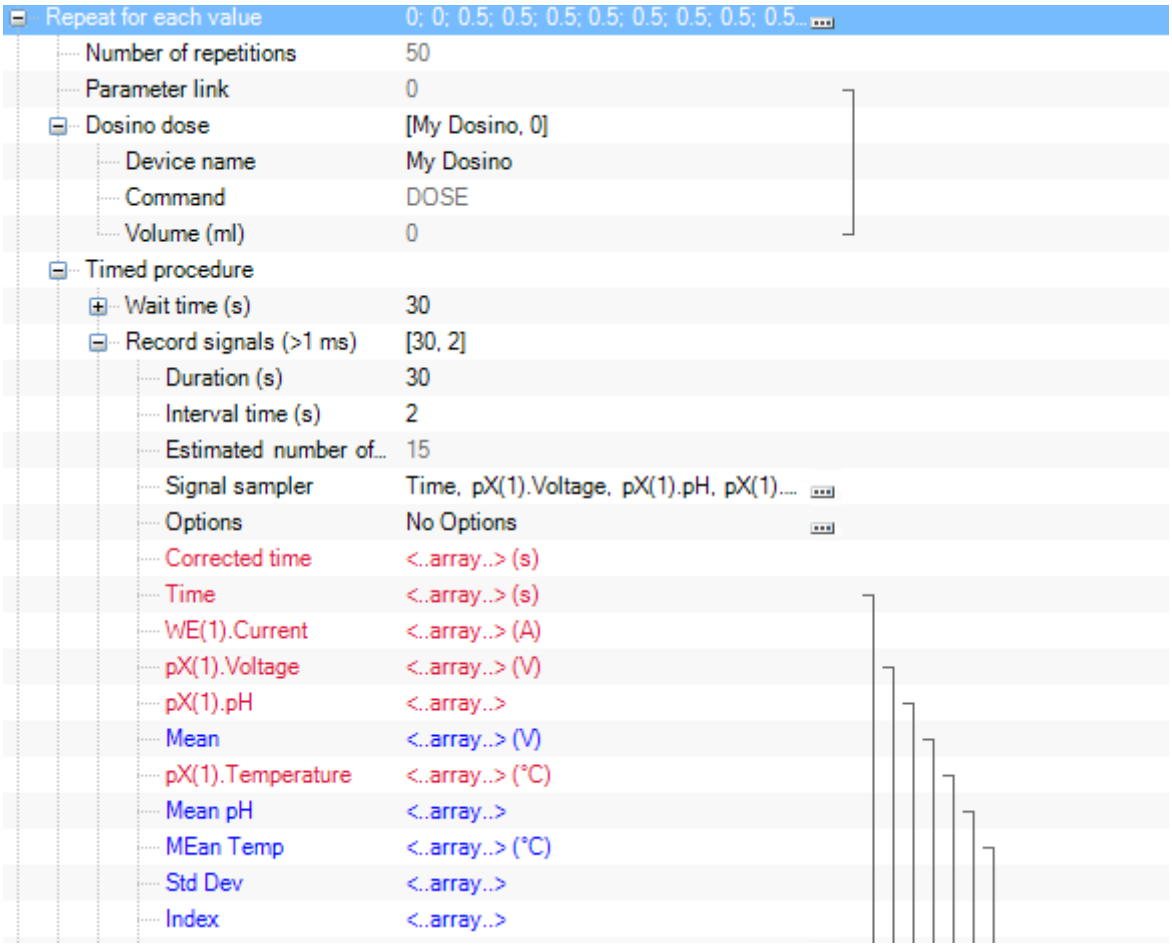

Figure 2.6: *Repeat for each value* command tree showing the parameters used for measuring the signals during the glass electrode calibration.

The *custom* commands shown in Figure 2.7 were used to give a visual representation of the measured data by drawing graphs as the experiment proceeded. Two graphs were displayed during this experiment: pX(1).Voltage vs time and pX(1).pH vs time. The signals

which are sampled (as indicated in red in Figure 2.6) were linked to the *custom* command via *links*, indicated but square brackets on the right of the commands.

The signals that were measured and calculated were saved in an ASCII file via the *Export ASCII data* command. The data required are *linked* to the respective columns in which the data must appear in the ASCII data file and are saved into the directory designated by the user. Within the *Export ASCII data* command, the *File mode* command determines how the data file should be saved. For the glass electrode calibration this option was set to *append* which allows the file to be rewritten and the data for the successive repeat loops to be added. Thus all the data measured for each repeat in the loop is then saved in one row and the completion of the next repeat saves the data in the next row of the file. The ASCII data file can then be opened in a spreadsheet in order to extract and utilize the experimental data.

The calibration procedure developed contained three repeat loops (Figure 2.8). It was decided to programme the procedure this way so as to take changing equilibration times into account. During the titration, equilibration times vary according to where along the titration curve the experiment is. At the beginning and near the end of the pH titration, 0.500 ml additions of base cause very little change in the pH, as indicated in the titration curve in Figure 2.9. However, near the end point the addition of 0.500 ml of base results in a large change in pH and as there is a large drift as the signal, so equilibration times in this region were made longer to obtain more stable values. It was therefore decided to have an initial *repeat loop* for the 0.500 ml additions up to a total of approximately 24 ml of base. The exact volume depended on the expected endpoint as determined by the standardised concentrations of the acid and base solutions used. During this repeat loop the *wait time* was set to 30 s. Thereafter a second repeat loop was included to add base for 4 repeats (collectively 2 ml of base added) around the end point of the titration and the *wait time* was changed to 300 s. This allowed adequate time for the system to reach equilibrium before measuring the signals. Standard deviations of the data collected in this region were $<10^{-5}$ mV signifying stable measurements. A third repeat loop was programmed to the same specifications as the first repeat loop. Here, the number of

0.500 ml additions were repeat until the desired stop volume was reached, which was approximately 40 ml of base in total for the glass electrode calibration procedure.

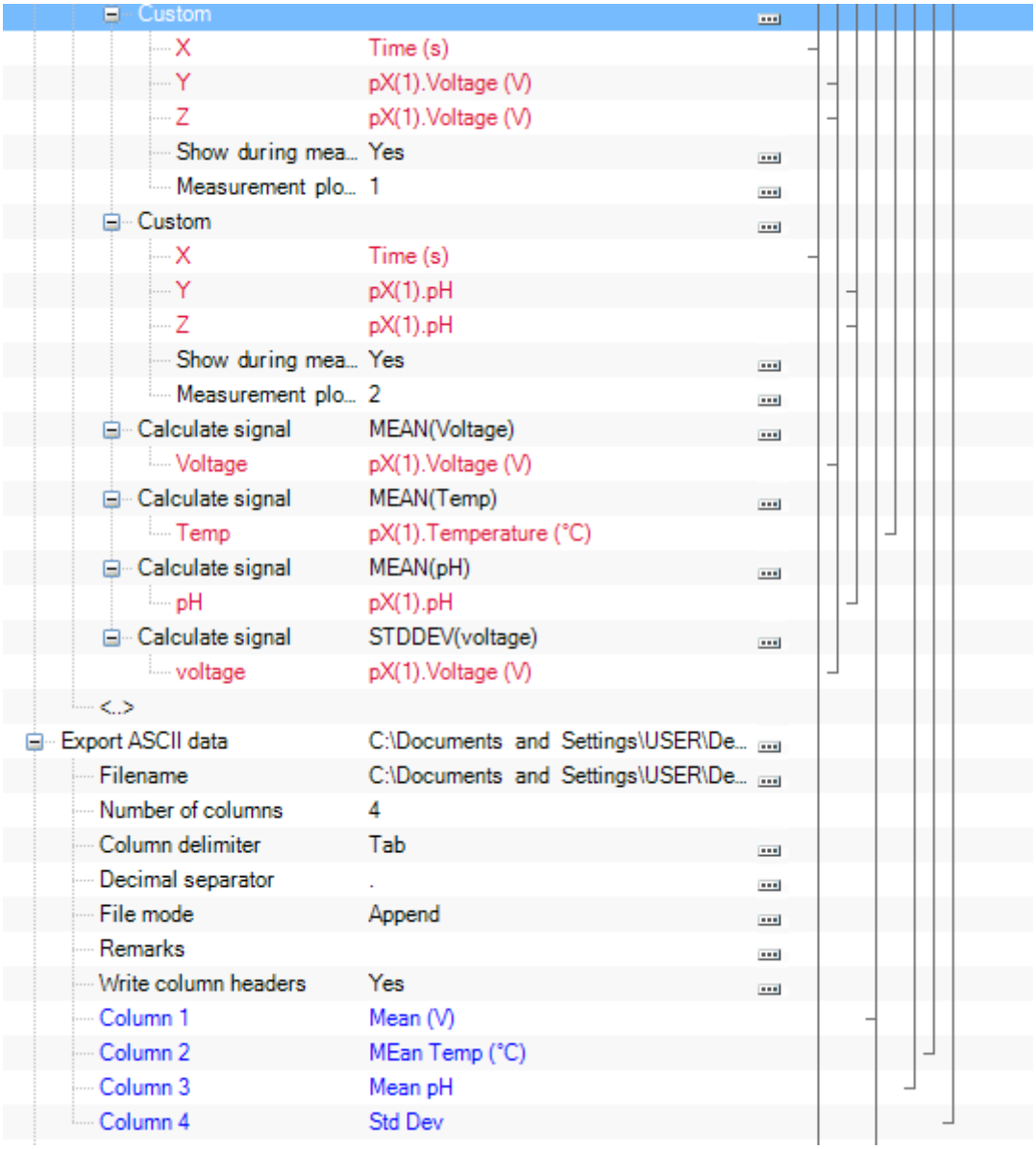

Figure 2.7: The *custom commands* used to plot the measured data during the experiment, and the commands used to perform calculations on the measured signals and save the data.

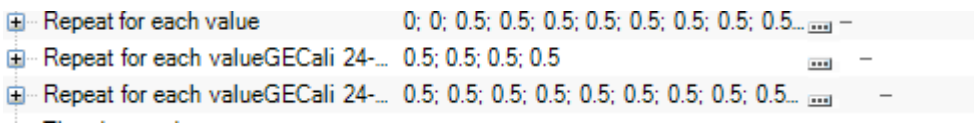

Figure 2.8: The three repeat loops in the glass electrode calibration to allow for longer equilibration times before measurements made close to the end point of the titration.

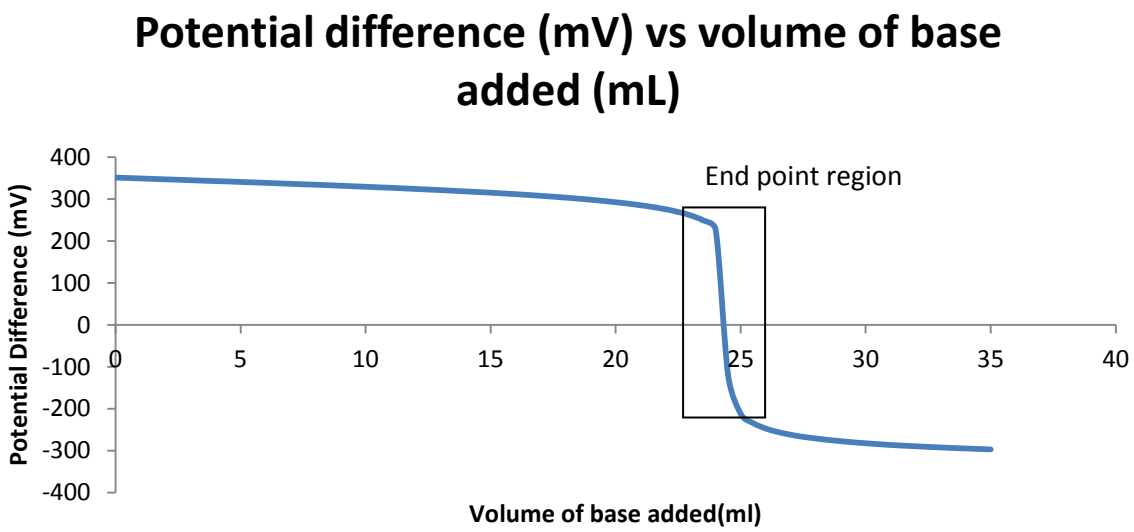

Figure 2.9: Potential difference vs volume added plot for the titration of 0.9945 M HNO_3 with 0.1012 M KOH at 25.0 ^{o}C. The end point region is highlighted to show the sharp change in gradient associated with measurement of potential difference, hence a longer equilibration time is needed.

2.4 Development of the NOVA procedure for the polarographic-pH titration

Due to limitations in the NOVA[4] software, a single experimental procedure which completes the entire metal-ligand experiment was unable to be employed. The multi-hour experiment unfortunately pushed the limits of the computers available due to the fact that NOVA[4] stores all the collected data in the RAM of the computer while the experiment is running and only saves the data to the hard drive once the entire experiment is complete. Since a large volume of data is generated during our experiment, there is insufficient RAM to successful complete of the entire experiment. The functioning of the NOVA[4] software was thus dependant on the computer available. It was decided to divide the experiment into two separate procedures, called Part A and Part B. This would allow the RAM of the computer to store the first part of the experiment, before carrying on with the next, thus preventing the computer RAM from running out of space.

Figure 2.10 shows a graphical representation of instrumental setup and the procedure used in both Part A and B, as will be discussed in detail shortly. The procedure for the

polarographic-pH titration was the same whether ligand was absent or present with the metal ions (Bi^{3+} and Tl^{+}) in solution (as is fully discussed in Chapter 3 sections 3.3.1 and 3.3.2). Essentially the procedure was designed to do a pH titration where pH data and a polarogram were collected at every 0.1 pH units. The volume of base required to change the pH by 0.1 unit varies throughout the titration, so in this case a fixed volume could not simply be specified. Instead a volume increment of base was defined and added, followed by a measurement of the pH. If the pH had not changed by 0.1, then another increment was added and the pH remeasured. This continued until the pH had increased by 0.1 units after which a DC polarogram was measured and the pH (as the GE voltage) accurately recorded. The titration process then continued as before. The details of the procedure are presented below.

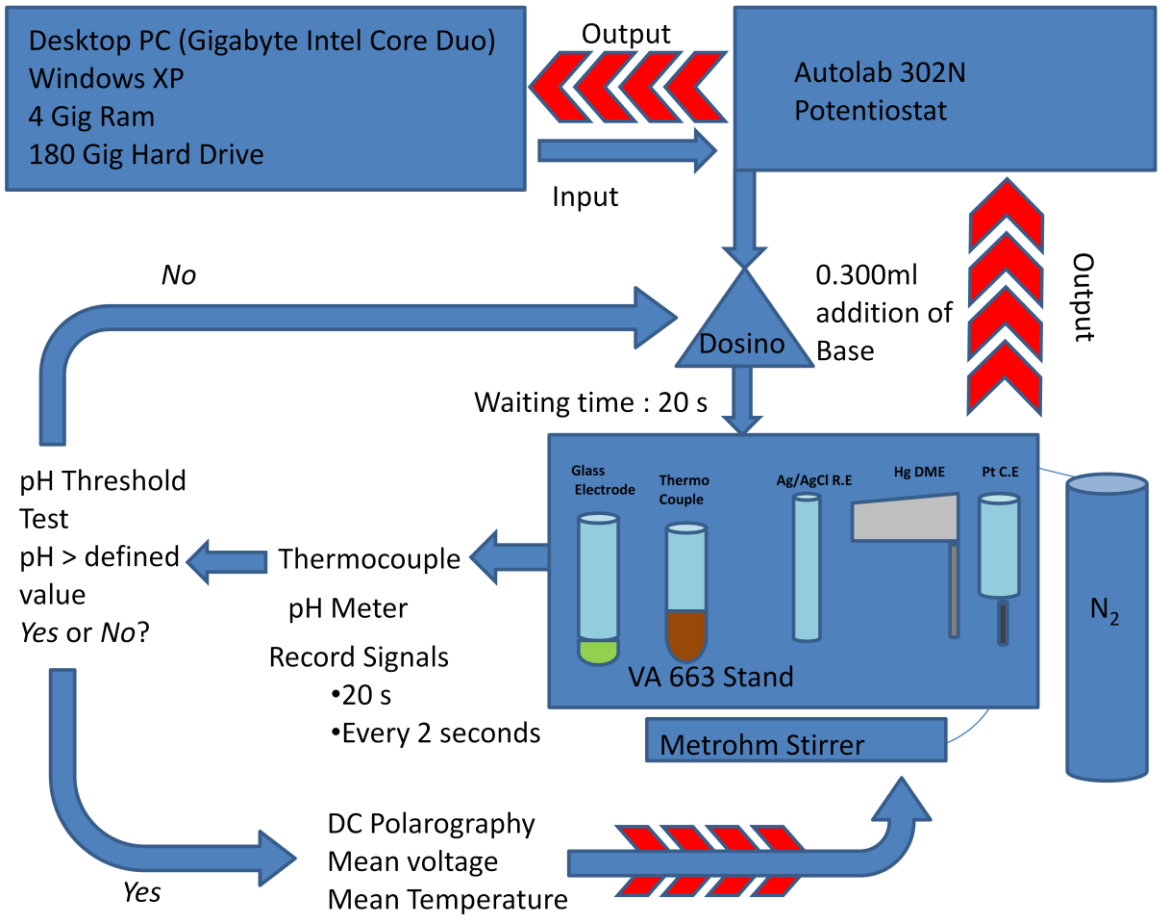

Figure 2.10: Schematic of the instrumental setup during the polarographic-pH titration procedure together with a flow diagram of the procedure.

2.4.1. Part A

As described in section 2.2 of this chapter, the opening command lines in a NOVA[4] procedure hold details of the type of potentiostat used and the signals which are to be measured. Figure 2.11 shows that the signals measured in this experiment were pH (pX(1).pH), voltage at the glass electrode (pX(1).voltage), temperature (pX(1).temperature), and the applied potential by the potentiostat and the current and actual measured potential at the working electrode (WE(1).Current and WE(1).Potential, respectively) for the polarographic data.

A *nested procedure* is a tool used for measurements that cannot be added to a *timed procedure*. The *nested procedure* command allows analysis and essential hardware commands to be grouped together. It is then easier to let one *nested procedure* contain all commands, than selecting each command individually. The first entry in the *nested procedure* is a *message box* which allows for the software to communicate with the user via text and is useful when certain actions need to be emphasised. The *message box* was utilized as a check that the Dosino to be used was prepared and ready to conduct the experiment. The Dosino had to be prepared manually before the start of the experiment to ensure the removal of air bubbles from the dosing system and that the solution in the outlet tubing was replaced by fresh solution as it may have absorbed CO_2 on standing. A further safety check which was added, is that the message box does not go away until the user clicks the *yes* tab, indicating that the Dosino is prepared and ready for use. Only then will NOVA[4] proceed to the next command. As before, the Dosino and magnetic stirrer must be *initialised* because they are used at various stages throughout the experiment. The next command is a *timed procedure* which houses the purge command while stirring the solution for a user-defined time period. This was generally set for a short time as the solution was deoxygenated in the initial data collection before the automated titration was commenced, as discussed in Chapter 3 (section 3.3.1).

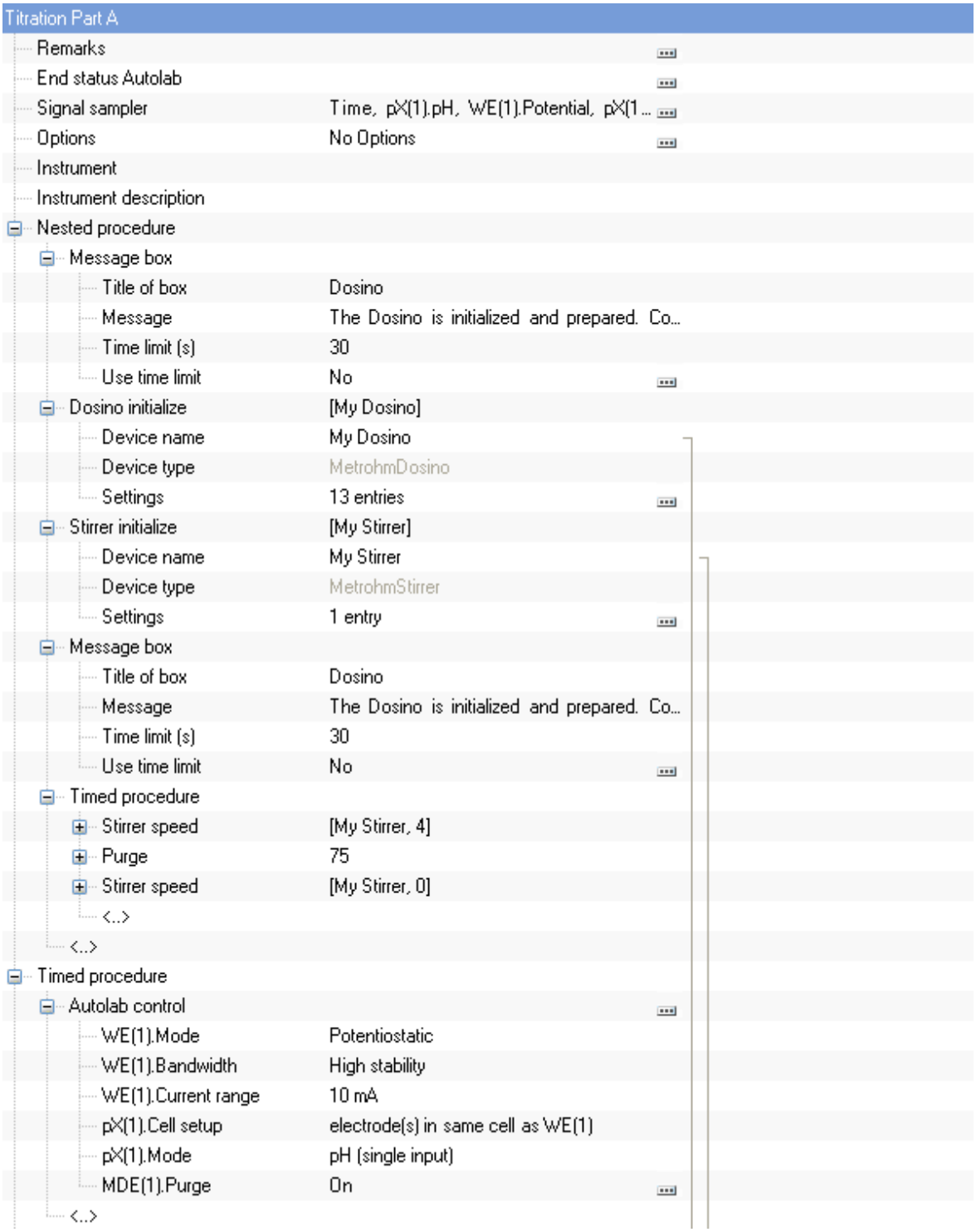

Figure 2.11: Initial steps in the procedure used for Part A of the polarographic-pH titration.

Figure 2.12 shows that the experimental procedure used to control the base addition to change the pH begins with a repeat loop. The *repeat for each value* command was used and within it the pH values were entered at which DC polarograms must be measured. As

discussed, a DC polarogram was required after a change in pH of 0.1 unit. Since initially a 0.1 M HNO_3 solution (containing lower concentrations of metal ions and ligand) was in the cell, the start pH was about 1 and so the repeat values inputted into the command are 1, 1.1, 1.2, 1.3 and so on until a final pH of approximately 2.3. The Dosino was set to add base in 0.300 ml increments for Part A. This ensured that the 0.1 pH step was never exceeded by a single addition, but that the increment was not so small as to spend unnecessarily long times on this step in the procedure.

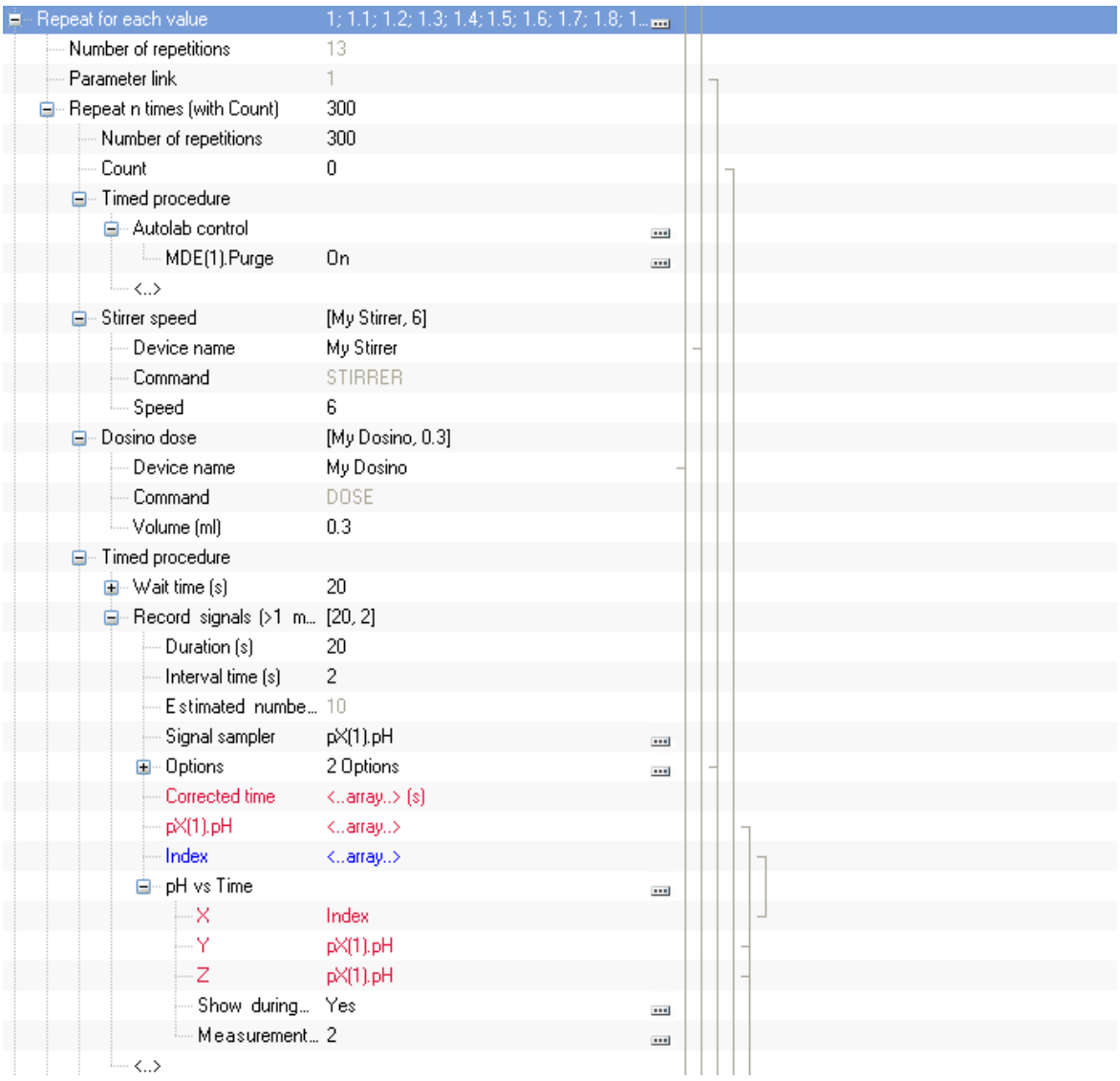

Figure 2.12: Various repeat loop commands were utilized to run the required experiment, namely the *repeat for each value* command as the primary tree command and the *repeat n times* command used to control the Dosino additions and run the pH threshold test.

A pH threshold test (see Figure 2.13) was included in the procedure to ensure sufficient base was added to change the pH by 0.1. The test applied an if-then type statement as the basis for determining how the experiment would proceed. To make the if-then statement viable, a parameter needed to be assigned to it in order for NOVA[4] to know how to proceed. The *parameter link* was the pH defined in the *repeat for each value* command, and the link is indicated by the square bracket the right. The *repeat n times with count* command allows whatever commands which are placed within it to be repeated until a stop value is reached. This version of the repeat loop command was required because increments of the base needed to added repetitively in order to achieve the pH change of 0.1, but the number of increments added would decrease as the pH increased. Once the pH has been measured there is a link from the measured pH value to the pH threshold value which calculates whether or not the pH is below or above the pH defined in the repeat loop.

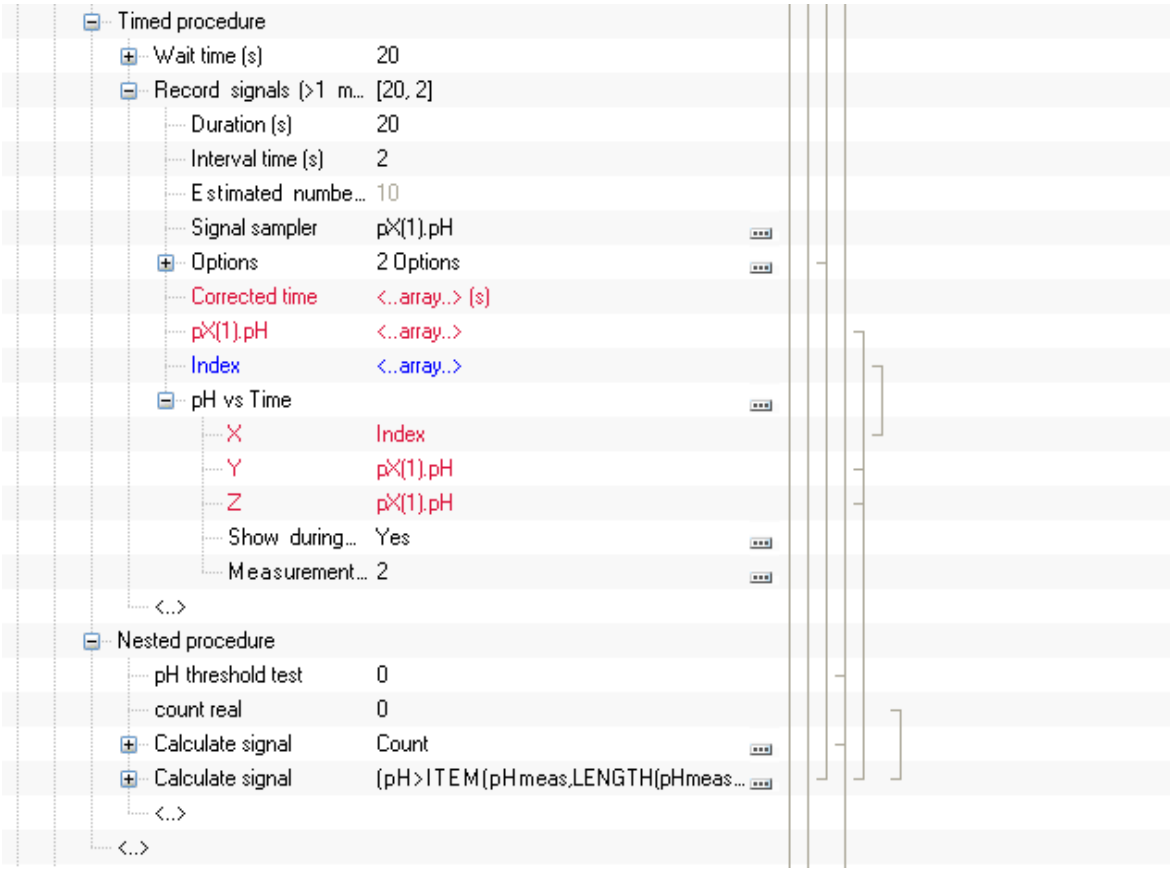

Figure 2.13: Command tree showing the pH measurement process. The *nested procedure* command for the pH threshold test is also shown.

In practice, the Dosino is programmed to dispense 0.300 ml increments of base at a time, while stirring and purging throughout. After each addition of base, a *timed procedure* allows a waiting time of 20 s for equilibration of the system. Then a *record signals* command allows the pH to be measured every 2 s for a 20 s interval (see Figure 2.13). The *signal sampler* tab shows that the only signal being recorded during this particular phase of the procedure is the pX(1).pH signal (and the corrected time as always). While the signals are being recorded, NOVA[4] can display a plot of the data, which was set to plot of pH vs index. The index array is the number of readings taken, which in this case is numbers 1 to 10 (as pH is measured every 2 s for 20 s, implying 10 readings). This plot was useful to monitor the progress of the experiment and it also indicated whether the experiment was running according to the given settings.

The *nested procedure* which follows was the second component which contributed to the programming of the if-then type statement. The pH threshold test allowed the NOVA[4] software to determine if it should carry on adding base or proceed to record a DC polarogram. The first *calculate signal* command gives the formula for the pH threshold test to obey. The second *calculate signal* command determines whether the pH is greater than that in the *parameter link* (shown in Figure 2.12). *IF* the pH is smaller than the valued defined by the *parameter link*, the *pH threshold test* returns a 0, which *THEN* causes the *repeat n times with count loop* to continue adding another increment of base. The procedure is repeated until there is a change in pH of 0.1 units. This will cause the signal calculated to be greater than that of the *parameter link*, which in turn causes the *pH threshold test* to return a value of 1 to the *repeat n times with count loop* and hence the repeat loop is stopped. The procedure then moves on to the measurement of the sampled DC polarograms, the glass electrode voltage and temperature of the solution.
The *sampled DC polarography* procedure is built into the NOVA[4] software, however, it can be amended to an extent according to the needs of the experiment. In our experiment (see Figure 2.14), the solution was purged for 400 s to remove oxygen introduced from the addition of the base before the DC polarogram is taken. The *stirrer speed* was also set to 3 so that it continued to mix the solution while purging. Once the purging was complete, the *stirrer speed* was set to 0 so that no stirring occurred during

the measurement of the signals. The *create new drop* command ensured that the measurement began with a fresh mercury drop at the electrode.

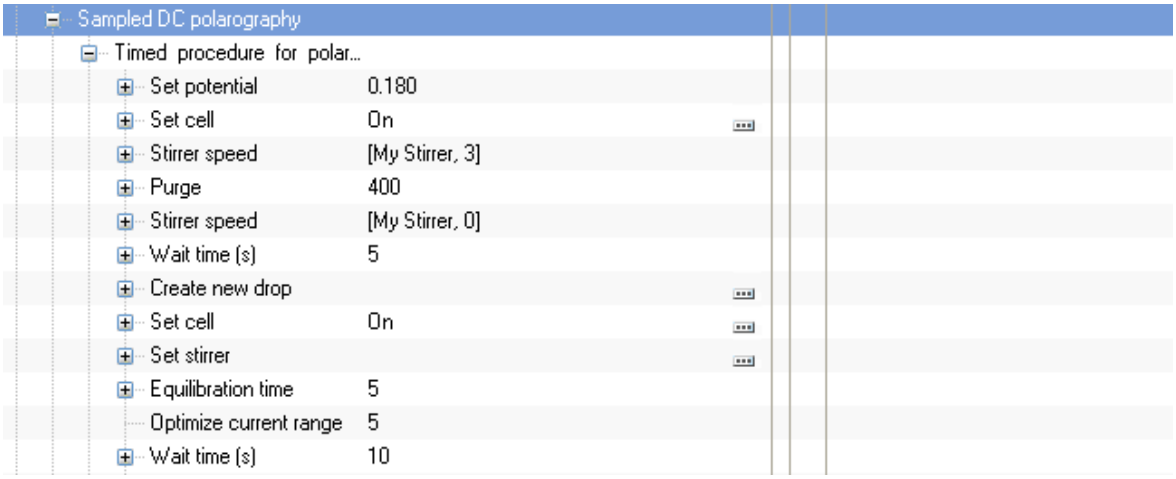

Figure 2.14: The layout of the pre-programmed *Sampled DC Polarography* command.

Figure 2.15 shows the parameters used to record the DC polarograms. The interval was from 0.180 V (*initial potential*) to -0.700 V (*end potential*). The *step potential* of –4 mV indicates by how much the applied voltage changes by for each step. An *interval time* of 1 s refer to the drop lifetime. The *signal sampler* was set to measure the applied potential, the current and potential at the working electrode (WE(1).Current and WE(1).Potential, respectively), as well as the pH and potential at the glass electrode and the temperature (pX(1).pH, pX(1).Voltage and pX(1).Temperature, respectively).

The polarogram of current vs applied potential was shown during the measurement. In order to plot the graph, these two parameters need to be defined as the axes of the graph. This is done by linking the WE(1).Current and applied potential data from the *signal sampler* to the respective axes of the graph (see Figure 2.16). During the collection of the DC polarogram, the pX1000 module simultaneously collects the voltage and pH at the glass electrode as well as the temperature at the thermocouple. As can be seen in Figure 2.17, *calculate signals* commands were added in order to determine the mean and standard deviation of the voltage at the glass electrode, the mean pH and the mean temperature of the system at the time of measurement. As before, although the pH values were collected they are merely used to indicate the approximate solution pH, but

the voltage values together with the glass electrode calibration curve were used to determine at actual pH.

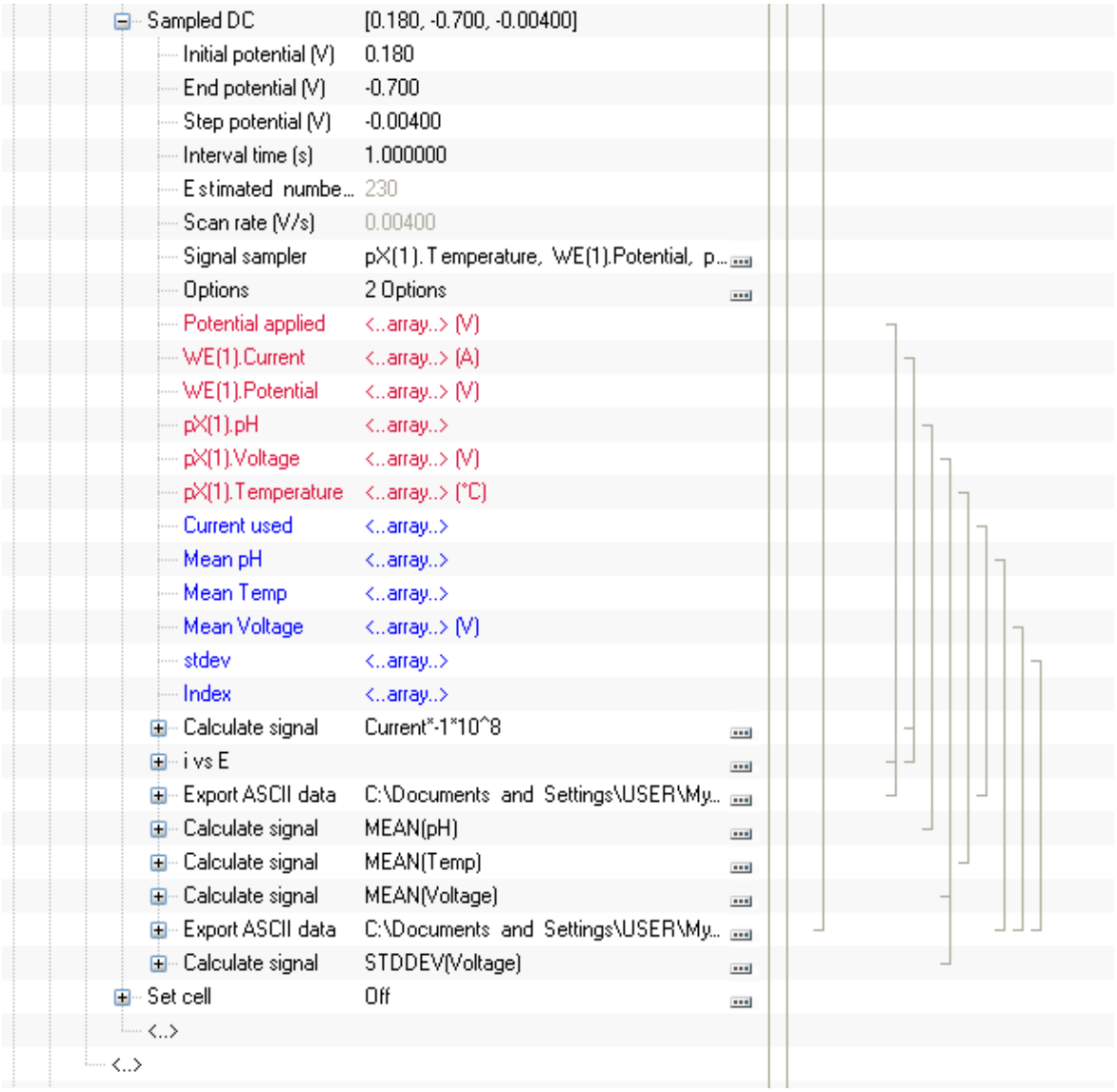

Figure 2.15: The parameters used for the DC polarogram as inputted into the NOVA[4] software.

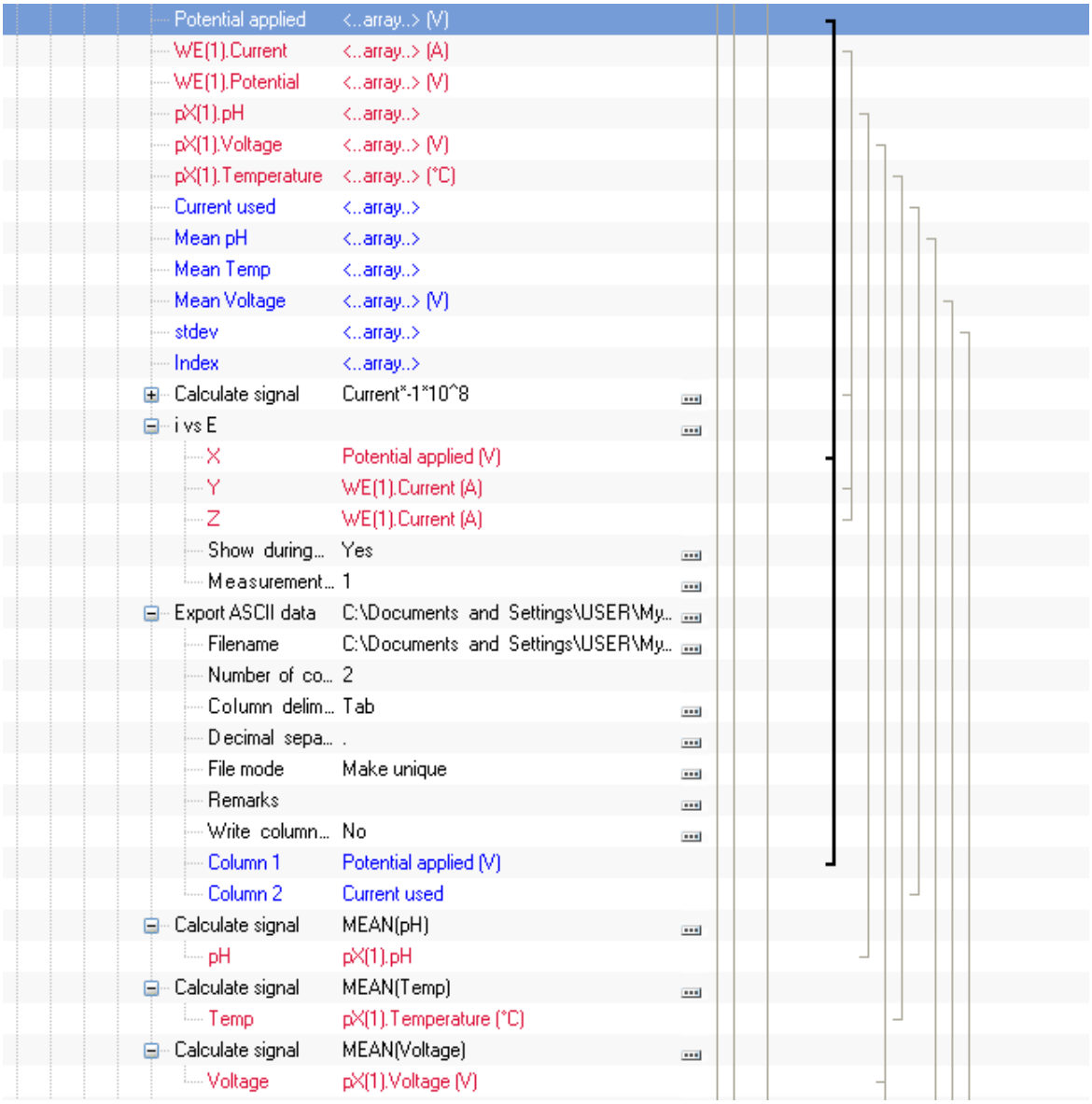

Figure 2.16: Highlighting the *link* (square brackets on the right) between the measured signals and the graphs plotted as well as the data saved in ASCII files.

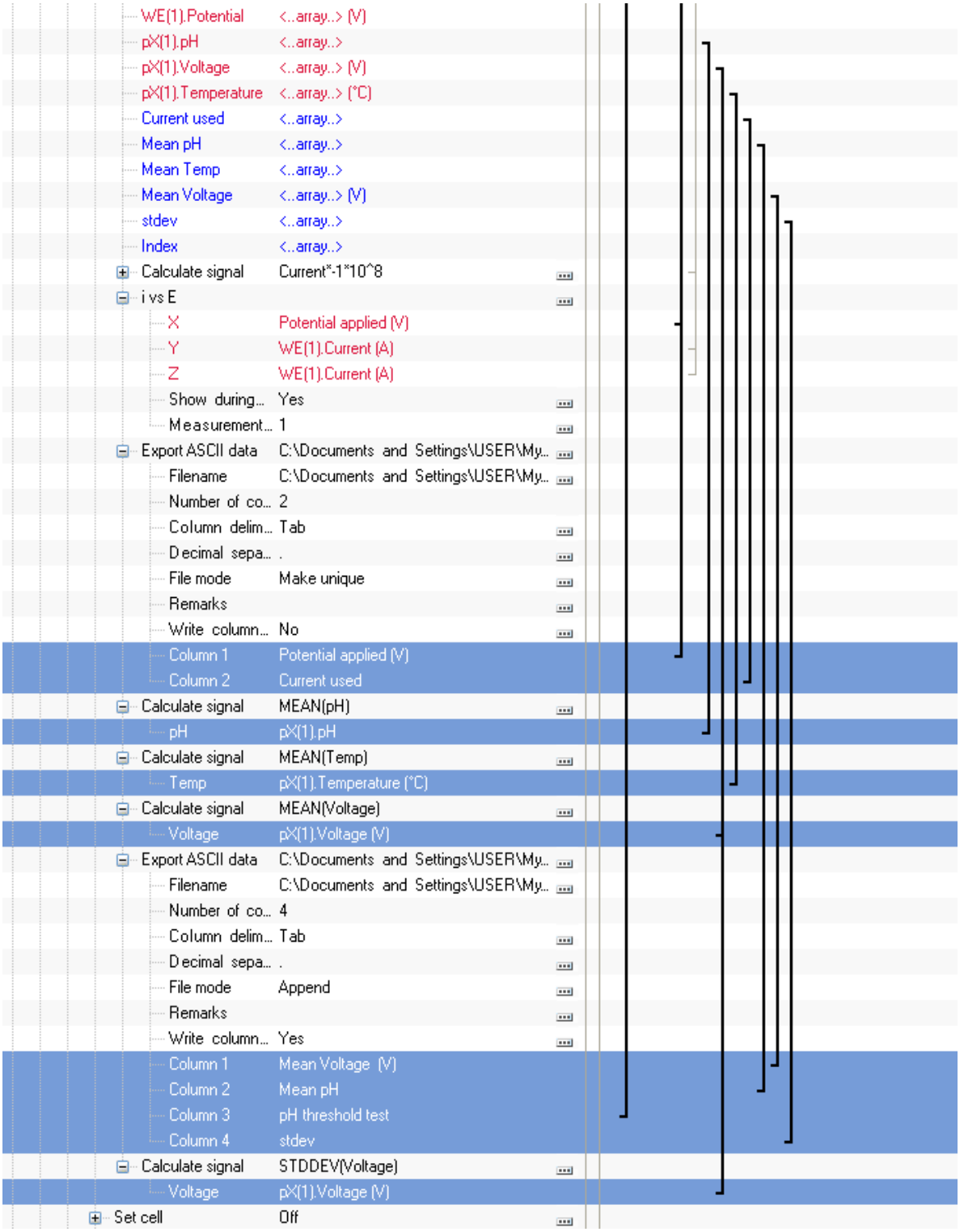

Figure 2.17: Highlighting the *calculate signal* commands which were linked to columns in ASCII data files for saving.

The signals collected were saved in two distinct ways. Firstly, data for each DC polarogram was saved in a file containing two columns for each respective signal (applied potential and WE(1).Current) using the e*xport ASCII data* command and linking the

columns to the required signals that must be saved (Figure 2.17). On hindsight, the WE(1).Potential rather than the applied potential should have been used, but in general the difference between these values was negligible. Since a polarogram was collected at each pH value, it was ensured that the data for each polarogram was saved in a separate file. In order to achieve this, the *file mode* was set to *make unique*. Each file (corresponding to one polarogram) uses the root file name followed by a number given in sequential order. Secondly, data collected via the pX1000 module was also needed and it was decided to save the calculated mean and the standard deviation of the voltage, the mean pH and the pH threshold test. The pH threshold test value is able to show us how many times the dosing increment was added before the loop could complete itself. This then allowed us to calculate the volume of KOH added by multiplying the threshold number by the dispensing volume. Since four signals were required, the *number of columns* was set to 4 and all collected data was saved in a single file for the entire experiment by setting the *file mode* to *append* under the e*xport ASCII data* command (Figure 2.17). The ASCII file was also given a name and a specific directory the on the hard drive for later analysis. The temperature measured at the thermocouple electrode was also monitored closely. This was to ensure that the temperature remained constant at 25.0 ± 0.2 ^{o}C since the calculations of stability constants are highly dependent on temperature. The temperature of the cell throughout the measurement was viewed in the analysis tab of the NOVA[4] software and any deviations throughout the entire measurement procedure could be highlighted.

Once the DC polarogram collected at pH 2.3 is complete (i.e. the last pH listed in the repeat loop), NOVA[4] software begins the ending phase for the procedure. In order for Part A to be valid, the Dosino and stirrer must be closed using the *Dosino close* and *stirrer close* commands (Figure 2.18). The cell is also turned off, but the purger and stirrer are set to be on because while Part B of the experiment is being selected, O_2 contamination is minimised.

Figure 2.18: Closing commands for the validation of the NOVA[4] procedure.

2.4.2. Part B

Part B for the polarographic-pH titration follows a similar procedure to Part A, and only the changes are highlighted here. The Dosino was programmed to add base in smaller increments of 0.025 ml. This was to ensure that data was not missed near the end point of the titration as the pH increases sharply even with small amounts of base added. The pH values for the *repeat for each value* loop were also changed; since Part A ended at a pH 2.3, Part B was set to begin with pH 2.3 and then increase in 0.1 pH steps up to a final pH value (Figure 2.19). In our experiments, the pH at which the procedure stops was generally set to pH 10.

Another important change which needed to be made in Part B was the naming of the files which contain data from the DC polarogram and pX1000 module respectively (Figure 2.20). The file names and directory for these files must be inputted by the user to ensure all data is collected and saved and that no data is overwritten. All other measurements and command lines are the same as those described in Part A.

Part B was completed by switching off the Dosino and stirrer using the *Dosino close* and *Stirrer close* commands (Figure 2.21). The *timed procedure* command which houses the Autolab control command was used to switch the purger off and finally the cell was switched off to prevent any potentials being applied across the electrodes while the cell was being emptied and cleaned.

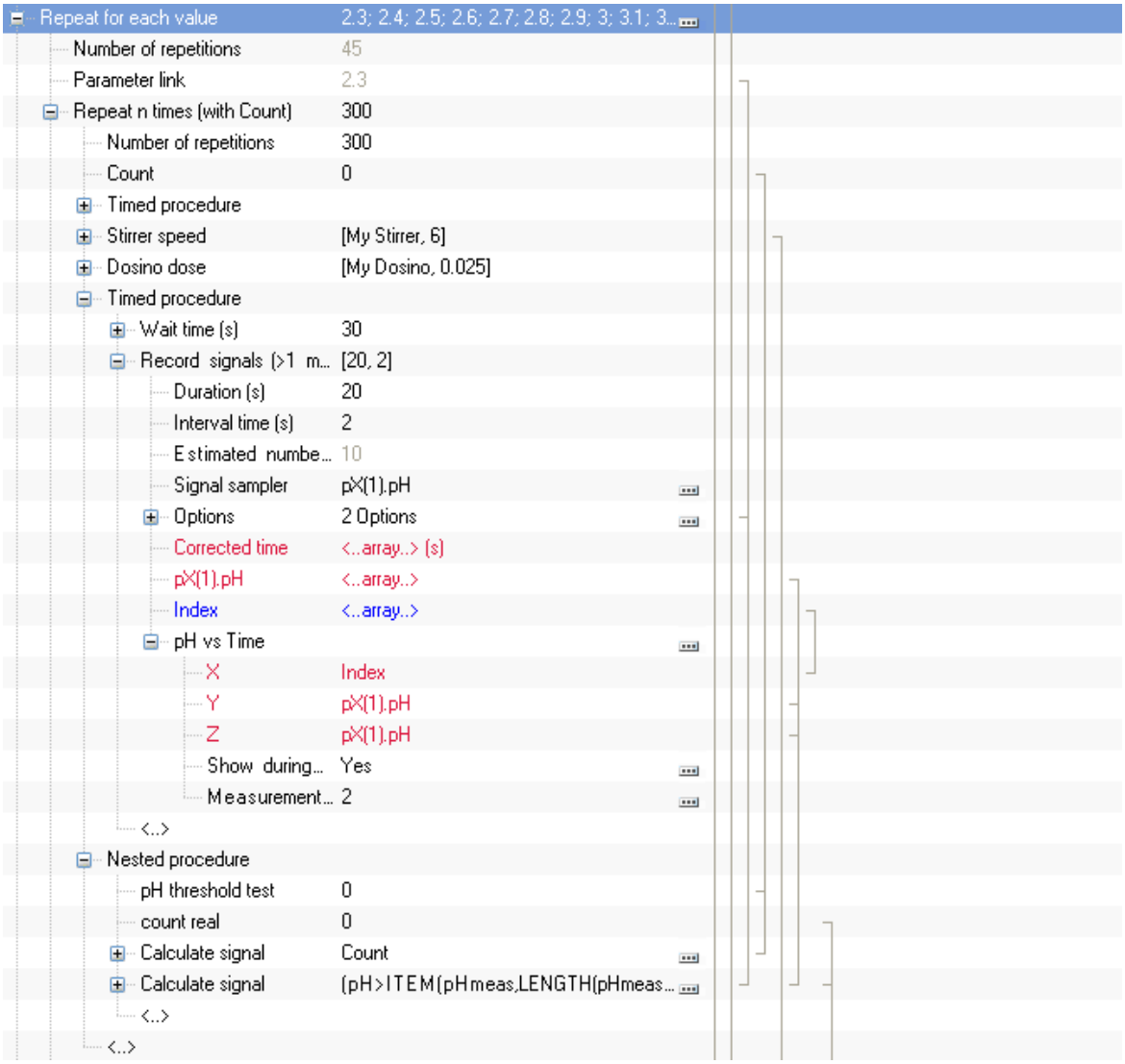

Figure 2.19: Repeat loops were utilised in the same manner as Part A. Part B was set to begin at the pH at which part A ended, therefore the first value in the loop command was pH 2.3.

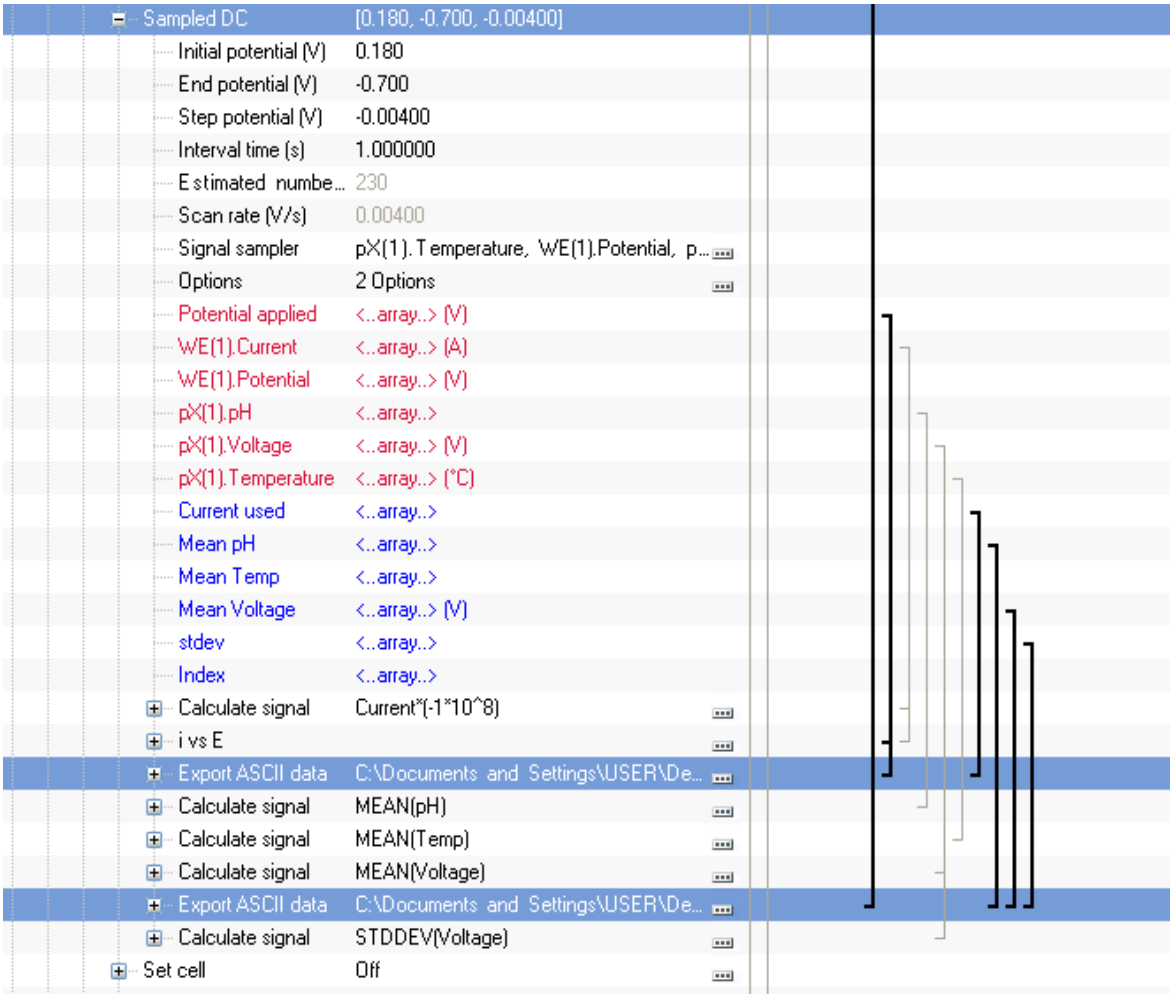

Figure 2.20: In Part B the export ASCII data commands are highlighted to emphasise that the directory and file names for the respective data must be changed.

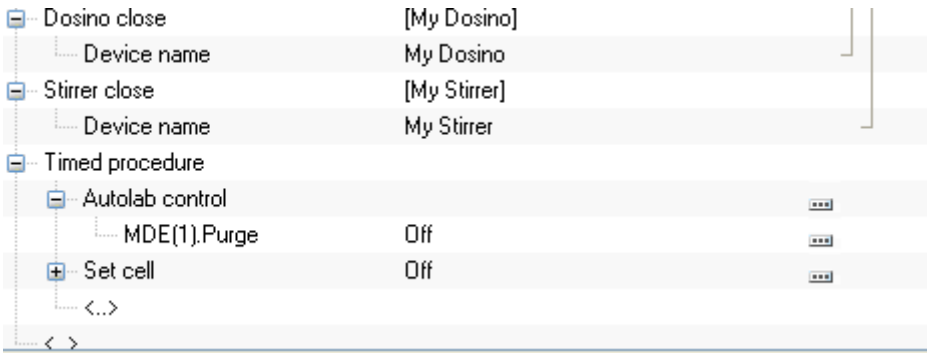

Figure 2.21: Closing Commands for the validation of Part B.

2.5 References

[1] J. H. Christie and R. A. Osteryoung, *J. Electroanal. Chem. Interfac. Electrochem.*,**1974**, *49*, 301.

[2] a) T. S. Mkwizu, Polarographic and potentiometric study of metal-ligand equlibria: instrumentation and investigations of sstems with non reversible electrode reactions, Masters Degree, Univeristy of the Witwatersrand, **2006**; b) I. Cukrowski, H. M. Marques, T. S. Mkwizu, P. P. Magampa and C. Serge, *Anal. Chim. Acta.*,**2007**, *590*, 203.

[3] Chance E, Vipin V, Wesley Z and H. Richard, *J. Lab. Auto.*,**2007**, *12*, 17.

[4] Metrohm-Autolab, NOVA, **2012**, (Utrecht, Netherlands)

Chapter 3: Experimental Procedures

3.1. Introduction

The experimental technique for the analysis of Bi^{3+} and its ability to complex with ligands was chosen to be polarography. The majority of metal-ligand studies in the past have utilized glass electrode potentiometry (GEP) in order to determine formation constants of the respective complexes in solution. Although GEP is a tried and tested technique, as was discussed in Chapter 1, Bi^{3+} hydrolyses at low pH and begins to precipitate at about pH 2, thus its coordination chemistry must be studied from pH below 2. GEP studies generally only start from pH 2 as it has been well documented that the formation constants determined by GEP using measurements below this pH have large errors. This is because only the measurement of the H^+ concentration in solution is utilized in these calculations. It is the concentration of H^+ due to the deprotonation of the ligand on complex formation that is important, but determining this value accurately in a solution below pH 2, where there is already be a large number of H^+ ions present from the strong acid background solution is impossible.

Polarography is also an ideal technique to use in these studies as low total metal ion concentrations can be used to postpone or suppress precipitation and a large ligand-to-metal ion concentration ratio, which is required for these measurements, also promotes complex formation at lower pH. When using polarography to determine stability constants, the formation of the Bi^{3+} hydroxide complexes, unfortunately, leads to an increased number of experiments and calculations that have to be done. These will be described in this chapter as well as in Chapter 4.

3.2. Glass Electrode Calibration

In order to calibrate the glass electrode, an acid-base titration was performed. Solutions of 0.1 M HNO_3 and 0.1 M KOH, were made by diluting the appropriate volumes of concentrated HNO_3 (65%, Merck) and KOH (45%, Sigma-Aldrich) and 0.4 M KNO_3 (Sigma-

Aldrich) was added to both solutions. The salt was added to maintain the ionic strength of solutions close to 0.5 M throughout the titration. It was important that the ionic strength of these solutions was kept constant since the concentration of H^+ (not its activity) was used in calculations, thus the activity coefficients need to remain constant throughout the experiment.

The KOH solution was standardized by dissolving ~0.5 g potassium hydrogen phthalate (Sigma-Aldrich), previously dried at 100 ^oC for at least two hours and then accurately weighed, in 5 mL of deionised water. The resulting solution was placed in a cell connected to the Metrohm Titrino Plus autotitrator. Nitrogen gas was bubbled through the solution so as to remove carbon dioxide and oxygen from the cell. The solution was purged while the potassium hydrogen phthalate was allowed to dissolve. The KOH solution was contained in a Metrohm dosing unit attached to the autotitrator and then allowed to titrate the potassium hydrogen phthalate solution while the pH was measured using a Metrohm Ecotrode glass electrode. The standardization of the KOH was repeated until a standard deviation less than 0.001 M was achieved. Once the KOH solution was standardized, it was then used to standardize the HNO_3 solution. An exact volume of 10.00 mL HNO_3 was placed into the reaction vessel and then titrated with KOH as before. The HNO_3 standardization was also repeated until a standard deviation less than 0.001 M was achieved.

The glass electrode used throughout this work was a Metrohm pH glass electrode (also termed Ecotrode), contains an incorporated 3 M KCl Ag/AgCl reference electrode. The glass electrode was calibrated by titration. Using a Metrohm Dosimat, 25.00 mL of HNO_3 was placed into a jacketed-cell connected to a waterbath and then allowed to reach 25.0 ± 0.1 ^oC (monitored using Metrohm thermocouple) while purging with N_2 gas. The automated glass electrode calibration procedure developed using Autolab NOVA software as described in detail in Section 2.3 was used. The programme allowed the addition of 40.00 mL of KOH in 0.500 mL increments to increase the pH. The potential difference at the glass electrode and the temperature were measured after each addition of 0.500 mL KOH. Enough KOH was added to allow the titration to surpass the

end point because the potential difference at the glass electrode was needed in both the acidic and basic regions for the calibration.

After standardization of the 0.1 M KOH and HNO_3 solutions, the concentrations were accurately known. Knowing the chemical equation to be:

$$HNO_3 + KOH \rightarrow KNO_3 + H_2O$$

the concentration of H^+ ions can then be calculated after each addition of 0.500 mL KOH. Therefore pH can be calculated after each addition of KOH. It is important to note that in this work the pH is calculated using the concentration of H^+ ions in solution, thus pH = -log $[H^+]$. The potential difference at the glass electrode obtained after each step of the titration was then plotted against calculated pH.

A procedure developed recently by Billing and Cukrowski[1] to calibrate the glass electrode in very acidic solutions by employing both linear and quadratic functions to fit the calibration graph was used. A linear function was fitted throughout all data points, and a quadratic function fitted through the acidic region so as to compensate for any slight curvature shown by glass electrodes in very acidic medium. The observed curvature is due to the diffusion junction potential at the reference electrode contained within the glass electrode. The acid error which occurs at low pH could also contribute to the slight curvature. This error is due to the large concentration of H^+ ions present which cause a saturation effect at the membrane of the glass electrode, however, since the lowest pH used in the majority of this study was 1, the acid error is not likely to be significant. When titrations were started in highly acidic solutions (pH ~0.3)[1] the deviation from linearity in the potential difference versus pH response is much greater than the deviation seen when started at pH 1, the pH which measurement commenced in this work. The higher the pH, the greater the decrease in $[H^+]$ and so the error due to diffusion junction potential decreases. Although not a standard practice, the quadratic equation was used so as to accurately represent the relationship between potential difference and pH even if the diffusion junction potential caused linearity to be compromised and hence minimize the error in pH calculations.

In order to calculate the pH values from measured potential values at the glass electrode during polarographic-pH titration experiments, the quadratic equation was used in very

acidic solutions and the straight line was used across the remainder of the pH range. The glass electrode calibration was also conducted before and after every polarographic-pH titration experiment in order to ensure the glass electrode remained in good working order and gave reproducible results.

3.3. Polarographic Studies

The use of polarography in the study of metal-ligand complexation was first described by Lingane.[2] Lingane derived the equation which is able to describe the extent of complexation as a function of the shift in wave potential. This method was developed for a ligand-metal system where a single complex species is formed to the virtual exclusion of all others over the entire ligand concentration working range. The equation was improved and extended by de Ford and Hume[3] so as to calculate formation constants of the metal-ligand system where several complexes are thought to form in a step-wise manner. A requirement for the validity of this equation is that the formation constants, must differ from one another to such an extent that each species has to predominate between fairly sharply defined limits of ligand concentration. More recently, Cukrowski[4] introduced a process whereby either ligand or pH titrations could be used and the restrictive conditions of having only a single species dominant in solution at a time no longer applied. In a pH titration, the ligand-to-metal concentration ratio is kept constant and the pH is increased by titrating the metal-ligand solution with a strong base (although under certain circumstances a strong ligand acid can be used). As the pH is increased, it promotes the complex formation reactions. In a ligand titration, the pH is kept constant and the ligand concentration is increased thereby promoting complex formation.

The equation used by Cukrowski[4] to determine formation constants relates the observed shift in the peak potential and a decrease in the peak height with a change in the concentration of the free metal ion in a solution. The equation is defined as:

$$\left\{E(M_{free}) - E(M_{comp})_{(i)}\right\} - \frac{RT}{nF}\ln\frac{I(M_{comp})_{(i)}}{I(M_{free})_{(i)}} = \frac{RT}{nF}\ln\frac{[M_T]_{(i)}}{[M_{free}]_{(i)}} \qquad (3.1)$$

where $E(M_{free})$ is the reduction potential of the free metal ion (without any complexed ligand) and $E(M_{comp})_{(i)}$ is the reduction potential of the complexed metal ion at a specific

pH or ligand concentration, depending on the type of titration done; [M_T] and [M_{free}] indicate the total and free metal ion concentrations at each step in the titration, respectively; $I(M_{comp})$ is the reduction current of the labile wave or peak recorded at each step; $I(M_{free})$ is the current observed from the reduction of the metal ion $M^{n+}(aq)$ at the pH value with the assumption that complexes of the metal ion were not formed. The term $\frac{RT}{nF}\ln\frac{I(M_{comp})_{(i)}}{I(M_{free})_{(i)}}$ is generally referred to as the correction factor and is also very close to zero in most cases.[2] This is true if the rate of diffusion of the complexed species is similar to that of uncomplexed hydrated species and if all species formed are labile. ΔE represents the difference between $E(M_{free})$ and $E(M_{comp})_{(i)}$, i.e. the shift in the half-wave or peak potential observed at each i^{th} pH value or ligand concentration to which the metal-ligand system was adjusted in the polarographic cell by titration with base or ligand solution, respectively. Thus the left-hand side of the equation 3.1 is thus called the corrected ΔE and is determined using the experimental data obtained from the polarographic titration experiment. In this work only pH titrations were used, the reason for which will become evident in later chapters. All further discussions will thus refer to pH titrations. In this case, the left-hand side of the equation plotted vs pH is called the experimental complex formation curve (ECFC) and the right-hand side of the equation plotted vs pH forms the calculated complex formation curve (CCFC)

The right-hand side of equation 3.1 is solved by employing mass balance equations of all possible species in solution. The mass balance equation for all species containing the metal ion is:

$$[M_T]_{(i)} = [M_{free}]_{(i)} + \sum_p \sum_q \sum_r p\, \beta_{M_pL_qH_r} [M_{free}]_{(i)}^{\,p} [L_{free}]_{(i)}^{\,q} [H_{free}]_{(i)}^{\,r} \quad (3.2)$$

Since the initial [M_T] added to the solution is known, $[M_T]_{(i)}$ is determined at each step in the titration by simply taking dilution into account. The [H_{free}] is determined from measuring the pH using the glass electrode and if r is a negative value it rather indicates [OH_{free}]. The [L_{free}] is determined from a second mass balance equation (equation 3.3) since the initial [L_T] is once again known and , $[L_T]_{(i)}$ is found by accounting for dilution.

$$[L_T]_{(i)} = \sum_K \beta_{H_kL} [H]_{(i)}^{\,k} [L_{free}]_{(i)} + \sum_p \sum_q \sum_r q\, \beta_{M_pL_qH_r} [M_{free}]_{(i)}^{\,p} [L_{free}]_{(i)}^{\,q} [H]_{(i)}^{\,r} \quad (3.3)$$

The concentrations of the free metal ion and the free ligand at each pH, as well as the stability constants, $\beta_{M_pL_qH_r}$, are refined simultaneously using a non-linear least squares refinement method. This is achieved by predicting the species present and giving initial estimates of their log β values such that the difference between the ECFC and the CCFC is minimised. In this refinement process, the stability constants for the metal-hydroxide complexes, the protonation constants for the ligand and the dissociation constant for water are all kept constant.

3.3.1 Polarographic-pH titrations: Experiments in the absence of ligand

This section describes the procedures used in the polarographic-pH titration of solutions containing the Bi^{3+} and Tl^{+} (as the witness ion) but no ligand. The results were used to obtain the free metal ion potential of bismuth ($E(Bi_{free})$) and thallium ($E(Tl_{free})$).

An exact volume of 25.00 mL 0.1 M HNO_3 (containing 0.4 M KNO_3) was added to a jacketed-cell. The cell was equipped with a dropping mercury electrode (DME), a 3 M KCl Ag/AgCl reference electrode inserted into a 0.5 M KNO_3 salt bridge, a platinum counter electrode, a glass electrode and a thermocouple (used to monitor the solution temperature throughout the experiment). All components used were supplied by Metrohm. After purging the solution with N_2 for 30 minutes, a background polarogram was recorded to ensure that there were no reduction processes occurring in the region of our analysis due to impurities.

Using a Hamilton syringe, 25.0 µL of a 0.0100 M $Bi(NO_3)_3$ (Merck) stock solution containing 1 M HNO_3 and 100.0 µL of 0.0100 M $TlNO_3$ (Sigma Aldrich) stock solution made up in 0.5 M HNO_3 were added to the reaction cell. The solution was purged again and polarograms were collected such that at least three overlapped so as to ensure accurate analysis of the reduction waves and that sufficient purging had taken place.

Using the NOVA method discussed in Chapter 2, Section 2.4, 0.1 M KOH (containing 0.4 M KNO_3) was added using a Dosino in 0.300 mL increments, until a final pH of 2.3 was reached in Part A, then KOH was added in increments of 0.025 mL until the end of the

titration in Part B. The addition of the KOH results in an increase of pH and polarograms were recorded only once enough KOH was added to cause an increase of about 0.1 pH units. The potential difference at the glass electrode was also accurately measured during the collection of the DC polarogram. Titrations were continued until a pH of 8 was reached so that an accurate value of $E(Tl_{free})$ could be calculated.

The parameters used in these polarographic-pH titration experiments are shown in Table A 1.1 in Appendix 1. The initial pause is the wait time before the experiment starts. It is important to allow all equipment to be properly initialized and for the computer to interface with the various components. The sample rate is how often the signals (in this case the potential difference at the glass electrode and the temperature) are measured. The sample rate is set at 2 seconds to allow for more stable measurements. The pH step indicates that a polarogram must be measured after each 0.1 pH unit change. Dose refers to the volume increment of base added by the Dosino. The polarographic parameters indicate how the DC polarogram was measured. The initial and final potential gives the potential range over which the DC polarogram is recorded. The step potential is the incremental change in applied potential (toward more negative values) at each new drop. The interval time is the mercury drop life. The stop conditions refer to the pH at which the titration must be terminated. It is impossible to change the pH by only 0.1 unit when adding 0.1 M hydroxide to solutions around pH 7 due to the very small buffer capacity of the solution in this region, so only approximate values that will cause termination of the experiment. In this work the Bi^{3+} precipitates as a Bi-hydroxy-nitrate species long before pH 8, however, the experiment was allowed to continue in order to obtain all Tl^{+} data which was used to calculate the free metal ion potential of thallium as accurately as possible.

3.3.2. Polarographic-pH titrations: Experiments in the presence of ligand

This section describes the procedures used in the polarographic-pH titration of solutions once again containing the Bi^{3+} and Tl^{+}, but in this case amino acid is added to the solution. These results were used together with that in section 3.3.1 to study bismuth-amino acid complexation.

The polarographic-pH titration experiment was run using the same parameters given in

except the stop condition was now set to pH 10 to ensure that there was always sufficient data to analyze where necessary. In these experiments, 25.00 mL of the HNO_3 solution was also added to a jacketed-cell containing the same components stated above. The metal ions (Bi^{3+} and Tl^{+}) were added and polarograms recorded as before. Ligand (accurately weighed to five decimal places) was then added to the cell and the system was purged. Three overlapping polarograms were collected with purging occurring between measurments to ensure no oxygen was present in the cell. Only then were the automated NOVA procedures initiated. The amino acids reported in this study will predominantly be Glutamic Acid, Histidine and Glutamine, however, Chapter 4 will show that other amino acids such as methionine and cysteine were also studied in order to demonstrate their complexing behavior with Bi^{3+}.

3.3.3 Fitting the polarograms

In order to determine the parameters from the recorded DC polarograms, the following equation was fitted to each polarogram:

$$f(x) = {I_d}\Big/\left(10^{\left(\frac{n\gamma\left(x - E_{1/2}\right)}{0.05916}\right)} + 1\right) + I_b \qquad (3.4)$$

where

$$I_b = a + bx + c^{dx} \qquad (3.5)$$

and I_d represents the diffusion limited current, I_b represents the background current, n represents the number of electrons transferred, $E_{1/2}$ represents the half-wave potentials for reduction of metal ions and γ represents the steepness of the wave. For a reversible electron transfer process, the γ value is equal to 1 and this implies that the rate of electron transfer is greater than the rate of mass transport and is described by Nernstian behavior. However, as described in previous work[5], a γ value for stability constant determination in the range of 0.9 - 1.0 was sufficient to indicate that the electron transfer process is fully reversible. A value between 0.9 - 0.5 indicates that the electron transfer process is quasi-reversible and a value less than 0.5 shows that the electron transfer process is irreversible.

The background current of the polarograms is described by equation 3.5 where the straight line terms refers to the capacitance current. The exponential term (c^{dx}) takes into account the exponential curvature of mercury oxidation (at the start of the Bi(III) reduction wave) and hydrogen reduction (at the end of the Tl(I) reduction wave in acidic solutions) Since the entire polarogram is too complicated to fit all at once (Figure 3.1), the data was split into two separate data sets, one containing the Bi^{3+} reduction data and the other the Tl^{+} data. Equation 3.2 was then fitted to each reduction wave separately.

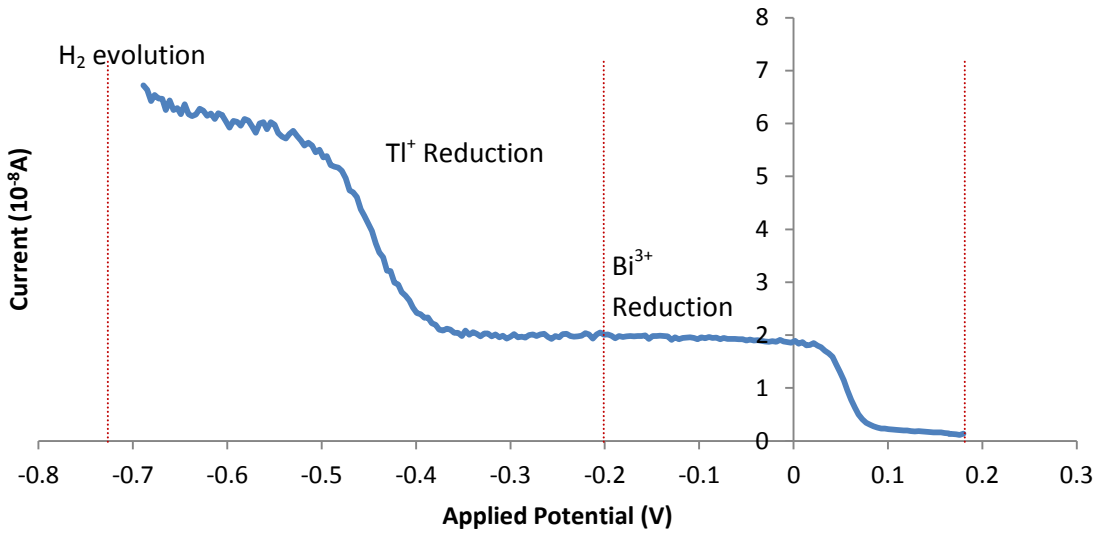

Figure 3.1: Typical DC polarogram showing the reduction of Bi^{3+} and Tl^{+} and H_2. [Bi^{3+}] = 9.95 x 10^{-6} M, [Tl^{+}] = 3.98 x 10^{-5} M, μ = 0.5 M, T = 25 °C

Since the reduction waves are fitted using a non-linear curve fitting programme, initial estimates of $E_{1/2}$, I_d, γ and background values were required. The estimates given are shown in Table A 1.2. in Appendix 1 and these values are then refined iteratively. Once all the parameters were found, the values for $E_{1/2}$, I_d and γ were all plotted against pH, for Bi^{3+} and Tl^{+}, respectively, and then analysed further.

3.3.4. Calculation of formation constants for Bi^{3+}-amino acid complexes

The 3D-CFC programme[6] was used to calculate the formation constant of the predicted solution species. This software essentially applies equation 3.1 to entered data. Initial parameters that need to be inputted into the software include the initial concentrations of total Bi^{3+} and ligand being studied and the total volume of the solution before any

KOH was added. Additionally the values for $E_{1/2}$ and I_d for free Bi^{3+} are required. The I_d values were obtained from the initial polarograms before ligand was added, but the process of determining $E(Bi_{free})$ is more complicated and will be discussed in Chapter 4. Data from the titration experiment that need to be entered are the $E_{1/2}$ values for Bi^{3+} reduction (that have been corrected for the diffusion junction potential, as will be explained in Chapter 4) with the corresponding I_d values, the pH of the solution in which each polarogram was collected and the volume of KOH for each corresponding pH. The hydrolysis constants for Bi^{3+} and the protonation constants for the ligand under study were also inputted into the 3D-CFC programme in order to take the competing reactions into account. Unfortunately the Bi^{3+}-nitrate complexes could not also be added as competing species due to restrictions of the software.

The method used to predict the type of species dominant in solution under a range of pH conditions was slope analysis[7] of the $E_{1/2}$ (corrected for E_j) vs pH. The extent of protonation of the ligands varies according to the pH of the solution. The pK_a values of a ligand indicates when two forms of the ligand differeing by only one proton, exist in equal amounts in solution (50% of each form of ligand). By finding the slopes of the plot of E_j corrected $E_{1/2}$ vs pH in the pH region where one form of ligand is dominant, it provides information about the type of metal-ligand species being reduced since the slope is given by:

$$slope = \frac{x\mathrm{H}^+ \times 60\ \mathrm{mV}}{n} \qquad (3.6)$$

where x is the number of H^+ ions that would react with the ligand to form the predominant species in solution. Also, 60 mV is the Nernstian slope (rounded off) for the a reversible process occurring at 25 ^oC and n is the number of electrons required for the reduction process of the metal ion.

Once the types of species in solution were predicted, these species are included in the 3D-CFC program and the log β values were estimated for those species. To improve the initial estimates the CCFC was calculated using these values and then compared to the ECFC. If the CCFC was too high above the ECFC, the log β value/s were decreased and if it was too far below, the formation constant/s would were increased. Once the CCFC was close

to overlapping with that of the ECFC, the values are refined to obtain a more accurate fit and to determine the standard deviation for the formation constant. Figure 3.2 gives an example of the ECFC and CCFC after the refinement process, illustrating that they should overlap throughout the pH range in order to be confident that the species predicted are correct and that their log β values are accurate.

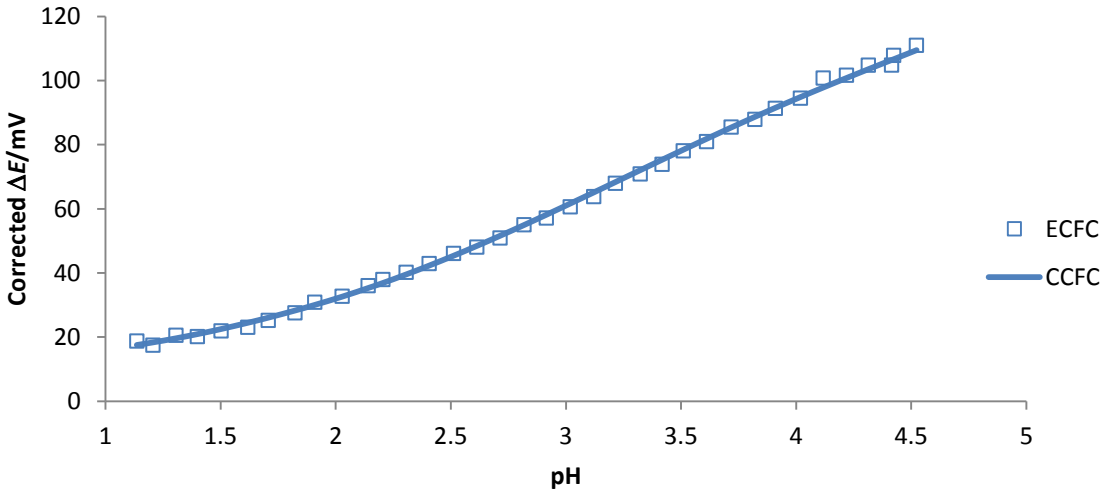

Figure 3.2: An example of an ECFC and a refined CCFC for a Bi^{3+}-amino acid system.

3.4. Investigating the bismuth precipitation product from a nitric acid solution

A 1 L 0.1 M HNO_3 solution was made and to it bismuth nitrate salt was added to it and dissolved such that $[Bi^{3+}] = 1 \times 10^{-2}$ M. The solution was then left to equilibrate for 3 hours. A pH electrode, calibrated using buffers, was used to monitor the pH of the solution. Concentrated KOH (11.5 M) was then added dropwise to the solution at a rate of 1 drop every 4 minutes while stirring. This was continued until precipitation occurred and then left to stand for 1 day. The precipitate was isolated using ACE 11.0 cm, 5 µm pore size filter paper and placed in a desiccator until all moisture was removed. The precipitate was then studied by Powder X-Ray Diffraction (PXRD) using a zero background holder. An experiment was also run where 1 L 0.1 M HNO_3 solution was made and both bismuth nitrate and glutamic acid (Glu) was added to it such that $[Bi^{3+}] = 1 \times 10^{-2}$ M and the ratio $[Glu]:[Bi^{3+}]= 1000$. Concentrated KOH was then added until precipitation occurred and the precipitate isolated and allowed to dry. The powder was then analysed using PXRD.

3.5. X-Ray Diffraction

The insoluble Bi^{3+} species which was indicated by a drop in I_d when polarography was employed proved a real obstacle in the full analysis of whether a Bi^{3+}- amino acid complex was forming. Additionally, the type of species which was precipitating was not fully known and only the previous literature studies by Olin[8], Bidleman[9] and Hataye[10] allowed an indication of the species present in solution. It was decided that a rudimentary exercise be performed in order to gain a better understanding of what type of Bi^{3+} species was precipitating. Powder x-ray diffraction (PXRD) was therefore employed in order to see if the species precipitating could be isolated and analysed.

PXRD involved targeting x-rays at the isolated precipitate sample and then the diffracted x-rays were measured. The K-alpha radiation is directed toward a detector once it has hit and diffracted off the specimen.[11] These x-rays, which are generated by an x-ray tube, are filtered to produce monochromatic radiation which is collimated and then directed toward the sample. The interaction of the incident rays with the powder produces a diffracted ray undergoing constructive interference when conditions satisfy Bragg's Law.

Bragg's Law is given as $n\lambda = 2d \sin\theta$[11] where λ is the wavelength of the x-ray, *d* is the spacing of the crystal layers (path difference), θ is the incident angle (the angle between incident ray and the scatter plane) and n is an integer. Subsequently, a spectrum in terms of intensity and 2θ are produced and the powder pattern can then be used to cross reference against other PXRD patterns of known structures within the ICSD.[11-12]

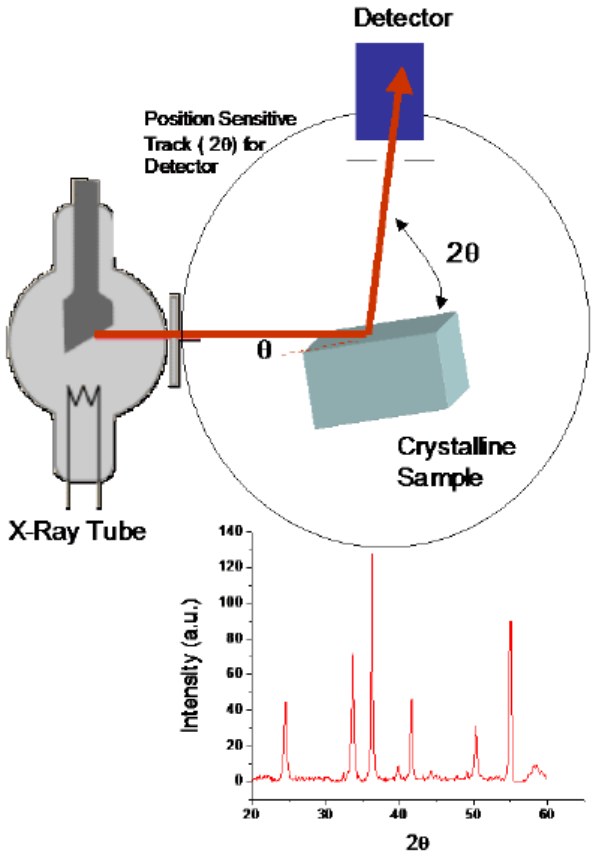

Figure 3.3: Schematic of the PXRD process whereby X-rays are emitted from an X-Ray Source and travel toward and reflect of a crystal/crystalline powder sample. The reflected X-rays are then detected and the structure of the complex must be calculated from the respective intensities and 2θ values which are present in the spectrum.[13]

The instrument to be used will be a Bruker D2 phaser diffractometer. The isolated precipitate was transferred to a pestle and mortar and ground until a fine powder was achieved. The powder was then placed onto a zero background stand and placed into the D2 diffractometer (instrument settings are shown in Appendix 1). PXRD (demonstrated in the schematic in Figure 3.3) is a useful technique for this study because once the XRD component of analysis has been completed, it can readily be compared with other PXRD

patterns or a suitable programme, such as Mercury, can be used to convert single crystal XRD data to predict the theoretical PXRD pattern. In our work we aim to examine the Bi^{3+}-hydroxy-nitrate precipitates and also investigate whether in the presence of ligand it is simply the Bi^{3+}-hydroxy-nitrate species that forms, or whether an amino acid is still bound to Bi^{3+} in the precipitate.

3.6. References

[1] C. Billing and I. Cukrowski, *S. Afr. J. Chem.*,**2009**, *62*, 168.

[2] J. J. Lingane, *Chem. Rev.*,**1941**, *29*, 1.

[3] D. Deford and D. N. Hume, *J. Am. Chem. Soc.*,**1951**, *73*, 5321.

[4] I. Cukrowski, *Anal. Chim. Acta.*,**1996**, *336*, 23.

[5] I. Cukrowski, H. M. Marques, T. S. Mkwizu, P. P. Magampa and C. Serge, *Anal. Chim. Acta.*,**2007**, *590*, 203.

[6] P. Franklyn and I. Cukrowski, 3D-CFC software, University of the Witwatersrand, **2003**, *Windows Version 1.2*, (unpublished)

[7] I. Cukrowski, *Electroanal.*,**1997**, *9*, 699.

[8] A. Olin, *Acta. Chem. Scand.*,**1957**, *11*, 1445.

[9] T. F. Bidleman, *Anal. Chim. Acta.*,**1971**, *56*, 221.

[10] I. Hataye, H. Suganuma, Ikegami H. and T. Kuchiki, *Bull. Chem. Soc. Japan*,**1982**, *55*, 1475.

[11] G. I. Analysis in *Single Crystal X-Ray Diffraction*, *2012* Science Education and Resource Centre, Montana State Univeristy, **2012**.

[12] A. Belsky, M. Hellenbrandt, V. L. Karen and P. Luksch, *Acta. Cryst.*,**2002**, *B58*, 364.

[13] C. Morris, B. Sieve and H. Bullen, *An Introduction to X-Ray Diffraction*, Highland Heights, KY 41099.

Chapter 4: Initial Bi^{3+} complexation studies

4.1. Introduction

The study of Bi^{3+} complexation with amino acids using polarography is not a technique which has been commonly used. Previous studies, as shown in Chapter 1, have utilized potentiometric studies in order to monitor complex formation. To monitor the success of our polarographic pH titrations, an initial analysis was completed. Studies by Lingane[1] and furthermore by Cukrowski[2] have shown that the successful complexation of a metal ion to a ligand, studied using polarography, will cause a shift in $E_{1/2}$. The aim of this Chapter is to show that the pH-polarographic studies completed in our study illustrate that complexation between Bi^{3+} and the respective amino acid ligand is actually occurring.

As described in Chapter 1 and Chapter 3, the calibration of the glass electrode used in this work was vital for the robustness of the data collected. Due to Bi^{3+} being largely insoluble in nitrate solutions above pH ~2, the initial work without ligand in solution took place in the pH range of 1 – 2. The calibration of the glass electrode was completed and its results were used to determine the worthiness of the glass electrode during the polarographic-pH titrations. This chapter will also aim to show how the determination of E_j was accomplished using Tl^+ data and subsequently determining the E_j correction on Bi^{3+}. Previous work[2a, 3] have shown the optimal conditions in terms of [L]:[M] for studies using polarography, however, during this work for the [L]:[M] conditions needed to be reassessed for amino acid ligands reacting with Bi^{3+}. Evidence presented in this chapter will show that conditions which proved fruitful in other studies, could not be employed in this study due to the complicated chemistry associated with Bi^{3+}.

4.2. Glass Electrode Calibration and determination of pH values.

The glass electrode calibrations were conducted in order to determine an accurate relationship between pH and voltage measured at the glass electrode. Figure 4.1 shows

a typical calibration plot of the measured potential difference at the glass electrode vs calculated pH. In this case the linear trendline fitted through all the data points which gave a slope of 59.101 mV which is close to the Nernstian slope at 25 ^{o}C. Although the glass electrode is not an ideal sensor, the calibration should be close to the theoretical slope, thus indicating that the glass electrode was in good working condition. Any outliers close to the end point region were removed from the calibration plot as larger errors could be expected in these values (due to large changes in the voltage occurring on addition of the base and also small errors in the standardized concentrations of the acid and base solutions are emphasized in this region).

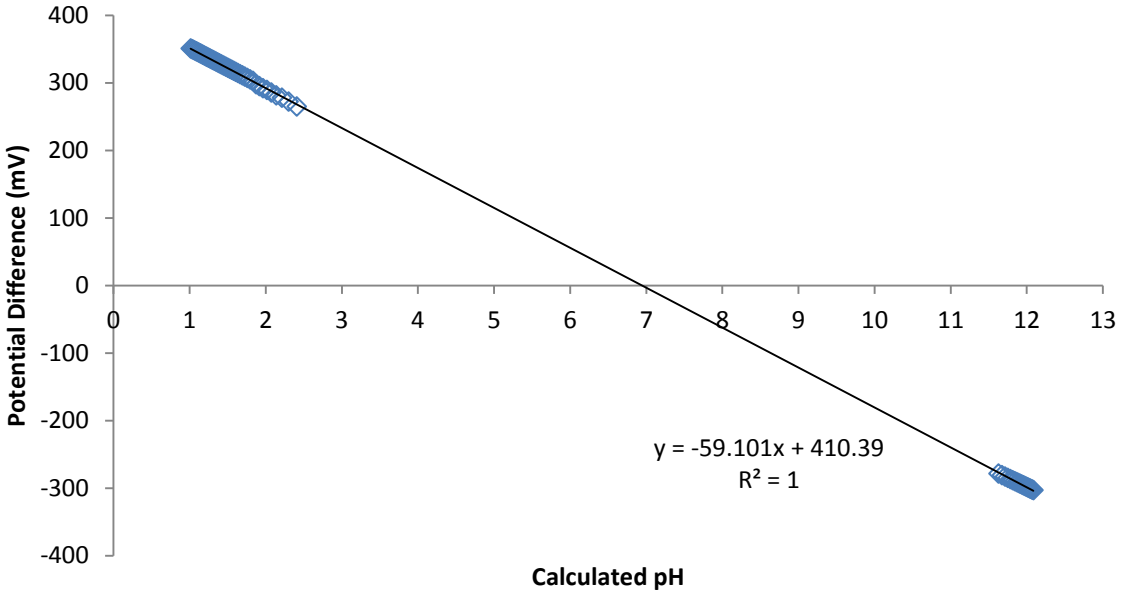

Figure 4.1: Potential difference at the glass electrode vs calculated pH for 0.1 M HNO_3 solution titrated with 0.1 M KOH solution (both in 0.4 M KNO_3) at 25.0 ^{o}C.

In order to fully compensate for the diffusion junction potential error at the lowest pH range, a quadratic function was also fitted to the data in the acidic region to establish the deviation from linearity, as described by Billing and Cukrowski[4]. **Error! Reference source not found.** shows the calibration curve in the very acidic region only. This shows that minimal deviations were observed in calibrations from pH 1 (work done by Billing and Cukrowski[4] started from pH 0.3 where more significant deviations were found). Even so, the quadratic function was always fitted to establish the extent of deviation, if any.

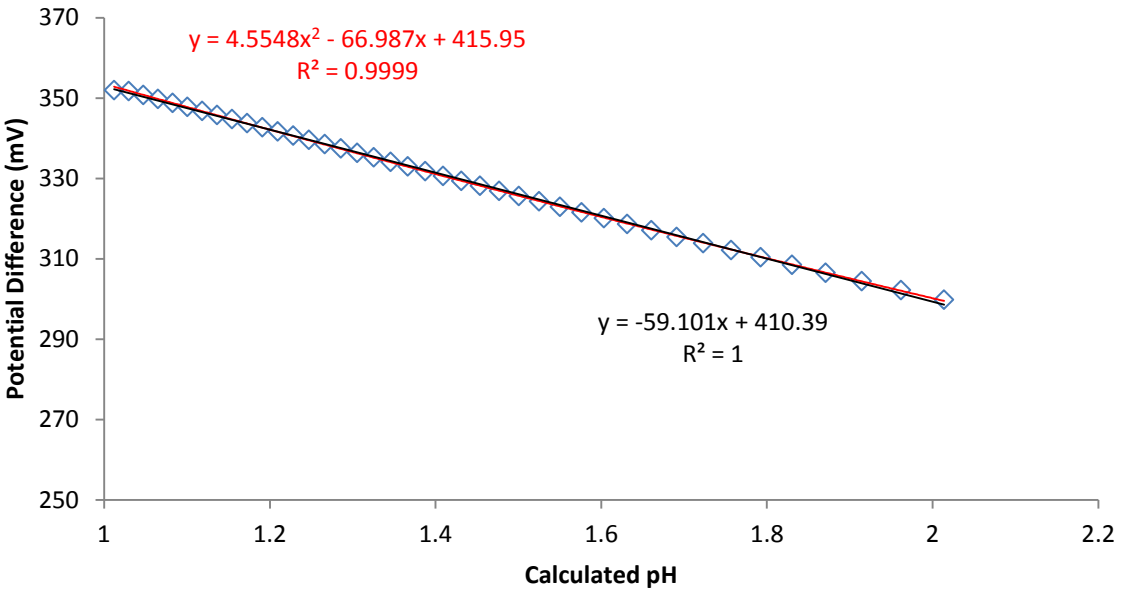

Figure 4.2: Glass electrode calibration curve in pH range 1 - 2 showing both the linear trendline (black) and the quadratic trendline (red) fitted.

The pH of the solution at each step in the polarographic-pH titration was calculated using the potential difference measured by the glass electrode and the calibration curves that were determined before and after each experiment. The pH values were taken from the quadratic curve only at the at the lowest pH values if the function was below the linear curve, and then subsequently calculated using the linear function for the remainder of the pH range. The results were only considered acceptable if the standard deviation between the calculated pH values using the before and after calibrations was less than 0.002 units. The average pH values from the two calibrations were then used.

A suggestion to test the condition of the glass electrode was given by Billing and Cukrowski[4] which gives guidelines to limits of acceptable slopes for the data fitted in either the acidic or basic regions. These guideline are shown in Table 4.1. Although the tests were applied to titrations using 0.5 M acid and base solutions,[4] it was always checked that the calibrations for this work fell in the suggested limits.

Table 4.1: Acceptable slope ranges for the calibration of glass electrode as described by Billing and Cukrowski.[4]

pH range	Acceptable slope range or difference/mV
Basic Region	
(1) 12.2-12.8	56-60
(2) 12.2-13.0	55-60
Δslope: (2)-(1)	<3
Acidic Region	
(3) 0.3-1.5	57-60
(4) 0.6-1.5	57-60
Δslope (4)-(3)	<1.0
(Acidic -Basic) Region	
Δslope: (4)-(1)	<1.5

4.3. Calculation of the diffusion junction potential, E_j

To quantify the diffusion junction potential (E_j) as a function of pH, the half-wave potential data for Tl^+ reduction ($E_{1/2}(Tl)$) was used. Figure 4.3 shows a graph of the $E_{1/2}(Tl)$ plotted against the calculated pH which shows that above about pH 2, the $E_{1/2}$ values begin to plateau and reach a somewhat stable value. This corresponds the free metal ion potential of thallium ($E(Tl_{Free})$) and is calculated by averaging these values. Deviations from $E(Tl_{Free})$ below pH 2 are due to the diffusion junction potential and are greater at lower pH. Thus below pH 2, the dependence of E_j on pH can be found by subtracting the $E_{1/2}(Tl)$ values from $E(Tl_{Free})$ (see Figure 4.34). In order to smooth the E_j vs pH data a quadratic function was fitted and used to calculate the E_j at a given pH.

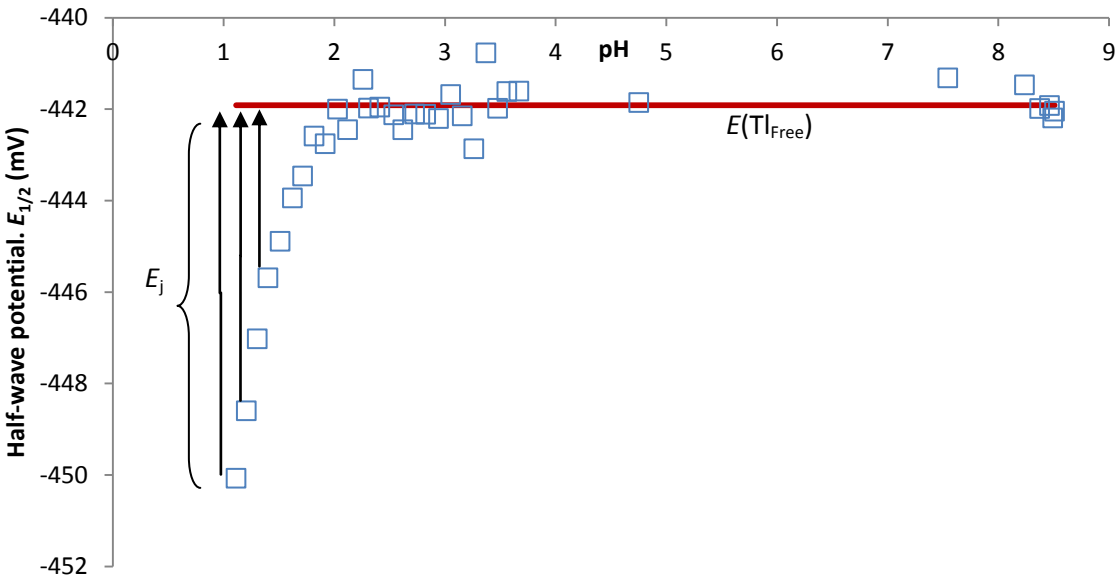

Figure 4.3: Half-wave potentials of Tl^+ vs pH showing the determination of E_j and $E(Tl_{Free})$. ($[Tl^+] = 1 \times 10^{-5}$ M).

The data presented in Figure 4.3 and 4.4 was obtained from an experiment that omitted the addition of ligand. However, Tl^+ was chosen to monitor E_j due to its general inability to form complexes with ligands especially in acidic solutions, so even if ligand was added to the solution, the plot produced should be very similar. Therefore Tl^+ was always added in all experiment - to solutions containing ligand and to solutions which did not contain ligand. This allowed for the determination of E_j in each experiment, under the specific cell conditions and was deemed this the most accurate method for the determination of E_j. To correct for the shift in $E_{1/2}$ for the reduction of Bi^{3+} due to E_j, the calculated E_j at each pH was added to the corresponding $E_{1/2}(Bi^{3+})$ value.

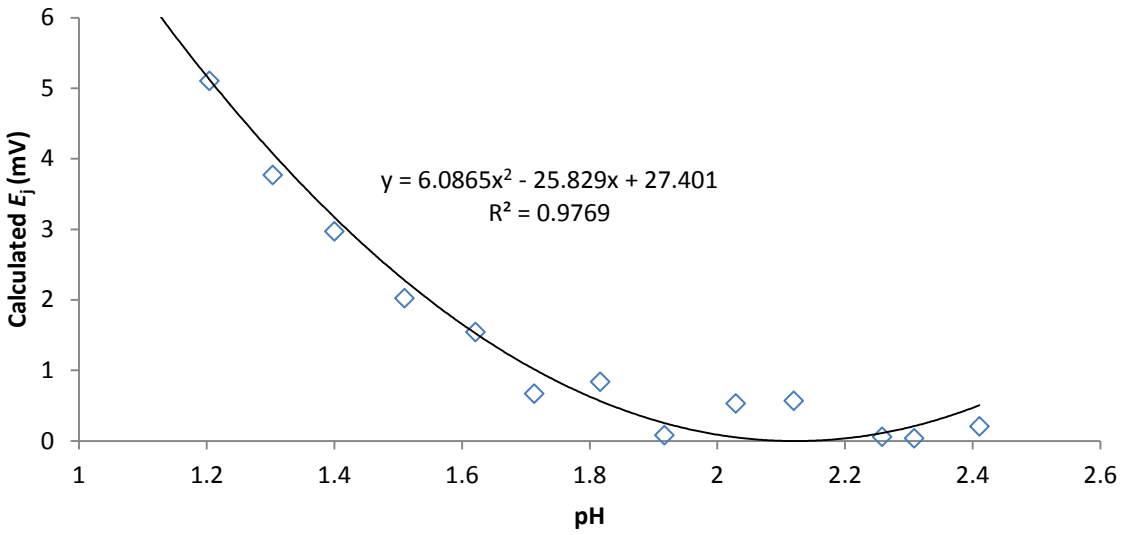

Figure 4.4: Calculated E_j vs pH for Tl^+ from a polarographic-pH titration.

4.4. Precipitation of Bi^{3+}-hydroxy nitrate species

Previous studies initially by Swinehart and Garrett[5] and Kragten *et al.*[6] showed that Bi^{3+} precipitates as a bismuth-oxy-nitrate species at pH ~2. In our work it was important that the point of precipitation was found because once out of solution information on complexation could no longer be obtained. One of the most useful indicators of when precipitation occured was the diffusion limited current (I_d). Figure 4.5 shows the I_d of Bi^{3+} vs pH plot when no ligand was added to the solution. Since current is directly proportional to the concentration of the solution species, the initial drop in current signified the dilution of the Bi^{3+} species as KOH was added to increase the pH. The sharp drop in current at a pH ~2.6 indicates precipitation as the current rapidly decreased to zero thereafter. Since experiments were started at pH ~1, there was only a very small range in which analyses could be done due to precipitation occurring at pH ~2.6 in the absence of ligand.

At the low concentrations of Bi^{3+} used (1 $x10^{-5}$M) it is not clear whether the precipitate formed exists as the mononuclear $BiONO_3$ (or $Bi(OH)_2NO_3$) species as suggested by Swinehart and Garrett[5] and Kragten *et al.*[6] or whether it is a hexanuclear type species as was found by Lazerini ($Bi_6O_4(OH)_4(NO_3)_6$ and $Bi_6O_5(OH)_3(NO_3)_5$).[7]

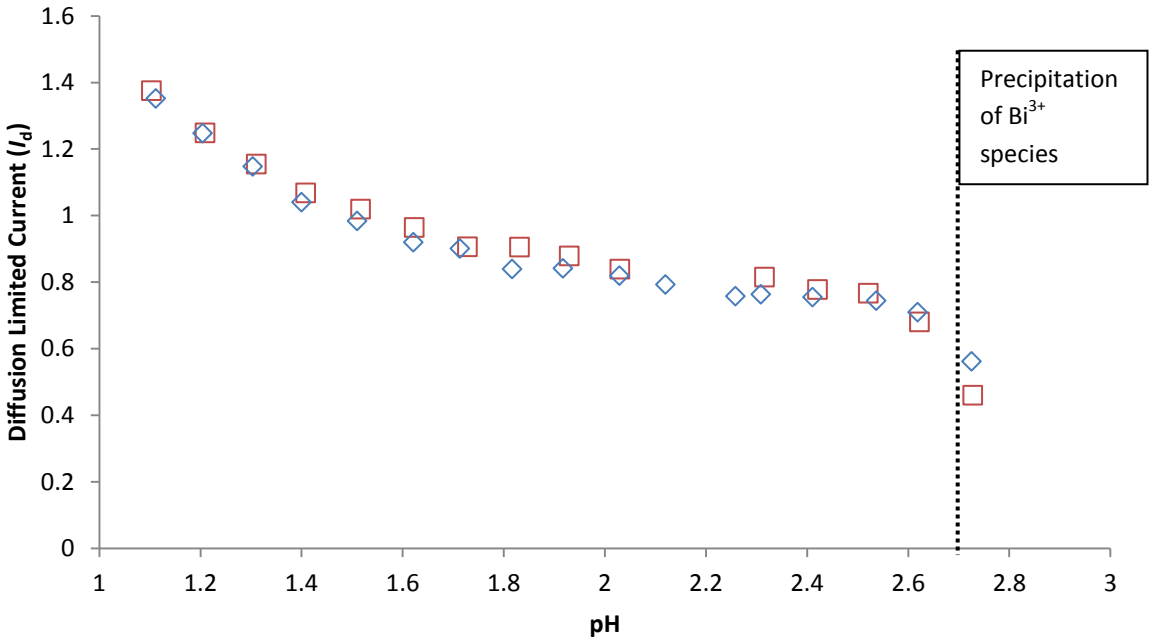

Figure 4.5: I_d values for Bi^{3+} vs pH for titrations with no ligand added showing dilution and then precipitation at pH ~2.6. $[Bi^{3+}] = 1 \times 10^{-5}$ M, μ= 0.5 M NO_3^-.

4.5. Determination of the free Bi^{3+} potential, $E(Bi_{free})$

As described in Chapter 1, Bi^{3+} readily forms nitrate and hydroxide complexes under acidic conditions. This presented a problem as $E(Bi_{free})$ must be determined for the calculation of formation constants as indicated in Equation 3.1. $E(Bi_{free})$ refers to the reduction potential of the free or uncomplexed Bi^{3+}, although in aqueous solutions it refers to the aqua form of Bi^{3+}. Since Bi^{3+} is never uncomplexed (it does not only exist as the aqua ion) in solution $E(Bi_{free})$ cannot be measured. Instead, it was calculated by taking into account the shifts in $E_{1/2}$ due to the formation of these bismuth nitrate and bismuth hydroxide complexes (as well as shifts due to E_j where needed).

In order to compute the shifts in half-wave potential due to Bi^{3+} nitrate and Bi^{3+} hydroxide complexation, the 3D-CFC programme[8] was utilized and the log β values shown in Table 4.2 and Table 4.3, respectively, were entered in the software. The Bi^{3+} hydroxide log β values were initially given for 0.1 M ionic strength,[9] but they were recalculated for 0.5 M ionic strength.[3b] The value for $E(Bi_{free})$ could only be calculated for experiments where no

ligand (in our case amino acid) was added because additional shifts in $E_{1/2}$(Bi) could not be accounted for as the formation constants are unknown (these were to be determined).

Table 4.2: Log β values for hydrolysis of Bi^{3+} in solution at 25 °C, μ = 0.5 M.[3b]

Species	**Log β**
$Bi(OH)^{2+}$	12.42
$Bi(OH)_2^{+}$	23.2
$Bi(OH)_3$	31.88
$Bi(OH)_4^{-}$	32.98
$Bi_6(OH)_{12}^{6+}$	162.78
$Bi_9(OH)_{20}^{7+}$	266.92
$Bi_9(OH)_{21}^{6+}$	276.76
$Bi_9(OH)_{22}^{5+}$	287.3

Table 4.3: Log β values for the formation of Bi^{3+} nitrate species at 25 °C.[9]

Species	**Log β**	**μ /M**
$Bi(NO_3)^{2+}$	0.72	0.5
$Bi(NO_3)_2^{+}$	0.94	0.5
$Bi(NO_3)_3$	0.7	1
$Bi(NO_3)_4^{-}$	0.6	2

Figure 4.5 shows the species distribution diagram plotted using the log β values in Table 4.2 and Table 4.3 and using the initial concentration conditions in our experiments. This shows that the Bi^{3+} nitrate species are present in solution till pH ~3 and are dominant in solution up till pH ~2. The $Bi(OH)^{2+}$ species starts forming at pH 0 already followed by $Bi(OH)_2^{+}$ just past pH 1. These were the only two hydroxide complexes formed before precipitation was observed.

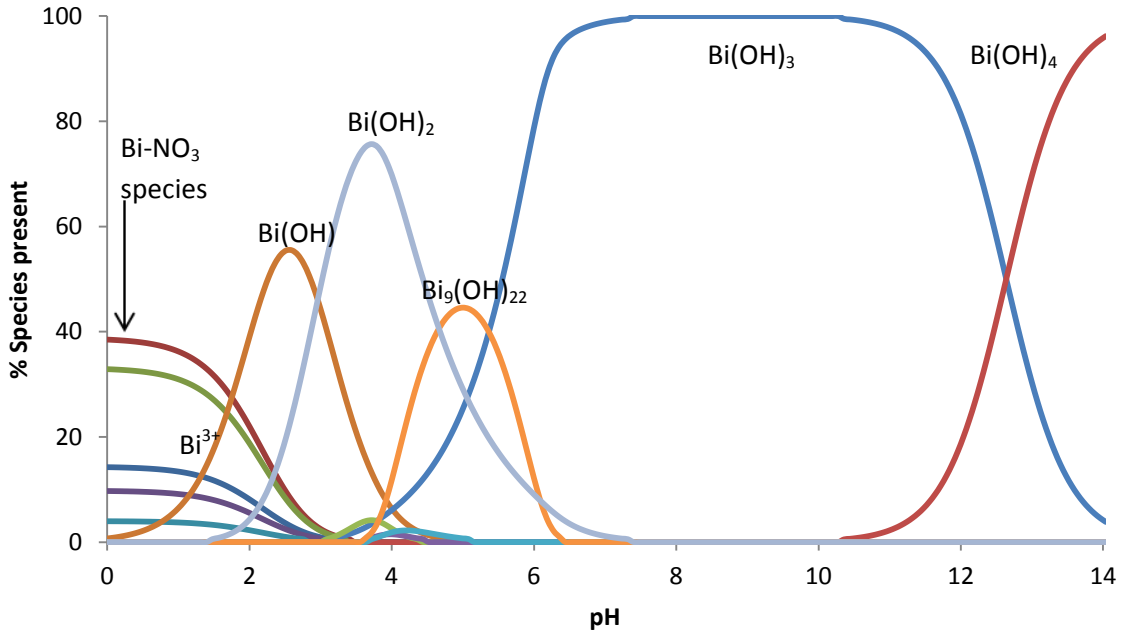

Figure 4.6: Species distribution diagram of Bi^{3+} nitrate and hydroxide species for [Bi^{3+}] = 1 x 10^{-5} M and [NO_3^-] = 0.5 M at 25 °C.

At each pH, where experimental $E_{1/2}$(Bi) values were obtained, the concentrations of total Bi^{3+} and NO_3^- were calculated by accounting for dilution due to the addition of the hydroxide solution. The expected potential shifts due to the formation of all Bi^{3+} nitrate and Bi^{3+} hydroxide species formed, as well as the percentage of the various species in solution, were then determined at each pH under the experimental conditions of the solution at that point using the 3D-CFC software.[3b]

In order to calculate the shift at each pH due to hydrolysis only ($\Delta E(\mathrm{OH})_{pH}$), the following equation was used:

$$\Delta E(\mathrm{OH})_{pH} - \frac{RT}{nF}\ln\frac{i(M_{comp})_{pH}}{i(M_{free})_{pH}} = \frac{RT}{nF}\ln\frac{[M_T]_{pH}}{[M_{free}]_{pH}} \qquad (4.1)$$

where the terms are the same as those seen in Equation 3.1. Since no polynuclear species are formed at the low Bi^{3+} concentration used, it was assumed that the rate of diffusion of the free metal ion (or more correctly the hydrated metal ion) and that of the hydroxide complexes is the same and that all hydroxide species were fully labile. Therefore $i(M_{comp})_{pH} = i(M_{free})_{pH}$ and the equation simplifies to:

$$\Delta E(\mathrm{OH})_{pH} = \frac{RT}{nF}\ln\frac{[M_T]_{pH}}{[M_{free}]_{pH}} \qquad (4.2)$$

$[M_T]$ at each pH was determined by accounting for dilution since the initial concentration added was known. $[M_{free}]$ was calculated using the percentage of hydroxide species present in solution at a particular pH as determined from the 3D-CFC software. This was completed by taking the known $[Bi^{3+}]$ and using the new volume amount present in the cell after the additionof enough KOH to change the pH by ~0.1 units.

Figure 4.7 shows the experimentally determined $E_{1/2}$ values (indicated by Δ), where only data up to the point of precipitation was used. The E_J values at each pH, as established from the Tl^+ data in the same experiment, were then added to the experimental $E_{1/2}(Bi^{3+})$ (indicated by ○). Thereafter, there was still a clear negative shift in the $E_{1/2}$ values, which was expected due to more Bi^{3+} hydroxide species being formed with increasing pH.

Error! Reference source not found. shows that both Bi^{3+} nitrate and Bi^{3+} hydroxide complexes are present in solution between pH 1 and 2.6 (the pH region in which $E_{1/2}(Bi^{3+})$ data was obtained) thus shifts in $E_{1/2}$ due to this complexation must be taken into account in order to obtain the true $E(Bi_{free})$ value. Therefore the shifts in potential due to the formation of all Bi^{3+} nitrate and hydroxide species, as determined using the 3D-CFC software, were then added to the E_j corrected $E_{1/2}$ values (indicated by □ in Figure 4.7). The average of these values was calculated and corresponds to the true $E(Bi_{free})$ value (called $E(Bi_{free})$). Additionally the shifts in potential due to the formation of the Bi^{3+} hydroxides only, calculated as described, were also added to the E_j corrected $E_{1/2}$ values (indicated by ◇ in Figure 4.7). The average of these values was also calculated and corresponds to a conditional $E(Bi_{free})$ value (called $E(Bi_{free})_{OH}$), which only applies to solutions containing 0.5 M nitrate. The $E(Bi_{free})_{OH}$ value is only useful in the region below pH ~2 where the Bi^{3+} nitrates are dominant in solution. Above pH 2 the values indicated by ◇ in Figure 4.7 increase as the concentration of Bi^{3+} nitrates in solution rapidly decrease. By pH 3, where the concentration of Bi^{3+} nitrates is insignificant, the values for ◇ and □ should intersect. Unfortunately precipitation occurs before this.

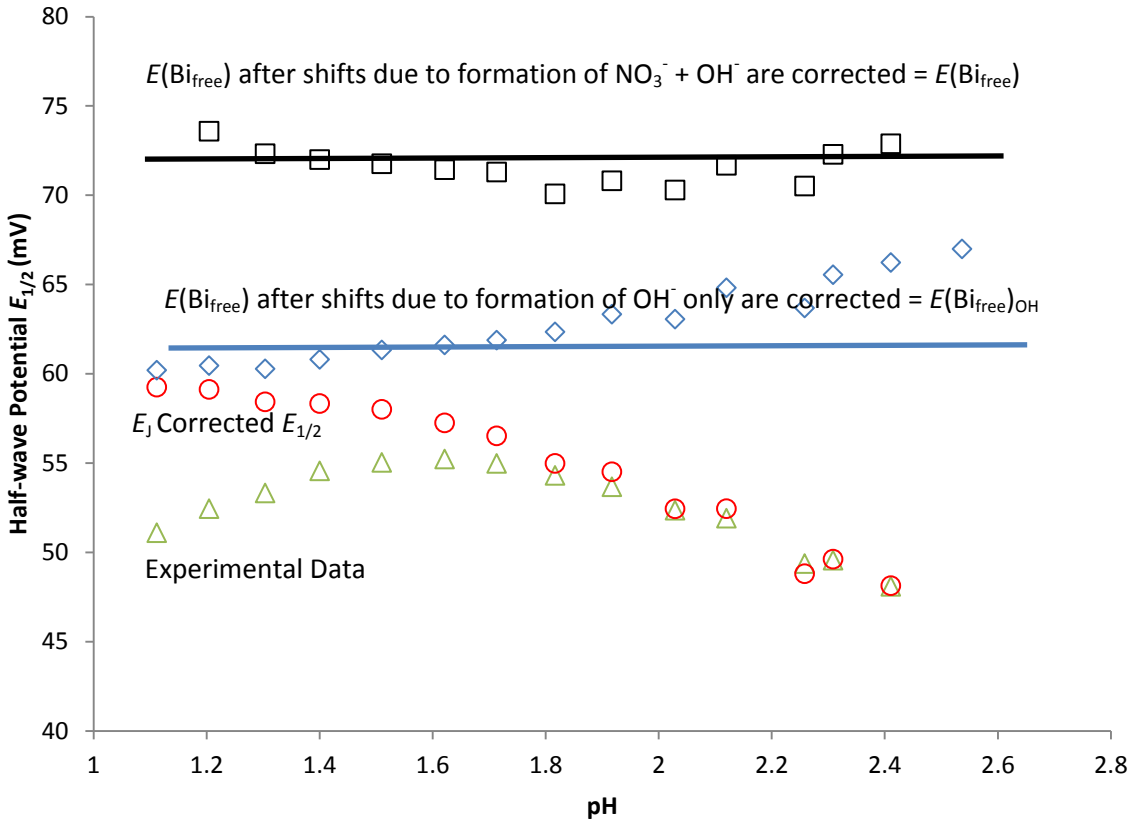

Figure 4.7: $E_{1/2}$ values of Bi^{3+} vs pH showing E_J corrections, as well as corrections for shifts due to formation of Bi^{3+} nitrate and hydroxide species or just Bi^{3+} hydroxide species. [Bi^{3+}] = 1 x 10^{-5} M and μ = 0.5 M.

The reason for finding the two types of $E(Bi_{free})$ values are calculated, $E(Bi_{free})_{OH}$ and $E(Bi_{free})$. Ideally the true $E(Bi_{free})$ value would be the best to use when determining formation constants, however, limitations in the 3D-CFC software prevented the addition of data due to Bi^{3+} nitrate formation together with that for the ligand and hydroxide. Only information about hydrolysis can be inputted while the formation constants for the Bi^{3+} ligand species are determined. The use of the two types of $E(Bi_{free})$ values will be discussed in Chapter 5.

Table 4.4 shows the $E(Bi_{free})$ and $E(Bi_{free})_{OH}$ values obtained for four different experiments. The average values were 72.05 ± 0.39 mV for $E(Bi_{free})$ and 63.02 ± 0.23 mV for $E(Bi_{free})_{OH}$. The difference of approximately 9 mV is due to the larger potential shift once Bi^{3+} nitrate species are accounted for. It has been shown that the $E(Tl_{free})$ and $E(Bi_{free})$ values may vary between experiments, however, the difference between these values $\Delta E(M_{free})$

remains constant and so it was very useful in Bi-ligand studies.[3b] The differences were calculated as follows:

$$\Delta E(M_{free}) = E(Tl_{free}) \text{ and } E(Bi_{free}) \quad (4.3)$$

$$\Delta E(M_{free})_{OH} = E(Tl_{free}) \text{ and } E(Bi_{free})_{OH} \quad (4.4)$$

These values as well as the average values are also given in Table 4.4.

Table 4.4: The $E(M_{free})$ values for Bi^{3+} and Tl^{+}, as well as the $\Delta E(M_{free})$ values.

Exp.	$E(Tl_{free})$ /mV	$E(Bi_{free})$ /mV	$\Delta E(M_{free})$ /mV	$E(Bi_{free})_{OH}$ /mV	$\Delta E(M_{free})_{OH}$ /mV
1	-442.75	72.22	514.96	62.83	505.58
2	-442.55	71.87	514.42	63.32	505.88
3	-442.67	72.50	515.17	63.10	505.77
4	-441.92	71.61	513.53	62.84	504.76
		Average	514.5	**Average**	505.5
		S.D.	0.7	**S.D.**	0.5
		RSD	0.14	**RSD**	0.10

In order to determine the $E(Bi_{free})$ value in an experiment where the amino acid ligand is added, the Tl^{+} potential data from that experiment was used to firstly determine $E(Tl_{free})$. Then, applying either equation 4.3 or 4.4 and using the average $\Delta E(M_{free})$ or $\Delta E(M_{free})_{OH}$ values, respectively, the value of $E(Bi_{free})$ or $E(Bi_{free})_{OH}$ can be determined for the ligand experiment, respectively. With a precise study as to how the metal ions (in the absence of ligand) behave during the polarographic-pH titration, an important link between Bi^{3+} and Tl^{+} reduction potentials has been established, as well as having a mechanism by which to determine $E(Bi_{free})$, which was found in terms of the true $E(Bi_{free})$ and the conditional $E(Bi_{free})_{OH}$.[10]

4.6. Initial Bi^{3+}-amino acid complexation studies

In previous complexation studies using polarography[2a, b, 11] it was found that [ligand]:[metal] used ranged from 10 to 100 for ligand titrations and from approximately 50-200 for pH titrations. Using polarographic-pH titration studies, many new complexes and their respective log β were able to be found, illustrating its success in monitoring

metal-ligand complexation. It was thus decided to conduct amino acid complexation studies using the conditions similar to those used in previous metal-ligand studies.

Therefore [ligand]:[metal] was set at about 100 with the initial $[Bi^{3+}] = 1 \times 10^{-5}$M. In these initial experiments the background solution consisted of 0.5 M HNO_3 and the titrant was 0.5 M KOH. It was later decided that since no complexation occurred at the lower pH range, to rather start in 0.1 M HNO_3 solutions where 0.4 M KNO_3 could be added to control the ionic strength better. The experimental parameters used were those set out in Chapter 3, section 3.3. The amino acids considered were glycine (Gly), methionine (Met), glutamic acid (Glu), cysteine (Cys) and glutamine (Gln).

As described in section 4.3, the diffusion limited current is an important indicator as to when precipitation occurs. Figure 4.8 shows the I_d vs pH plot for several amino acids when [ligand]:[metal] $\approx$ 100, and indicates that precipitation occurs around pH 2. It is in this pH range that precipitation was detected when no ligand was added to the solution, implying that complexation did not take place with the amino acids and the precipitate formed was most likely a Bi^{3+}-hydroxy nitrate species. It is expected that complex formation would be indicated by increased solubility of the Bi^{3+} ion and precipitation occurring at a higher pH.

It should be noted that the initial experiments with the various amino acid were conducted using on the older Labview system described in Chapter 2, except for the initial Gln studies which were conducted using the new NOVA system. The values of I_d for the Gln system were thus slightly different to that for the other amino acids shown in Figure 4.8. Also, precipitation occurred at slightly higher pH since the titration was done a bit faster using the NOVA system (as was also observed when no ligand was added to the solution). This kinetic effect was observed previously by Billing.[2a, b, 11]

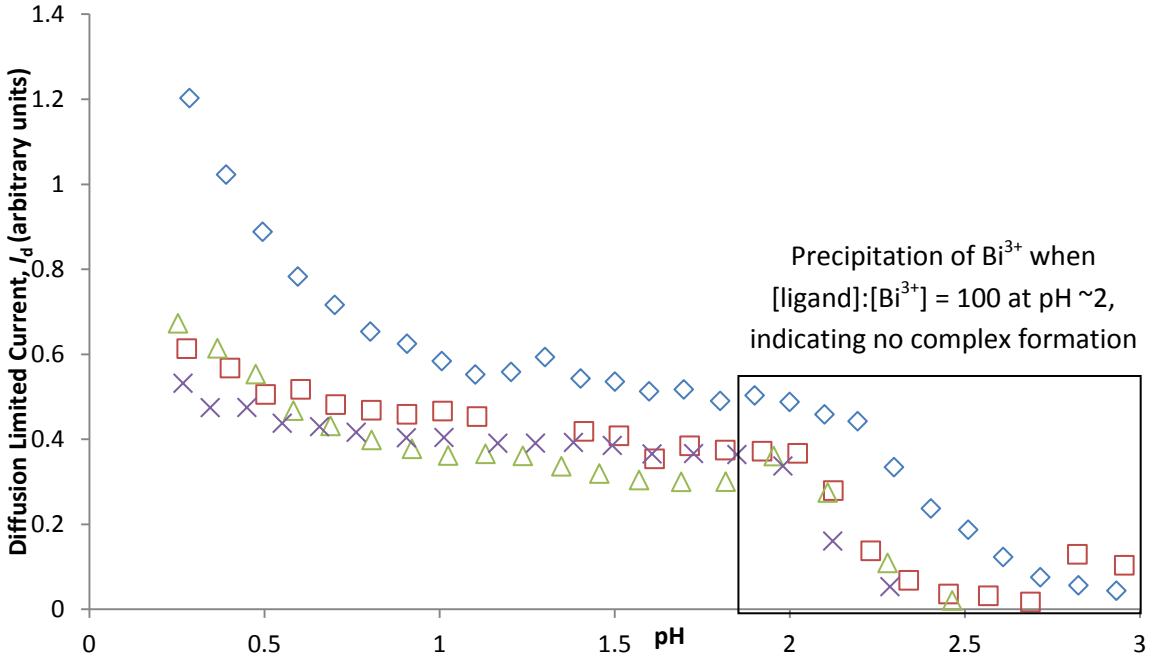

Figure 4.8: Diffusion limited current vs pH for (×) Glutamic Acid, (☐) Glycine, (Δ) Methionine and (◇)Glutamine at [ligand]:[metal] = 100. [Bi^{3+}] = 1 x 10^{-5} M.

Figure 4.9 illustrates the E_j corrected $E_{1/2}$ values for Bi^{3+} vs pH plot for the various amino acids initially studied. Also plotted for convenience is the $E_{1/2}$ for an experiment run without any amino acid present. Even though the experiment without any ligand (∗) began at a higher pH of 1 compared to the initial studies with amino acids, the $E_{1/2}$ values were similar in all cases, thereby indicating that no complexation was occurring between the amino acids and Bi^{3+}, and that any potential shifts occurring were comparable to those for Bi^{3+} nitrate and hydroxide complexation. The data from the experiment including Gln was a bit noisy, but since no conclusive complex formation was observed this experiment was not repeated.

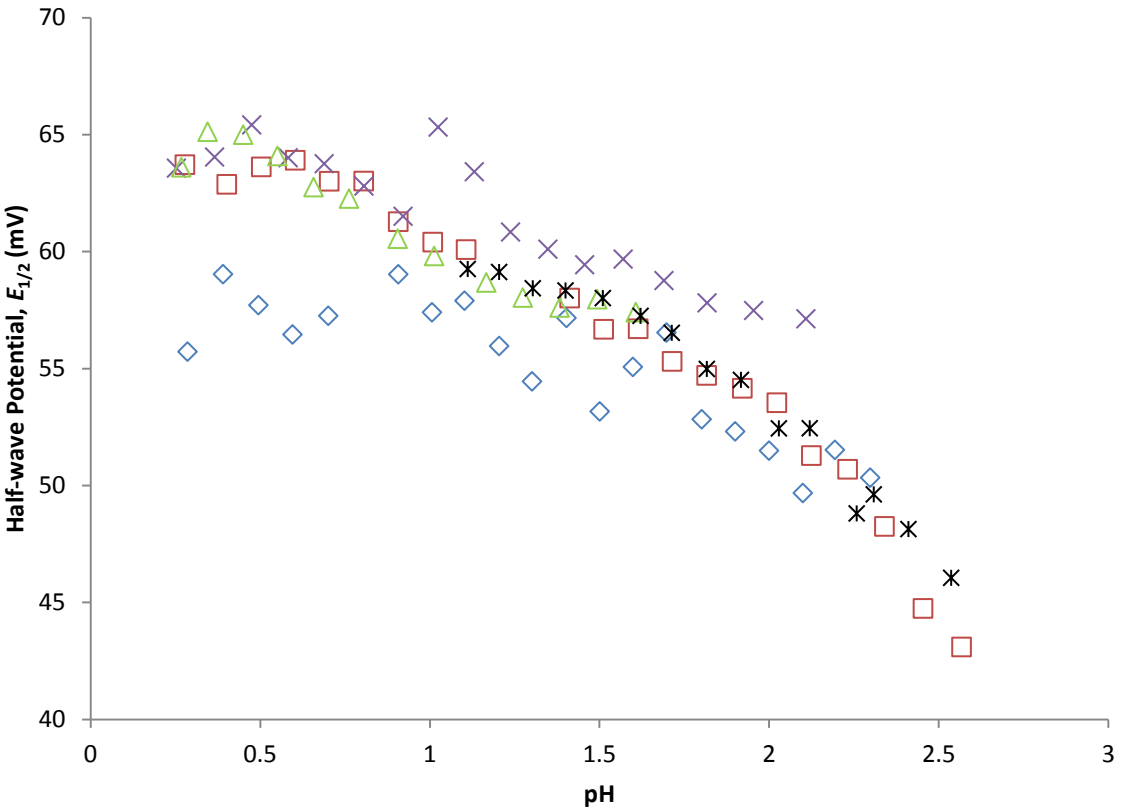

Figure 4.9: E_j corrected $E_{1/2}$ for Bi^{3+} vs pH plot for experiments where [L]:[M] ≈ 100 and L refers to (×) Glutamic Acid, (☐) Glycine, (Δ) Methionine and (◇) Glutamine. (✳) shows values in absence of ligand where Bi^{3+} is only present ($[Bi^{3+}] = 1 \times 10^{-5}$ M).

Bismuth has been shown to be thiophillic[12] and as a result the most well studied bismuth ligand complexes are those in which the ligands contain thiolate groups. These types of complexes are vital in the coordination chemistry of bismuth, as described by Atwood *et al.*[13] and some complexes are pictured in Figure 4.10. In these complexes, bismuth exhibits coordination numbers of three, four, five and six with thiolate ligands. Due to the fact that Bi^{3+} is a borderline metal ion, it is not unexpected for it to bind strongly to the thiolate-sulphur which is considered to be a soft donor group.

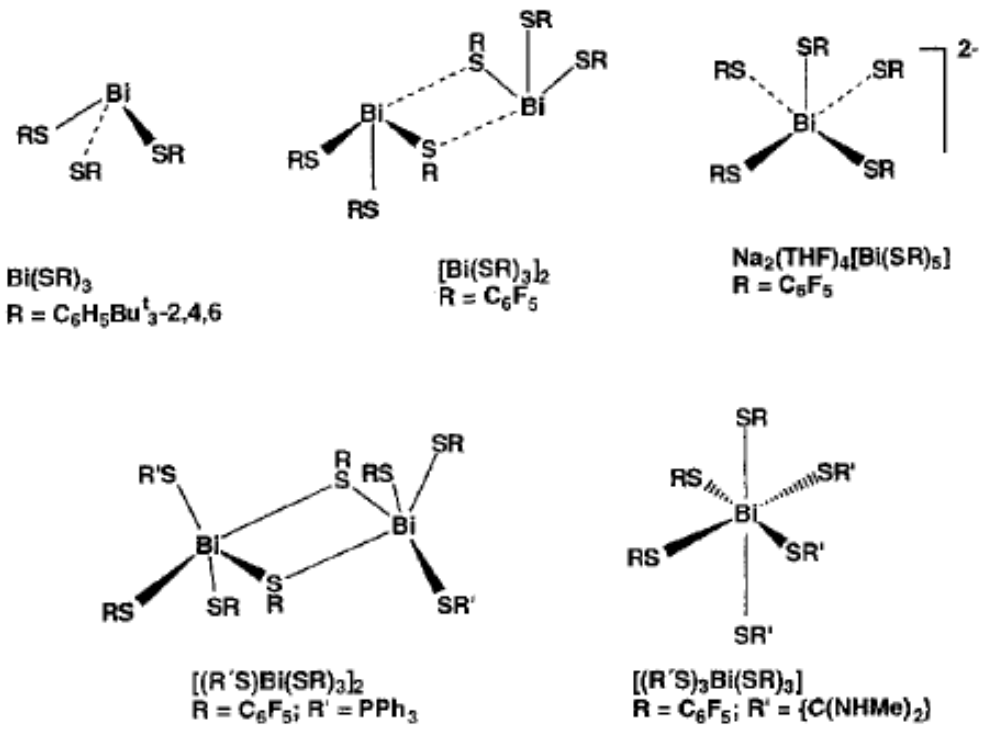

Figure 4.10: Various thiolate ligands attached to the bismuth metal ion shows its ability to vary coordination numbers for various ligands.[12b]

As such, the amino acid which contained the highest probability of complexation with Bi^{3+} out of those considered in this project was cysteine (Cys) since it contains a free thiol moiety. The pK_a values for Cys are 2.05 for the carboxylic acid moiety, 8.00 for the side chain thiol group and 10.25 for the amine group.[9] The problem encountered when adding Cys to the solution was the adsorption of the thiol group onto the mercury electrode, even in highly acidic solutions. This resulted in the Bi^{3+} reduction wave being severely swamped by the adsorption effects. Previous studies[14] have shown that the adsorption of thiol containing molecules, especially Cys, is common. These studies have suggested the use of a molecule with detergent-like characteristics, such as sodium dodecyl sulphate (SDS), which is able to suppress the adsorption[14a] when added into solution. Polarographic-pH titrations with SDS added at various concentrations ([Cys]:[Bi^{3+}] = 20-100) were thus conducted. Unfortunately, the addition of SDS did not improve the vast extent of adsorption of Cys, therefore the complexation of Bi^{3+} with Cys using polarography could not be investigated.

4.8. Powder X-ray Diffraction of Bi^{3+}precipitate

As described in Chapter 1, Bi^{3+} precipitates due to the formation of insoluble Bi-hydroxide species at low pH and the initial analysis of amino acid complexation with Bi^{3+} gave evidence to this. Studies by Moussa and Sammour[15] showed that in solutions containing Bi^{3+}, $HClO_4$ and chloride, the precipitate formed was the solid bismuth-oxy-chloride species, BiOCl. Kragten[16] was able to predict the formation of $BiONO_3$ species in nitrate solutions, however, studies[7a, 17] building upon this work were able to show that the species which could possibly be forming is the hexameric structure, $Bi_6O_4(OH)_4(NO_3)_6$. Due to precipitation being a major obstacle in this study, it was thus decided to attempt to isolate the Bi^{3+} precipitate at pH ~2. The solutions of Bi^{3+} and NO_3 were prepared according to Chapter 3.4. The white precipitate was isolated and then analysed by PXRD (Section 3.5). The PXRD pattern obtained is shown in Figure 4.11 and included in the PXRD pattern is the superimposed calculated PXRD pattern obtained from single crystal data studied by Lazarini.[7] The PXRD patterns show that the precipitate formed consists of the hexamer or hydroxy-nitrate species of Bi^{3+}, $Bi_6O_5(OH)_3(NO_3)_5(H_2O)_3$, partly described by Granier *et al*.[18] The experimental method used to isolate the precipitate used a $[Bi^{3+}] = 1 \times 10^{-2}$ M solution whereas during the polarographic analysis $[Bi^{3+}] = 1 \times 10^{-5}$ M. However, the latter would not allow a significant amount of precipitate, if any to be isolated.

The success of isolating the Bi-hydroxy-nitrate precipitate then begged the question of whether adding a substantial amount of amino acid to the system, would allow for the isolation of an insoluble Bi-hydroxy-amino acid complex or was the Bi-hydroxy-nitrate species simply formed in this case too. Since work on glutamic acid (Glu) had already been initiated, the ratio used for attempting isolation of precipitates was $[Glu]:[Bi^{3+}] = 1000$. The precipitate formed was analysed by PXRD, but the pattern produced could only be compared to the PXRD pattern of L-glutamine, showing that the complex formation was difficult to achieve. The only reason higher $[Glu]:[Bi^{3+}]$ was not used is because the large amount of amino acid needed in the solution was at the limit of the solubility of Glu.

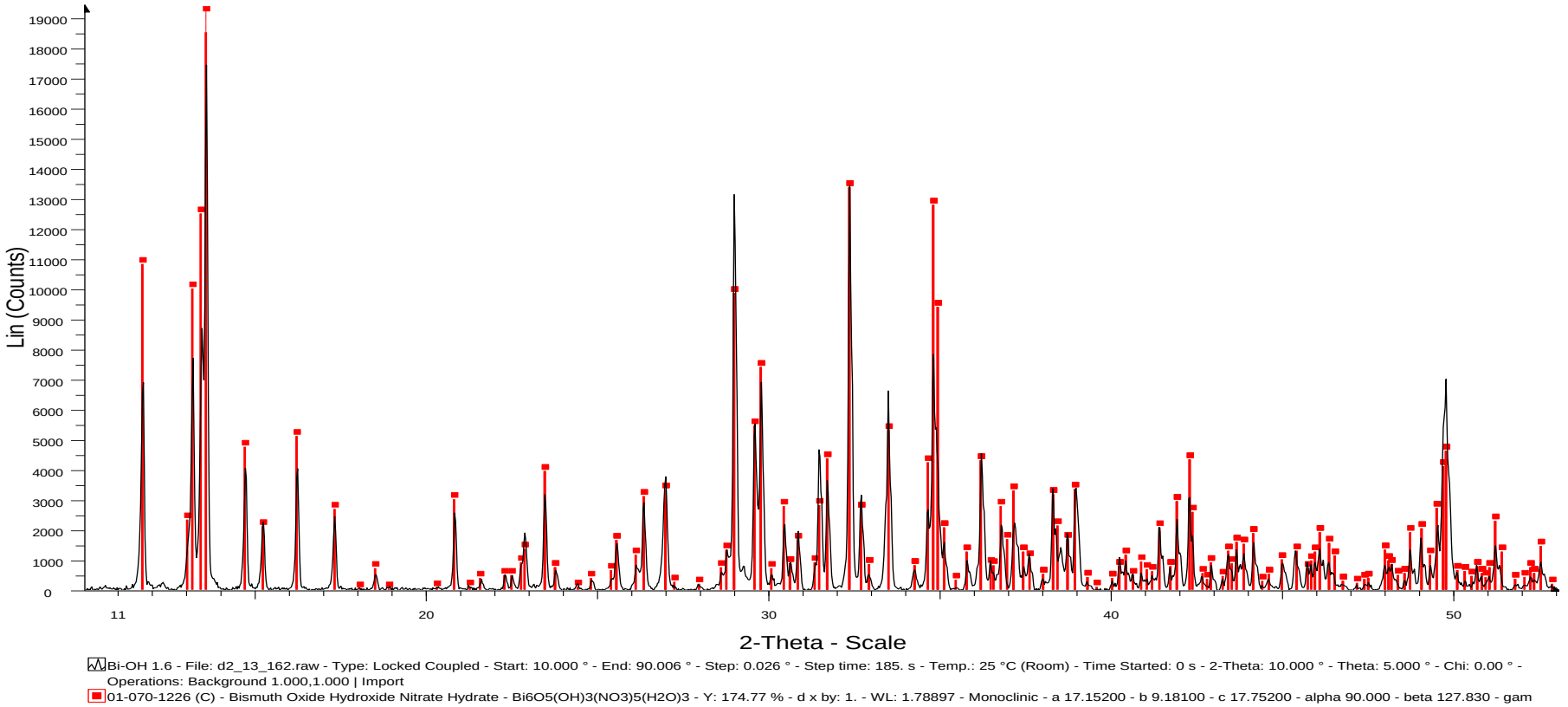

Figure 11. PXRD pattern collected from isolated precipitate as described by Chapter 3.4. The calculated PXRD pattern from single crystal data by Lazarini[7], showing $Bi_6O_5(OH)_3(NO_3)_5(H_2O)_3$, is superimposed onto the pattern (in red).

4.7. Conclusion

For experiments where [amino acid]: $[Bi^{3+}]$ = 100, it was noted that precipitation occurred at a similar point to experiments whereon amino acid was present. Additionally, the potential shifts were similar in the absence or presence of amino acid indicating the lack of complexation. These observations indicate that there is very little or no complexation occurring at this [amino acid]:$[Bi^{3+}]$. The aim of this study was to show the complexation of Bi^{3+} with amino acids and the question now was how we could possibly do this. The answer to this question came in the form of Le Chatelier's Principle. As described by Le Chatelier in his proposal for the equilibrium of a chemical reaction, if large concentrations of reactants or products are added to the chemical system, the system will shift in the direction which will allow for the chemical equilibrium to once again be reached. Using this theory, it was decided to introduce a large concentration of ligand to the the system under analysis. The increase in the [amino acid]:$[Bi^{3+}]$ would theoretically drive the equilibrium of the complexing reaction in the forward direction, allowing Bi^{3+} complexes to form with the respective ligands. The $[Bi^{3+}]$ was not increased as this would allow precipitation to occur at an even lower pH, making our window of study even smaller. Although studies initially began at lower concentrations, the change to higher [amino acid]:$[Bi^{3+}]$ is a more direct indication of what could be occurring within the body, as the concentration of amino acids would be much greater than 100 times more than Bi^{3+}. This work will be discussed further in Chapters 5-7.

In the case of studying Cysteine as a ligand, we did not develop a procedure around the adsorption of the free thiol moiety to the mercury electrode. One of the most interesting techniques which could be utilized is the Anodic Stripping Voltammetry (ASV).[19] ASV involves firstly pre-concentrating a metal onto a solid electrode surface or into a mercury drop, at negative potentials[19]. The metal is then selectively oxidized during an anodic potential sweep which allows very low detection limits. ASV is a useful technique to be used in this study as it may negate the precipitation of bismuth from solution since it will be plated into the mercury electrode[19].

PXRD analysis of the Bi^{3+} precipitate where $[Bi^{3+}]$ = 1 x 10^{-2} M, showed that the Bi^{3+} hexamer $Bi_6O_5(OH)_3(NO_3)_5(H_2O)$species was formed. With the addition of glutamic acid as the ligand, no complexation was found and PXRD analysis of the precipitate showed that it consisted of L-glutamic acid.

4.8. References

[1] a) J. Lingane, *Industrial & Engineering Chemistry Analytical Edition*,**1943**, *15*, 583; b) J. J. Lingane, *Chem. Rev.*,**1941**, *29*, 1; c) J. J. Lingane, *Chem. Rev.*,**1941**, *29*, 1.

[2] a) I. Cukrowski, *Anal. Chim. Acta.*,**1996**, *336*, 23; b) I. Cukrowski and R. C. Luckay, *Anal. Chim. Acta.*,**1998**, *372*, 323; c) R. D. Hancock, I. Cukrowski, I. Antunes, E. Cukrowska, J. Mashishi and K. Brown, *Polyhedron*,**1995**, *14*, 1699.

[3] a) I. Cukrowski, H. M. Marques, T. S. Mkwizu, P. P. Magampa and C. Serge, *Anal. Chim. Acta.*,**2007**, *590*, 203; b) I. Cukrowski, R. D. Hancock and R. C. Luckay, *Anal. Chim. Acta*,**1996**, *39*, 319.

[4] C. Billing and I. Cukrowski, *S. Afr. J. Chem.*,**2009**, *62*, 168.

[5] Swinehart and D. F. Garrett, *J. Am. Chem. Soc.,* ,**1951**, *73*, 507.

[6] J. Kragten, L. G. Decnop-Weever and P. Gründler, *Talanta*,**1993**, *40*, 485.

[7] a) F. Lazarini, *Acta. Cryst.*,**1979**, *B35*, 448; b) F. Lazarini, *Acta. Cryst.*,**1978**, *B34*, 3169.

[8] P. Franklyn and I. Cukrowski, 3D-CFC software, University of the Witwatersrand, **2003**, *Windows Version 1.2*, (unpublished)

[9] A. E. Martell and R. M. Smith, NIST Standard Reference Database 46 Version 8.0, NIST Critically Selected Stability Constants of Metal Complexes,USA, **2004**

[10] C. Billing, Study of bismuth chemistry toward medicinal applications, PhD, University of the Witwatersrand,, **2013**

[11] R. D. Hancock, I. Cukrowski, J. Baloyi and J. Mashishi, *J.Chem. Soc., Dalton Trans.*,**1993**, 2895.

[12] a) L. J. Farrugia, F. J. Lawlor and N. C. Norman, *J. Chem. Soc. Dalton Trans.*,**1995**, 1163; b) H. Sun, H. Li and P. J. Sadler, *Chem. Ber. Recueil.*,**1997**, *130*, 669.

[13] D. A. Atwood, A. H. Cowley, R. D. Hernandez, R. A. Jones, L. L. Rand and C. M. Nunn, *Inorg. Chem.*,**1993**, *32*, 2972.

[14] a) M. Heyrovský and S. Vavřička, *J. Electroanal. Chem.*,**1997**, *423*, 125; b) H. Sun, H. Li, I. Harvey and P. J. Sadler, *J. Biol.l Chem.*,**1999**, *274*, 29094; c) G. G. Briand, N. Burford, M. D. Eelman, N. Aumeerally, L. Chen, T. S. Cameron and K. N. Robertson, *Inorg. Chem.*,**2004**, *43*, 6495; d) N. Golovnev, A. Leshok and G. Novikova, *Russ. J. Coord. Chem.*,**2009**, *35*, 73; e) G. Alonzo, N. Bertazzi and M. Consiglio, *Inorg. Chim. Acta.*,**1983**, *85*, L35.

[15] A. A. Moussa and H. M. Sammour, *J. Chem. Soc.*,**1960**, 2151.

[16] J. Kragten, L. G. Decnop-Weever and P. Gründler, *Talanta*,**(1993)**, *40*, 485.

[17] a) B. Sundvall, *Inorg. Chem.*,**1986**, *22*, 1906; b) B. Sundvall, *Acta. Chem. Scand.*,**1979**, *A33*, 219; c) I. Grenthe and I. Toth, *Inorg. Chem.*,**1985**, *24*, 2405.

[18] F. Graner, A. Olin and L. G. Sillén, *Acta. Chem. Scand.*,**1956**, *10*, 476.

[19] Electroanalytical Chemistry-Anodic Stripping Voltammetry, www2.chemistry.msu.edu/courses/cem837/Anodic%20Stripping%20Voltammetry.pdf, (Date Accessed: 12-05-2012)

Chapter 5: Bi-Glutamic Acid Complexation

5.1 Introduction

Glutamic acid (Glu) is one of the twenty common amino acids. It helps with the transportation of potassium across the blood-brain barrier, although it itself does not pass this barrier that easily.[1] Figure 5.1 shows the fully protonated Glu. As can be seen, there are 3 potential sites which can be protonated and the protonation constants are pK_a^1 = 9.49, pK_a^2 = 4.07 and pK_a^3 = 2.16 at 25°C and 0.5 M ionic strength.[2] This show the versatility of Glu to perform a range of functions due to its degrees of freedom regarding the potential complexing sites. To associate the protonation site of Glu with a particular protonation constant it was compared to similar molecules. Glutaric acid (Figure 5.2), which has the carboxylic acids in the same positions as that for Glu, has protonation constants of pK_a^1 = 4.87, and pK_a^2 = 4.10 at 25°C and 0.5 M ionic strength.[2] Glutaric acid lacks the amine group on C2, thus both pK_a values are similar as the moieties present are equivalent and it is expected that the carboxylic acid furthest from the amine group in Glu would have a similar pK_a value. In Glu, the carboxylic acid adjacent to the amine group will be affected by the electronic properties of this electronegative amine group and therefore will have a lower a pK_a, hence the value of 2.16 is associated with this moiety. The NH_3^+ present in Glu remains protonated to the highest pH and therefore it is allocated the pK_a = 9.49.

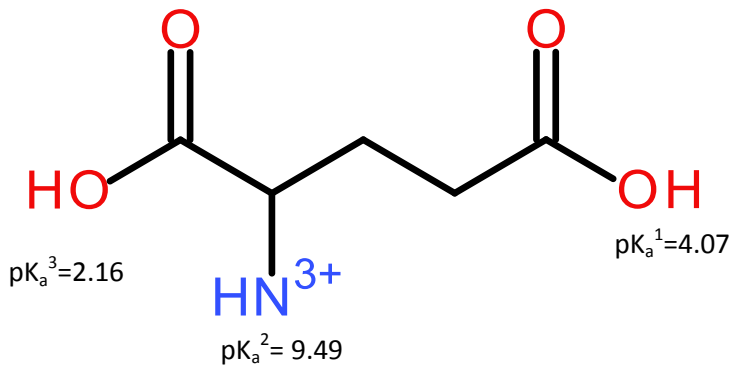

Figure 5.1: Structure of fully protonated glutamic acid indicating the respective pK_a values.[2b]

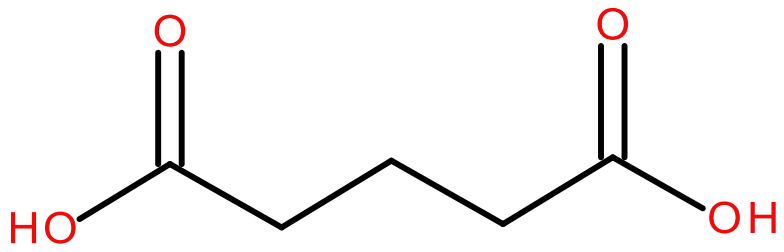

Figure 5.2: Structure of fully protonated glutaric acid.[2a]

Glu is used as fuel in the brain, and attaches itself to nitrogen atoms in the process of forming glutamine. The resulting action allows the detoxification of the body from ammonia, a natural byproduct of the body utilizing energy. This action is the only way in which the brain can be detoxified from ammonia, an important process of ensuring the growth and maintenance of a healthy brain and subsequent function. The detoxification action of Glu is also important for the rest of the body, where it is an important aid in cellular metabolism where it plays an important role in the body's disposal of excess or waste nitrogen. In humans, dietary proteins are broken down by digestion into amino acids, which serve as metabolic fuel for other functional roles in the body.

The process by which Glu achieves its detoxification action is by firstly undergoing deamination, an oxidative reaction catalysed by glutamate dehydrogenase[3] and is illustrated by the chemical equation :

$$Glu + H_2O + NADP^+ \rightarrow \alpha\text{-ketoglutarate} + NADPH + NH_4^+$$

Ammonia is excreted predominantly as urea, synthesised in the liver.[2a, 3] Transamination can thus be linked to deamination, effectively allowing nitrogen from the amine groups of amino acids to be removed, via a glutamate as an intermediate, and finally excreted from the body in the form of urea. The fluid produced by the prostate gland also contains amounts of Glu and may play a role in the normal function of the prostate.[2a, 3]

Along with the ability to dispose of waste nitrogen, Glu also serves an important role in the action of neurotransmitters.[4] Glutamate is stored in vesicles near the beginning of the pre-synaptic nerve. Once the appropriate nerve impulses are triggered, a signal is

sent to release the glutamate molecules which travel to the nerve, and allows the electrochemical signal to be passed on to the brain, thereby resulting in the intended reaction.[4]

5.2 Aim

Results presented in Chapter 4 show that the complexation of Bi^{3+} with amino acid ligands at [L]:[M] = 100 did not occur before Bi^{3+} formed a precipitate. The aim of this study is to investigate the conditions at which complex formation will be favored before Bi^{3+} precipitates. The study will also aim to investigate the best approach to calculating the stability constants in a medium conducive to Bi^{3+} forming complexes with NO_3^- at low pH especially when the ligand of interest (glutamic acid in this case) is rather weakly binding.

5.3 Experimental

Experiments were run as in Chapter 3 using the NOVA procedures developed in Chapter 2. In order to drive the complexation reaction of Bi^{3+} with Glu, experiments were run with [Glu]:[Bi^{3+}] significantly greater than 100. Here three experiments were run with [Glu]:[Bi^{3+}] of 1970, 3076 and 5000 (these experiments will be referred to as the rounded values of 2000, 3000 and 5000). On addition of Glu to the solution, particularly for the highest ratio, the pH of the solution increased. In hindsight the pH should then have been adjusted closer to the starting pH 1 before starting to titrate with KOH, but instead data was analysed from the pH the solution had attained.

5.4 Results

5.4.1. Modelling the Pb^{2+}-Glu system

Since amino acids are such a large component of biological systems, many have studies have been conducted where complexation to biological metal ions such as Cu, Fe and Zn were used. Complexation of Bi^{3+} with Glu is not well studied, so it was decided to see what happens to the species in solution when the solution conditions were changed by modelling the Pb^{2+}-Glu system since Pb^{2+} is isoelectronic with Bi^{3+}.

For the Pb^{2+} system it is seen that the MLH, ML and ML_2 species form (log β = 11.43, 4.53 and 6.80, respectively, at 25°C at 1M ionic strength).[2b] In the species distribution diagram (Figure 5.3) using the conditions $[Pb^{2+}] = 1 \times 10^{-5}$ M, and [Glu]:[Pb] = 100 (i.e. that used in the experiments with Bi^{3+} in Chapter 4), both the ML and MLH species were present above pH 3 but only to small extents and the ML_2 species is not formed under these conditions. The fact that the MLH species forms gives evidence that protonated species are viable. The formation constants of PbOH are shown in the Appendix 2.

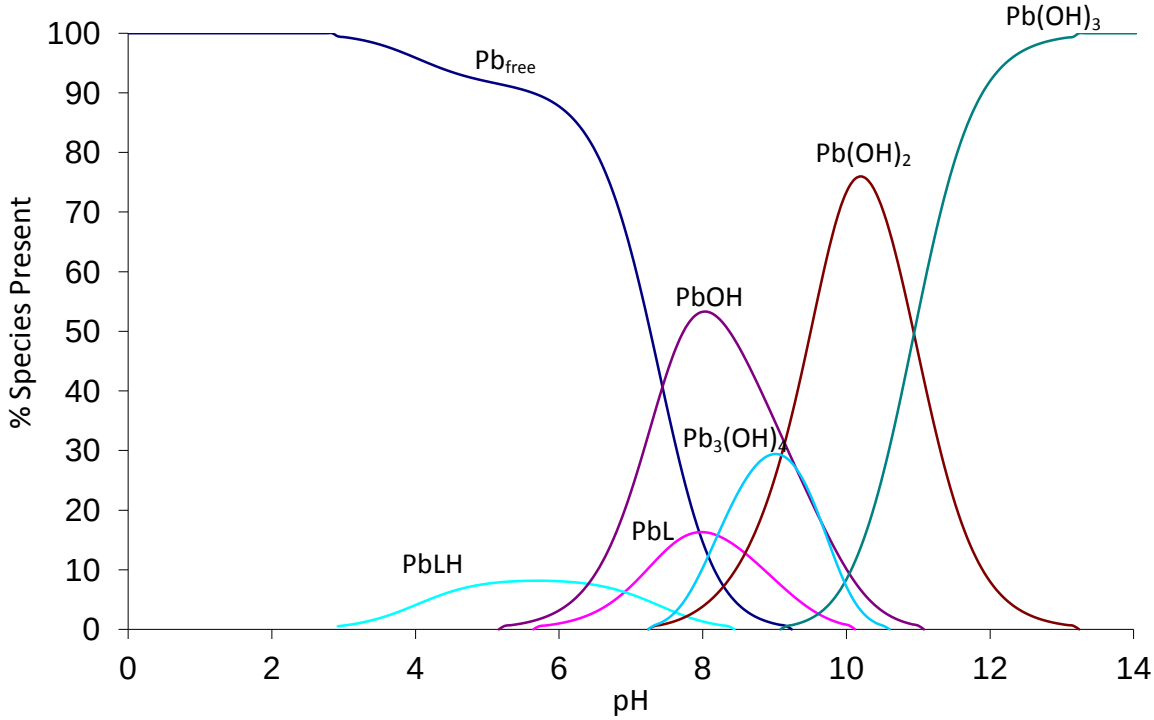

Figure 5.3: Species distribution diagram for the Pb^{2+}-Glu system where [Glu]:$[Pb^{2+}]$ = 100 and $[Pb^{2+}] = 1 \times 10^{-5}$ M at 25°C.

Moreover, when the $[Pb^{2+}]$:[Glu] was increased to 1000 (Figure 5.4), we see the formation of the MLH species in a much higher percentage and it starts forming at pH ~2. It can also be seen that significantly more of the ML species forms, almost three times greater than that of when [Pb]:[Glu] = 100. The formation of the ML_2 species also occurs above pH ~7 which indicates that as the concentration of the ligand is increased while that of the metal ion is kept the same, complexation increases as expected from Le Chatelier's principle.[5] An additional consideration is that since the Glu concentration is

increased, the concentration of deprotonated Glu (deprotonated to varying extents depending on pH) also increases. The increase in concentration of these deprotonated species must also have an effect in driving the reaction forward.

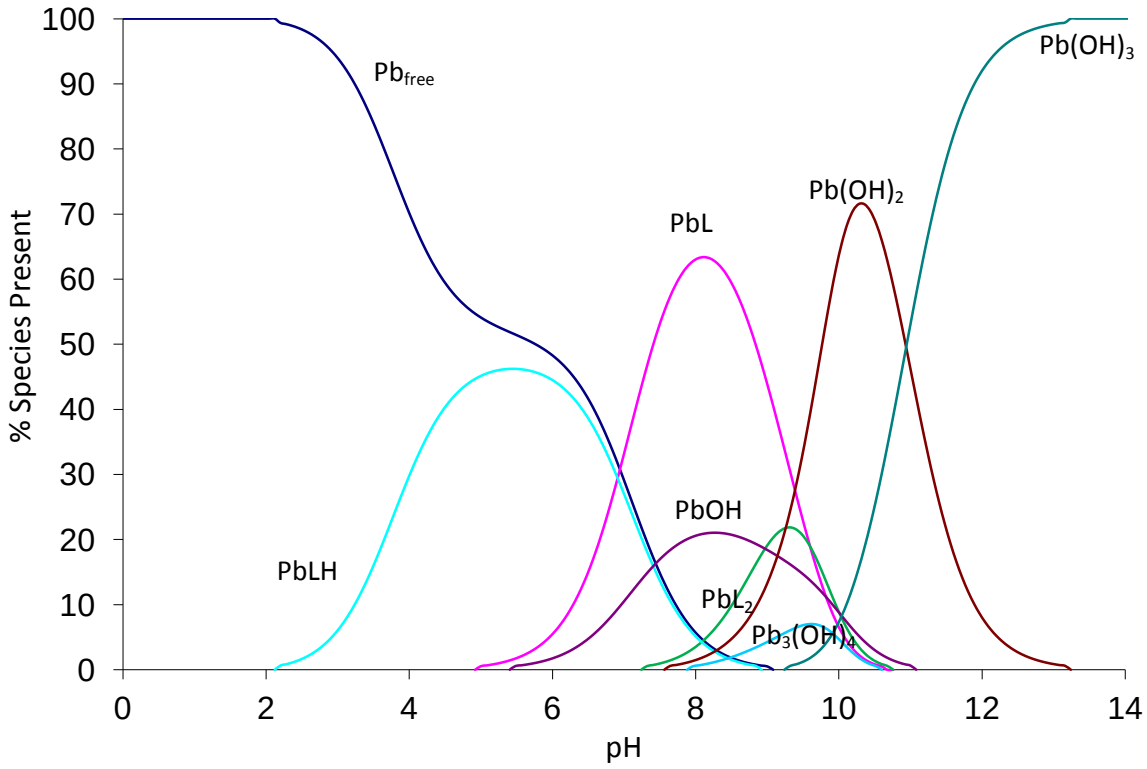

Figure 5.4: Species distribution diagram for the Pb^{2+}-Glu system where [Glu]:[Pb^{2+}] = 1000 and [Pb^{2+}] = 1 x 10^{-5} M at 25°C.

For interest, it was also decided to view how the increase in [Pb^{2+}] affects the species formed. As can be seen in Figure 5.5, when [Pb^{2+}] = 1 x 10^{-4} M and [Glu]:[Pb^{2+}] = 100, the MLH and ML species are once again much higher when compared to that in Figure 5.3 where [Pb^{2+}] = 1 x 10^{-5} M and [Glu]:[Pb^{2+}] = 100. It was realized that in keeping [Glu]:[Pb^{2+}] = 100, both the [Pb^{2+}] and [Glu] was increased 10-fold. Although a viable option when studying Pb^{2+}, this was not a chosen method when performing experimental studies with Bi^{3+} because by increasing [Bi^{3+}], precipitation of the Bi-hydroxy-nitrate species would occur at lower pH and decrease the already small window of analysis. The investigation into how Pb^{2+} complexes with Glu illustrates that by increasing either [M] or [L] results in promoting complex formation.

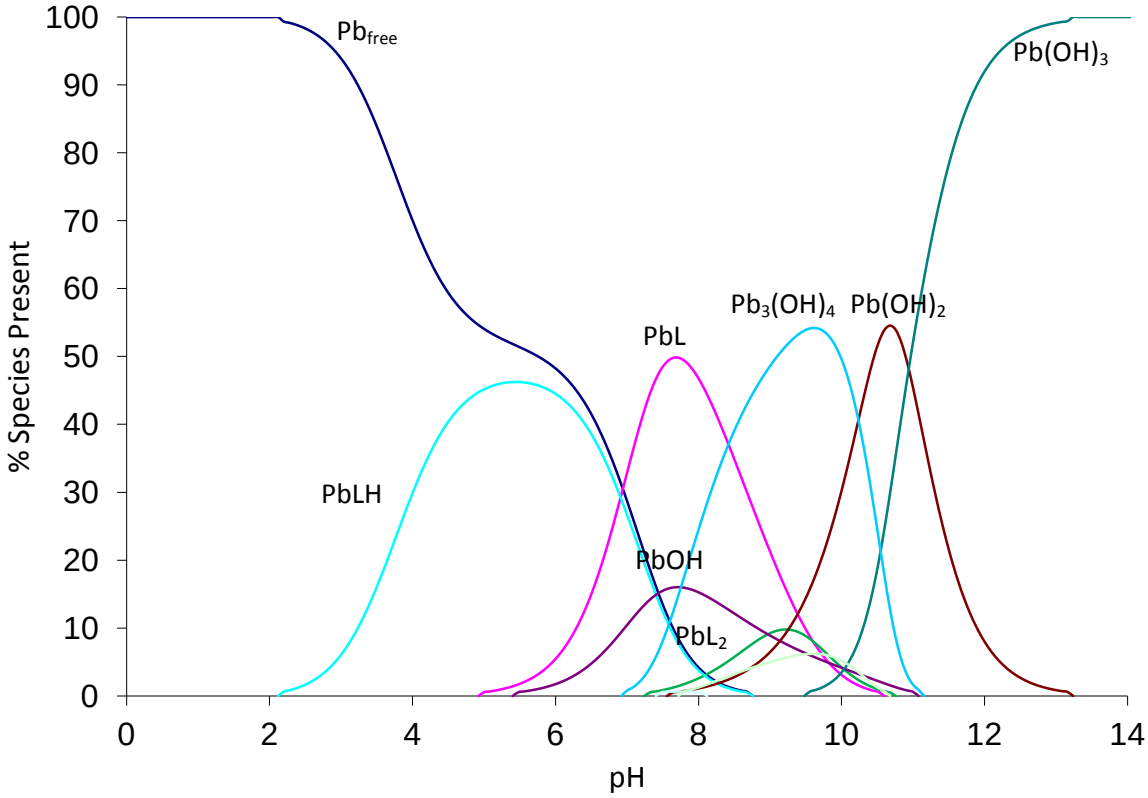

Figure 5.5: Species distribution diagram for the Pb^{2+}-Glu system where [Glu]:[Pb^{2+}] = 100 and [Pb^{2+}] = 1 x 10^{-4} M at 25°C.

5.4.2 Bi^{3+} complexation with Glutamic acid

As described in Chapter 4, the initial studies with [Glu]:[Bi^{3+}] = 100 indicated no complexation occurred and precipitation ensued at pH ~2 (see Figure 4.8), the region we would expect Bi^{3+} (with a concentration of ~10^{-5} M) to precipitate if 0.5 M NO^-_3 were present. One of the possible reasons for no significant complexation formation taking place at low pHs is that the third protonation constant of Glu is 2.16.[2b] At the low [Glu]:[Bi^{3+}] of 100 there is not enough deprotonated Glu to allow complex formation with the Bi^{3+}. If considering only the form in which the ligand is present, Figure 5.6 shows that ~90% of Glu exists in the form Glu-H_3 at pH 1 and therefore only 10% of the singly deprotonated Glu is available for complexation at that pH. Above pH 2.2 the dominant species present is Glu-H_2, however, at this stage Bi^{3+} is close to precipitation in the NO_3^- solution. As was also illustrate using the Pb-Glu system, the concentration of Glu plays an important role in the formation of complexes with metal ions since at different pHs there are different percentages of protonated and deprotonated species present in solution.

For example, consider a solution at pH 1 where 10% of Glu is in the form Glu-H_2. If the solution contains 1 x 10^{-5} M metal ion and [Glu]:[M] = 100, then 10% of 1 x 10^{-3} M = 1 x 10^{-4} M Glu-H_2. However, when the [Glu]:[M] = 1000, 10% of 1 x 10^{-2} M results in [Glu-H_2] = 1 x 10^{-3} M available to complex to the metal ion in solution.

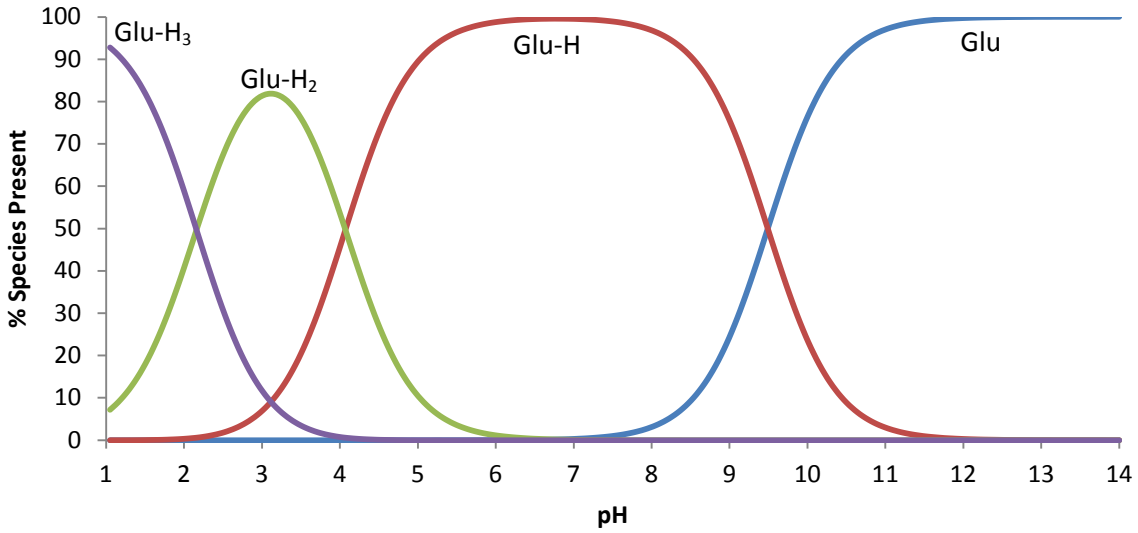

Figure 5.6: Species distribution diagram of glutamic acid in aqueous solutions at 25^{o}C.

Increasing the [Glu]:[Bi^{3+}] to 2000 (or more precisely 1970) and still using [Bi^{3+}] = 1 x 10^{-5} M resulted in the Bi^{3+} only precipitating at pH ~4.5 (Figure 5.7) which indicates that some soluble Bi-Glu complex formed under these conditions.

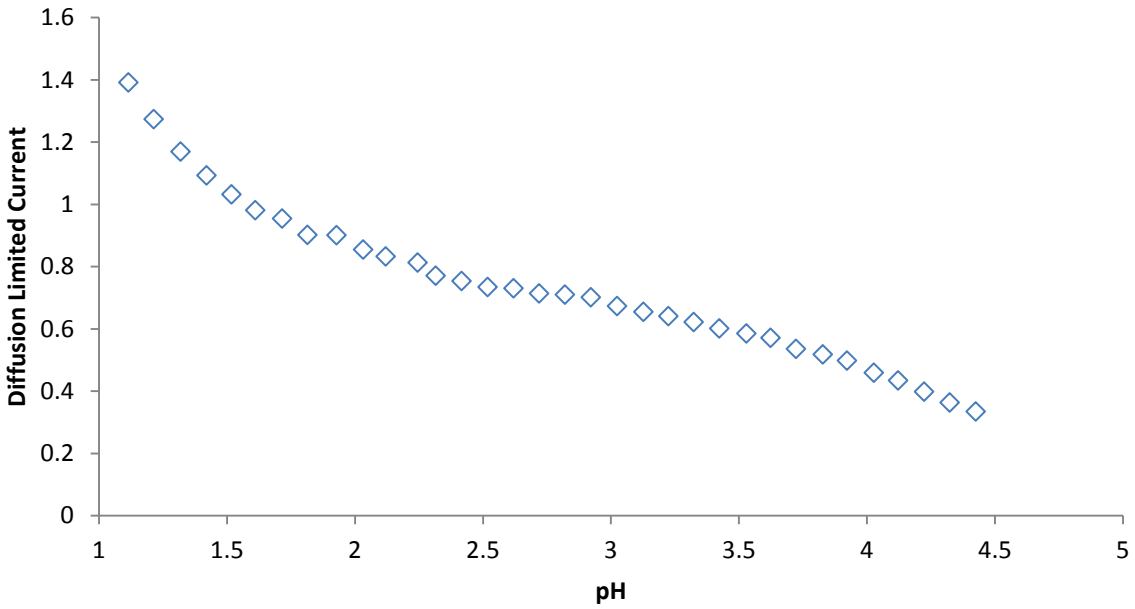

Figure 5.7: I_D vs pH for Bi^{3+} from solutions with [Glu]:[Bi^{3+}] = 2000 and [Bi^{3+}] = 1 x 10^{-5} M.

Before the $E_{1/2}$ values could be used in further analyses, E_j had to be corrected for first. E_j was calculated at each pH using Tl^+ potential data which was collected during the same experiment as that for Bi^{3+}. Figure 5.8 compares the experimental data obtained and the E_j corrected $E_{1/2}$ values. It can be seen that the correction is significant at the lowest pHs and becomes minimal from pH ~2.

A clear change in the $E_{1/2}$ vs pH plots for Bi^{3+} was noted when no ligand was added compared to when [Glu]:[Bi^{3+}] = 2000 (Figure 5.9). The addition of large concentrations of Glu thus resulted in the formation of Bi^{3+}-Glu complexes as evident from the more negative $E_{1/2}$ values in the presence of the ligand which is due to the Bi^{3+} centre becoming more difficult to reduce.

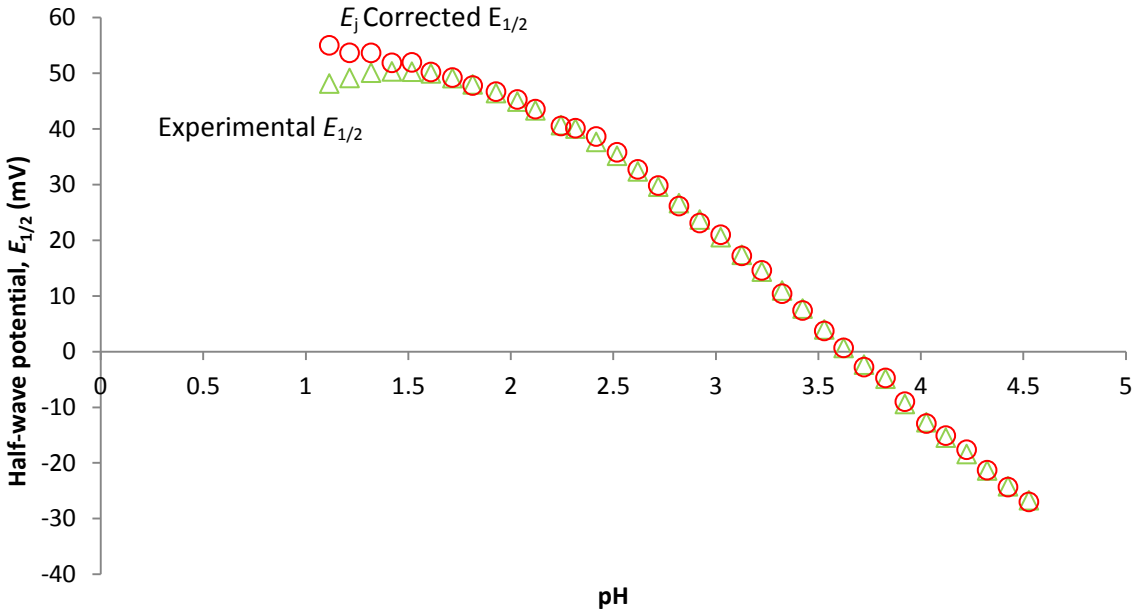

Figure 5.8: $E_{1/2}$ for Bi^{3+} vs pH with [Glu]:[Bi^{3+}] = 2000 showing both the experimental and E_j corrected $E_{1/2}$ values.

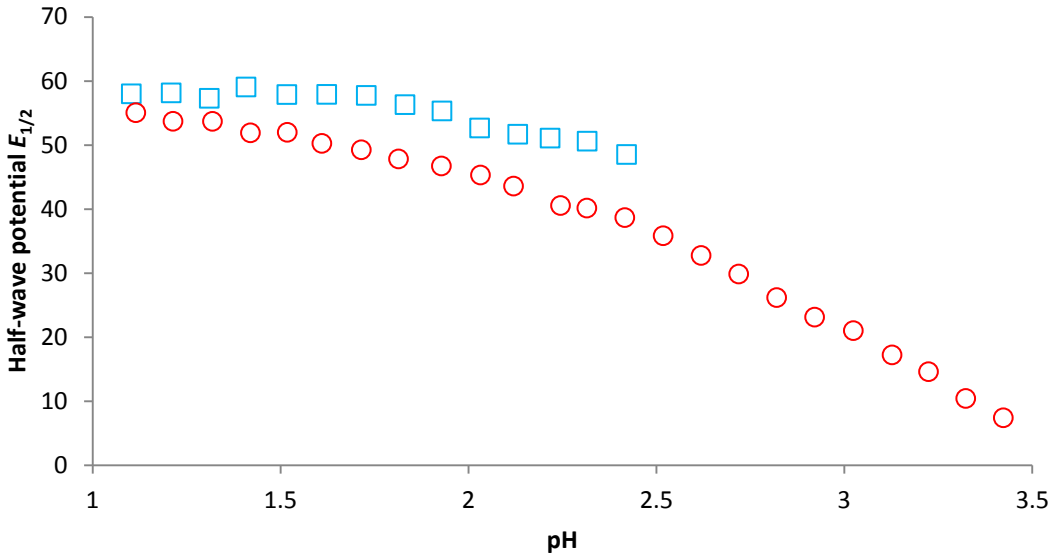

Figure 5.9: $E_{1/2}$ for Bi^{3+} vs pH with (□) no ligand added and (○) [Glu]:[Bi^{3+}] = 2000.

As can be seen in Figure 5.10, an increase in [Glu] results in greater negative shifts in $E_{1/2}$ as the pH is increased. The type of complexes formed and the resulting concentrations of these complexes would all contribute to the extent of the negative shift in $E_{1/2}$ all showing that that complexes between Bi^{3+} and Glu were indeed forming. An indication of both

$E(Bi_{free})$ and $E(Bi_{free})_{OH}$ is also given as it is the difference between the free metal ion potential and that of the complexed ion that are used in calculating formation constants (see equation 3.1). It can be seen that even from the lowest pH complexation was already taking place for these experiments with the significantly increased ligand concentration.

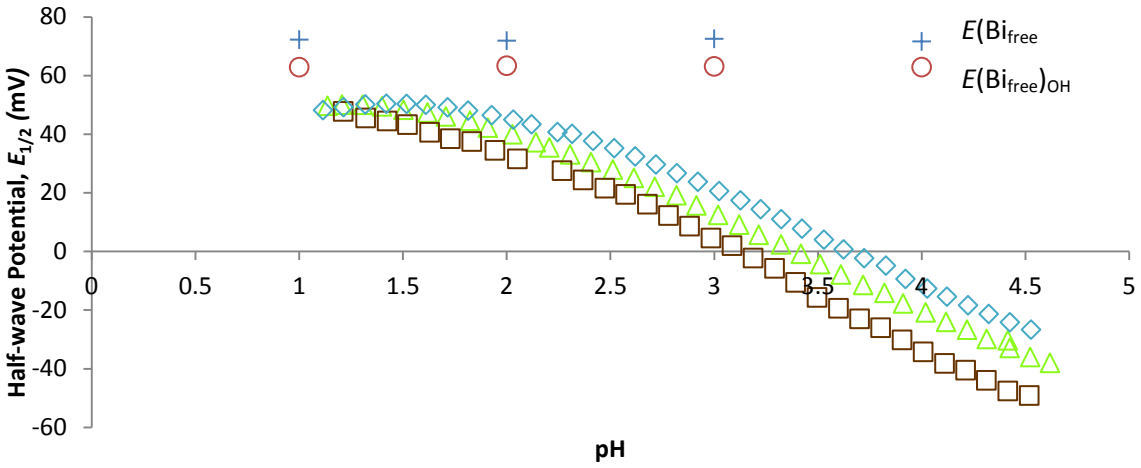

Figure 5.10: $E_{1/2}$ for Bi^{3+} vs pH for the three experiments where [Glu]:[Bi^{3+}] = (◇) 2000, (Δ) 3000 and (□) 5000.

The values of γ obtained from fitting the polarograms (see equation 3.4) should be between 0.9 and 1 to indicate a electron transfer process is reversible, which is required for equation 3.1 to produce a correct analysis of stability constants.[6] If quasi-reversible and irreversible $E_{1/2}$ values are used, greater shifts in $E_{1/2}$ would be predicted compared to the reversible case and formation constants would be overestimated. For [Glu]:[Bi^{3+}] = 5000 the γ value began to fall below the reversible threshold of 0.9 above pH 3.5 (see Figure 5.11). As will be described fully in Chapter 7, the reversibility of the polarographic waves which tended toward quazi reversibile and irreversible was then fitted using a software programme termed Fitbrink, which allows for the γ values to be fixed in the range of acceptable reversibility.

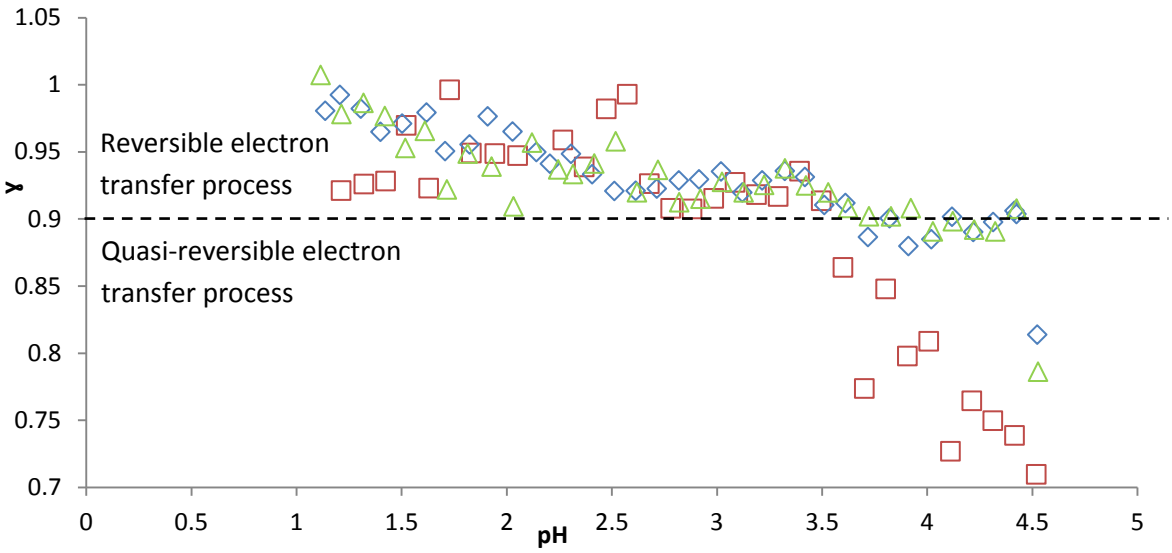

Figure 5.11: Graph indicating the extent of reversibility, *γ*, vs pH for the Bi^{3+} polarograms for [Glu]:[Bi^{3+}] = (◇) 2000, (Δ) 3000 and (□) 5000.

One of the most useful methods used to predict the type of metal-ligand species formed in solution is to analyse the slopes[7] of the E_j corrected $E_{1/2}$ vs pH graphs. As described in Chapter 3, Section 3.3.4, in a specific pH range there is a dominant form of ligand species present in solution, where these forms vary only by the extent of their protonation. We find the slopes of the graph using equation 3.6 within a pH range, which should indicate the type of species present in solution that is being reduced at the electrode. As an example, slope analysis conducted on the [Glu]:[Bi^{3+}] = 5000 data is illustrated here. The reduction of the Bi^{3+}-Glu species results in the formation amalgamated Bi^0 and the bond/s with Glu is/are then broken. Glu remains in solution and the pH of the solution is then the major determinant of the extent to which Glu would be protonated. Using the predicted complexes (Bi-Glu-H_2, Bi-Glu-H and Bi-Glu in this case), we take into account the number of electrons required to reduce the Bi^{3+} centre and the number of protons required to form the predominant ligand species at that respective pH range.

Figure 5.12 gives the expected slopes for the reduction of suggested species in the indicated pH ranges. Below pH 2.16, the expected slope for the reduction of the Bi-Glu-H_2 complex is 20 mV. As can be seen in Figure 5.13, a slope of 20 mV was found for the experimental data in the same pH region, thus indicating that the Bi-Glu-H_2 complex

probably formed under these conditions. If the other species were to form in this pH range, the slope would be considerably higher.

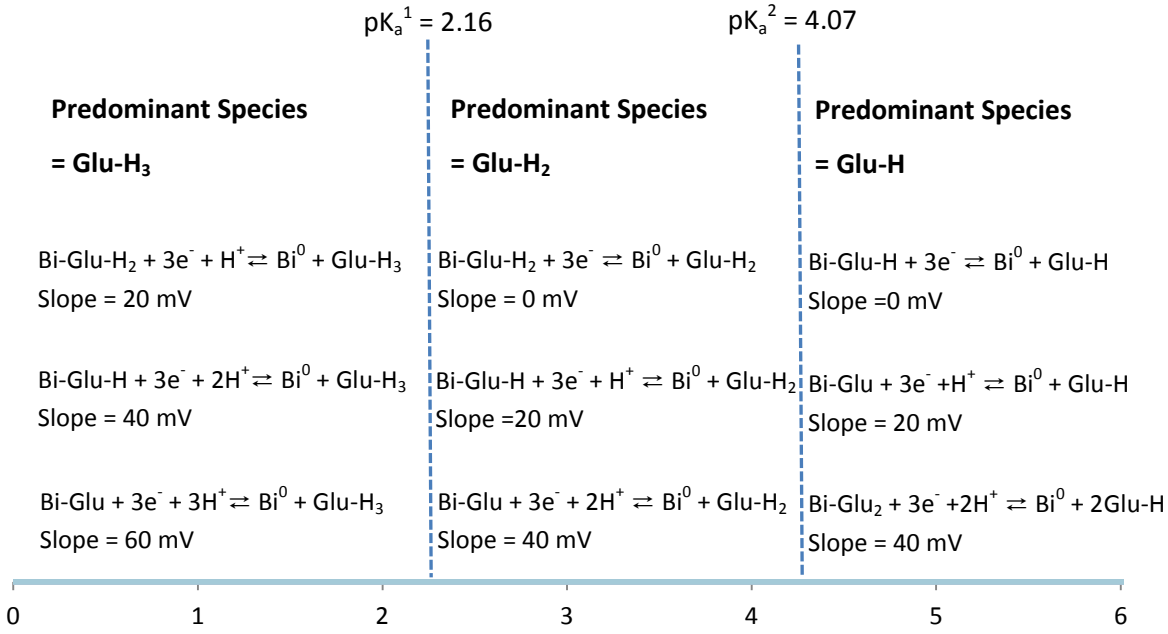

Figure 5.12: Diagram illustrating the predominant ligand species in a specific pH range and the calculated slopes which indicate the type of complex which could be present in solution.

For the pH range 2.16 to 4.09, the Bi-Glu-H_2 complex is expected to give a slope of 0 mV meaning that this reduction process will be independent of the pH. However, the reduction of the Bi-Glu-H and Bi-Glu species would produce slopes of 20 or 40 mV respectively. As can be seen in Figure 5.13, there are two distinctive slopes in this pH range. In the pH range 2.3 – 3.1, the slope of 32 mV lies between the two expected slopes and is a strong indicator that both Bi-Glu-H and Bi-Glu are present in solution. Between pH 3.1 - 4.1 the slope is 39 mV, which is close to the slope indicating the dominance of the Bi-Glu complex.

For the pH range greater than 4.09, we would expect the slope to be approximately 20 mV for the reduction of Bi-Glu and 40 mV for the reduction of Bi-Glu_2. In Figure 5.13 a slope of 30 mV was found above pH 4.1 which could indicate that both Bi-Glu and Bi-Glu_2 are present. However, this was in the very small pH region between pH 4.1 - 4.5 before

precipitation occurred. From the species distribution diagram in Figure 5.6 it can be seen that at pH 4.5 there is still ~30% Glu-H_2 in solution. Thus in this narrow pH range it could be that on reduction of Bi-Glu, both Glu-H and Glu-H_2 are produced, thereby giving an average slope of ~30 mV.

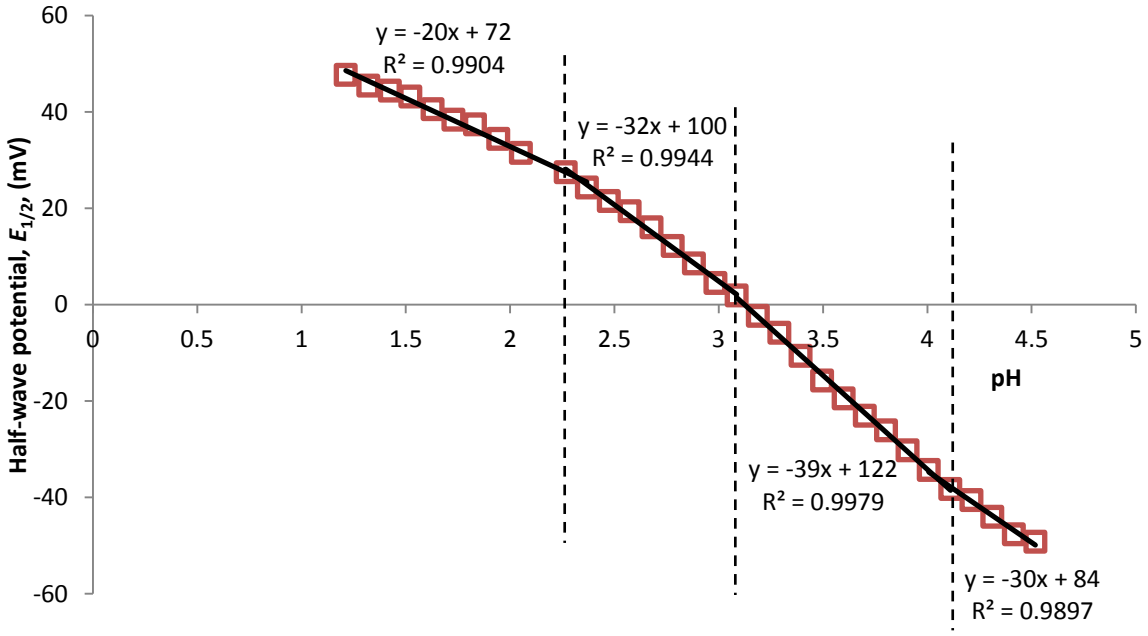

Figure 5.13: E_j corrected $E_{1/2}$ for Bi^{3+} vs pH with [Glu]:[Bi^{3+}] = 5000. Slope analysis has been completed in different pH ranges in order to help predict which Bi^{3+}-Glu complexes are present in solution.

The 3D-CFC programme[8] was used to plot the ECFC and CCFC as described in Chapter 3. The two free Bi^{3+} potential values, determined as discussed in Chapter 4, were utilized in order to obtain a better representation of the formation constants of complexes formed between Bi^{3+} and Glu. This is as a result of existing speciation software being unable to take into account the existence of NO_3^- species simultaneously with the OH^- and ligand (of interest) species. The ECFC and CCFC were therefore plotted using both $E(Bi_{free})$ and $E(Bi_{free})_{OH}$ values which were calculated as described in section 4.5. By determining log β values using both $E(Bi_{Free})$ and $E(Bi_{Free})_{OH}$, we can conclude that the true log β for the respective Bi^{3+}-Glu complexes is between these two values. The reason for this deduction is that initially below pH 1 the Bi^{3+} nitrate species predominate in solution (Figure 5.14). If the true $E(Bi_{free})$ value is used, then shifts due to the formation of Bi^{3+} nitrates could

erroneously be allocated to the formation of Bi^{3+}-Glu complexes. Thus the value of $E(Bi_{free})_{OH}$ is rather used in the low pH region to give better estimates of the formation constants. However, as pH increases the concentration of these Bi^{3+} nitrate species begin to decrease and that for the Bi^{3+} hydroxide species increase. Above pH 3 the Bi^{3+} nitrate species are negligible and there is no need to account for nitrate as a competing ligand. Above pH 3 when using the true $E(Bi_{free})$ value, good approximations of the formation constants are obtained. Between pH 1-3 the formation constants should be between the values calculated using the two $E(Bi_{free})$ values. We actually really need software that can account for the competition between decreasing Bi^{3+} nitrate species, increasing Bi^{3+} hydroxide species as well as the formation of the Bi^{3+}-Glu species which we propose are forming.

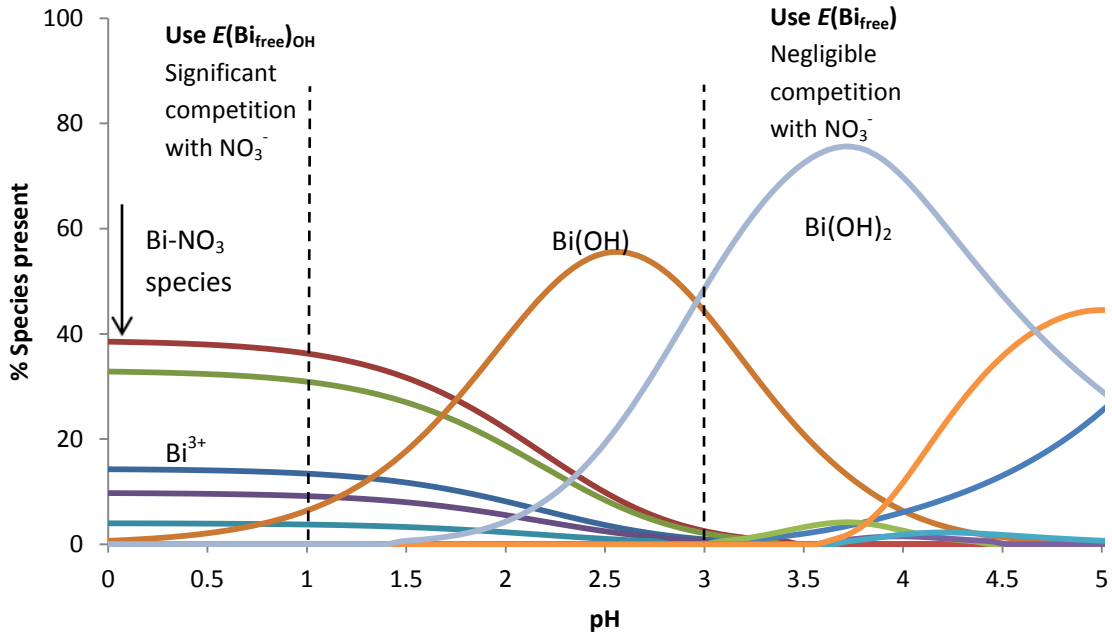

Figure 5.14: Species distribution diagram of Bi^{3+} species vs pH in a NO_3^- solution at 25°C in pH range 1 - 5. $[Bi^{3+}] = 1 \times 10^{-5}$ M.

Figure 5.15 to 5.17 show the ECFC and CCFC curves calculated using the true $E(Bi_{free})$ for the Bi^{3+}-Glu complexes for the various [Glu]:$[Bi^{3+}]$ values. As described in Chapter 3, the CCFC is fitted to the ECFC (using equation 3.1) by refining the formation constants for the respective Bi^{3+}-Glu complexes formed in solution. Using the information from the slope analysis, we were able to deduce that three Bi^{3+}-Glu complexes were predicted to form in

the accessible pH range. These complexes were then entered into the 3D-CFC programme[8] where the respective log *β* values were estimated iteratively by minimizing the difference between the CCFC and ECFC. Once the estimated values give a sufficiently good fit, the values are then refined using the non-linear least squares curve fitting procedure. Ideally, the two curves should overlap in order to obtain an accurate log *β* for complex formation. Better fits between the ECFC and CCFC were obtained for [Glu]:[Bi^{3+}] of 3000 and 5000, indicating a higher confidence in the log *β* values calculated for these experiments. The ECFCs and CCFCs were also calculated using $E(Bi_{free})_{OH}$ where the curves looked similar but all shifts were about 9 mV smaller and hence the calculated formation constants were also smaller. All formation constants are quoted in Table 5.1: .

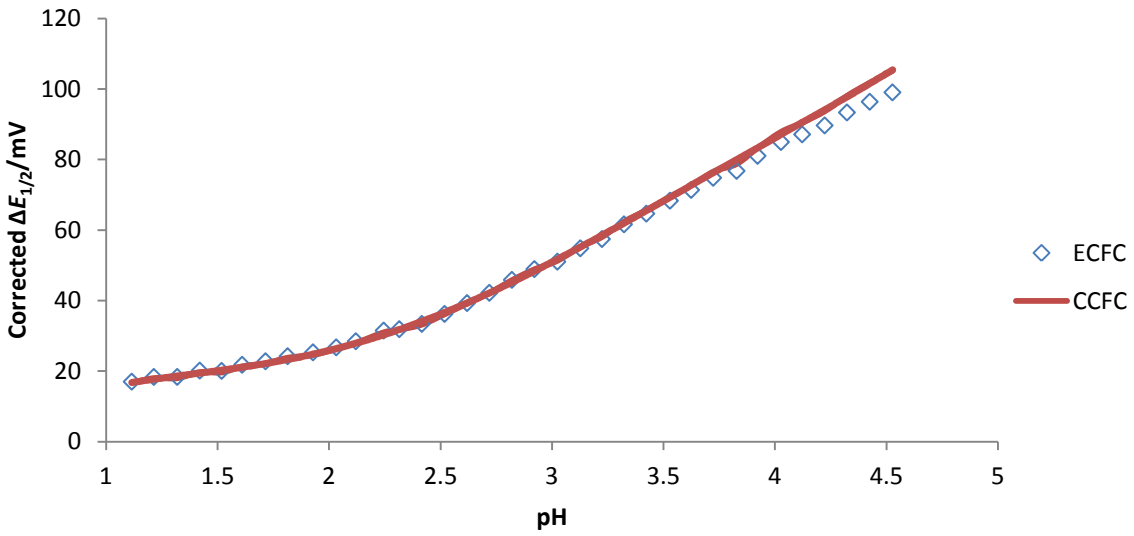

Figure 5.15: CCFC and ECFC for a Bi^{3+}-Glu complexes where [Glu]:[Bi^{3+}] = 2000.

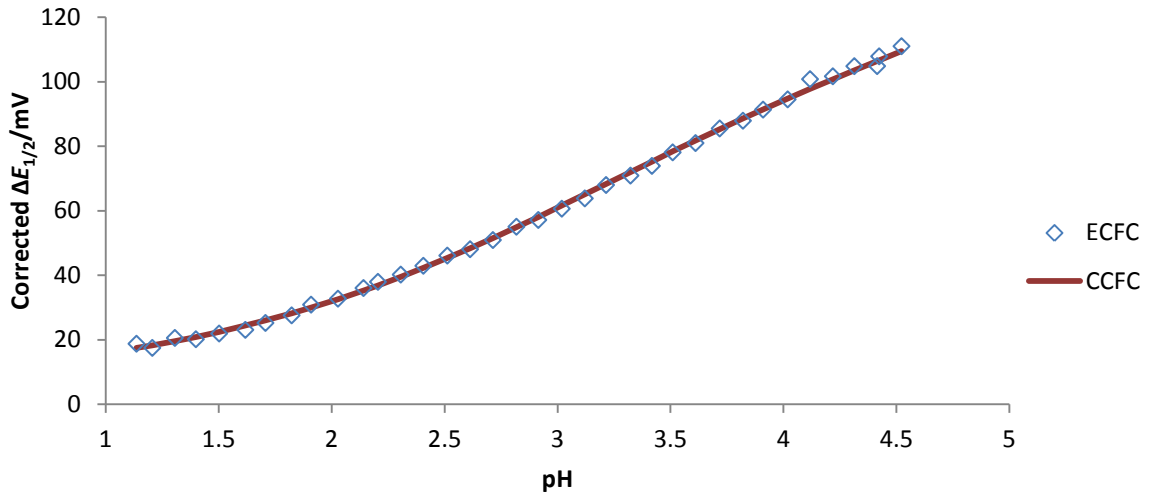

Figure 5.16: CCFC and ECFC for a Bi^{3+}-Glu complexes where [Glu]:[Bi^{3+}] = 3000.

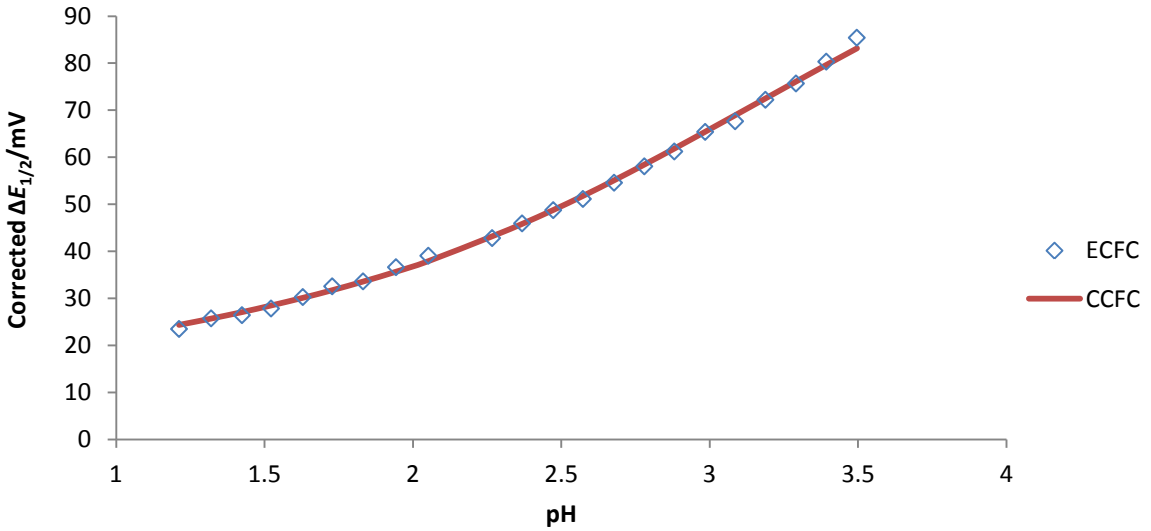

Figure 5.17: CCFC and ECFC for a Bi^{3+}-Glu complexes where [Glu]:[Bi^{3+}] = 5000.

The species model required to fit the data consisted of Bi-Glu-H_2, Bi-Glu-H and the Bi-Glu complexes except, as can be seen in Table 5.1: , the log β value for Bi-Glu-H for the ratio [Glu]:[Bi^{3+}] = 2000 could not be refined and could be a result of the low [Glu]:[Bi^{3+}] ratio used. For the remaining two experiments the Bi-Glu-H species was required to give a good fit and the log β values for Bi-Glu-H were reproducible. The average log β values for the three complexes are given in Table 5.1: $\pm$ the standard deviation for the three experiments, where the latter indicated good reproducibility.

Table 5.1: Calculated log β values for the formation of the Bi^{3+}-Glu complexes using using both the $E(Bi_{free})$ and $E(Bi_{free})_{OH}$ values and the 3D-CFC software. (Charges were omitted in equilibria reactions.)

[L]:[Bi^{3+}]	2000	3000	5000	Average
(a) Using $E(Bi_{Free})$		Log β		
Bi + LH_2 ⇄ Bi-LH_2	17.05 ± 0.02	16.87 ± 0.04	17.00 ± 0.03	16.97 ± 0.09
Bi + LH ⇄ Bi-LH	-	14.88 ± 0.05	14.77 ± 0.10	14.82 ± 0.08
Bi + L ⇄ Bi-L	12.09 ± 0.02	12.34 ± 0.02	12.47 ± 0.03	12.30 ± 0.19
Overall Fit	1.08	3.80	0.64	
(b) Using $E(Bi_{Free})_{OH}$				
Bi + LH_2 ⇄ Bi-LH_2	16.08 ± 0.05	16.03 ± 0.02	16.25 ± 0.05	16.12 ± 0.12
Bi + LH ⇄ Bi-LH	-	14.39 ± 0.06	14.05 ± 0.14	14.22 ± 0.24
Bi + L ⇄ Bi-L	11.12 ± 0.06	11.76 ± 0.09	11.84 ± 0.03	11.57 ± 0.39
Overall Fit	0.84	0.78	1.36	

Species distribution diagrams were plotted (using SOLEQ)[9] employing the formation constants calculated by using $E(Bi_{Free})$ (Figure 5.18) and $E(Bi_{Free})_{OH}$ (Figure 5.19). These plots are in agreement with the occurrence of the different species in various pH ranges as estimated by the slope analysis (Figure 5.13). From slope analysis it was predicted that between pH 2.3 – 3.1, Bi-Glu-H and Bi-Glu exist together in comparative concentrations, and above a pH of 3.1 the dominant species was Bi-Glu. The Bi-Glu-H_2 complex was predicted to be dominant below pH 2.3. This is clearly the case in Figure 5.18 and 5.19. The actual values for the formation constants are between those determined when using using $E(Bi_{Free})$ and $E(Bi_{Free})_{OH}$, and hence the species distribution diagram is also somewhere between the two given in Figure 5.18 and 5.19.

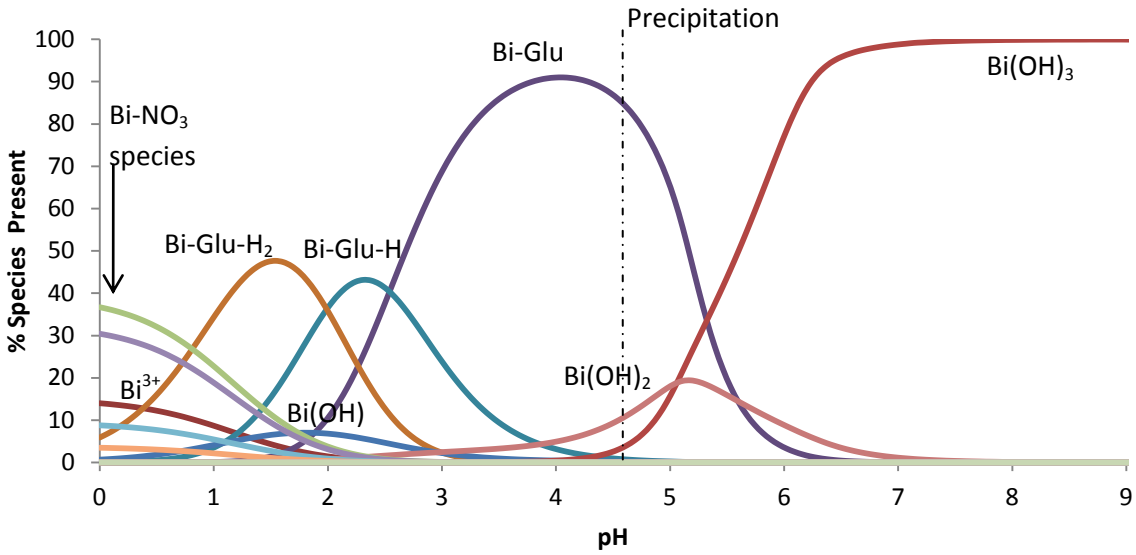

Figure 5.18: Species distribution diagram for the Bi^{3+}-Glu system where [Glu]:[Bi^{3+}] = 5000, [Bi^{3+}] = 1 x 10^{-5}M and [NO_3^-] =0.5 M. The formation constant used were those calculated using the true $E(Bi_{Free})$.

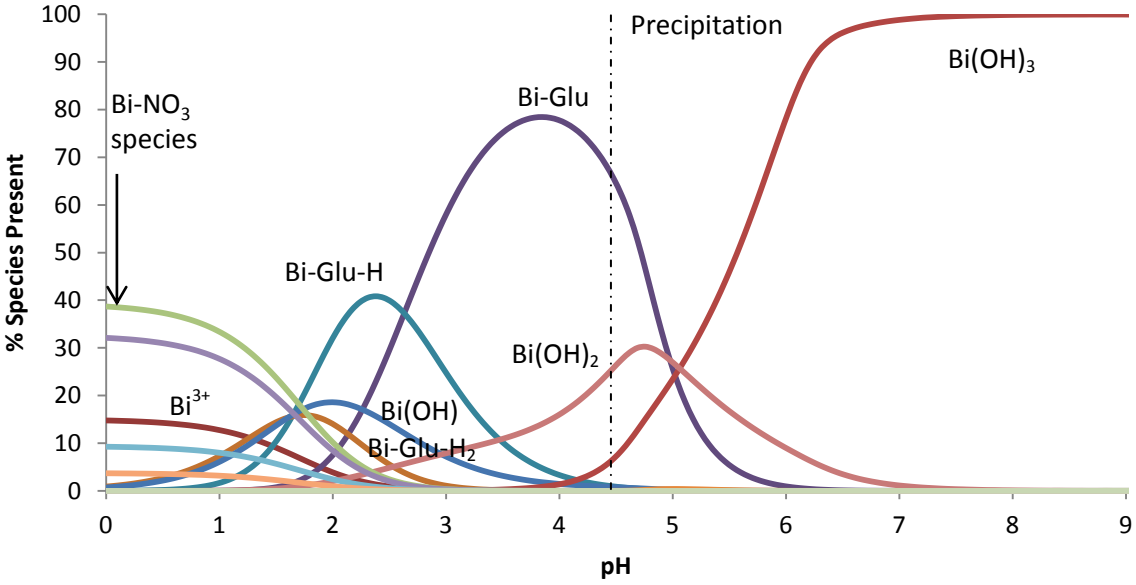

Figure 5.19: Species distribution diagram for the Bi^{3+}-Glu system where [Glu]:[Bi^{3+}] = 5000, [Bi^{3+}] = 1 x 10^{-5}M and [NO_3^-] =0.5 M. The formation constant used were those calculated using $E(Bi_{Free})_{OH}$.

The only work found in literature concerning Bi^{3+}-Glu complexation was by Singh and Srivastava.[10] They used glass electro potentiometry starting with solution containing 1 x 10^{-3} M Bi^{3+}, 4 x 10^{-3} M Glu, 0.1 M $NaClO_4$ and 1 x 10^{-3} M $HClO_4$ and then titrating with 0.2 M NaOH till about pH 11. They did not mention precipitation and found the ML, ML_2 and

ML_3 species in solution. It has been shown that Bi^{3+} is more soluble in ClO_4^- than NO_3^- solutions.[11]However, perchlorates were not used in this work as it the reduction of Bi^{3+} is not reversible in this medium.[12]Since Bi^{3+} is even less soluble in a Cl^- medium[11], the results in NO_3^- solutions should be more indicative of what could happen in the body. The log β values determined for the ML, ML_2 and ML_3 species were 10.47, 18.75 and 22.25, respectively.

Previous studies[13] conducted on glutamic acid complexation with various metal ions shows that the range log β values for complex formation is extremely broad. The only metal ion which behaved similar to Bi^{3+} was gallium(III). It was interesting to note that the solution species found were Ga-Glu-H_2, Ga-Glu-H and Ga-Glu with log β values of 16.97, 12.78 and 11.3, respectively.[13] These formation constants are similar those found for the Bi^{3+}-Glu complexes in this study. One of the most important findings was the presence of the MLH_2 complex to substantiate our finding the Bi-Glu-H_2 complex, especially since it could be contentious due to its presence in a pH region predominated by the formation of Bi^{3+} nitrate complexes. Ga^{3+} also forms an insoluble $Ga(OH)_3$ species with a log K_{sp} of -37[13] which results in precipitation just above pH 4, thus these species were also found under acidic conditions. Appendix 2 shows the species distribution diagrams of Ga^{3+} with Glu. It is interesting to note that by increasing the [Glu]:[Ga^{3+}] = 5000, as in this study with Bi^{3+} formation of insoluble $Ga(OH)_3$ is delayed to pH ~ 5.

Looking at the possible structure of the Bi-Glu-H_2 complex where Glu has only one deprotonated site, it is suggested that deprotonation of the carboxylic group with pK_a = 2.16 occurs and the Bi^{3+} coordinates to two oxygens as shown in Figure 5.20 This type of coordination was seen before in the crystal structure of the MLH species for the Cd^{2+}-picolinic acid (2-pyridinecarboxylic acid) system.[14]

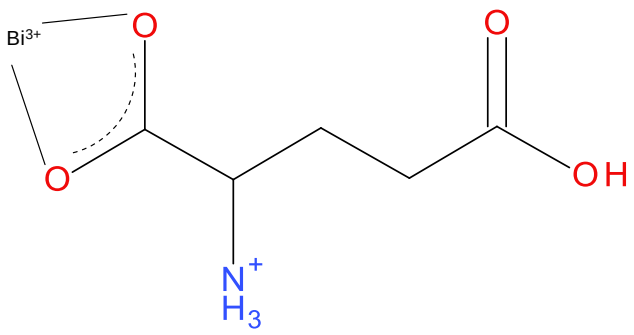

Figure 5.20: Proposed structure of the Bi-Glu-H_2 complex.

The Bi-Glu-H complex could have two possible chelation structures. Coordination could occur via both carboxylic acid groups as they are deprotonated before the amine group, as shown in Figure 5.21. However, this is not likely as a large 8-membered ring system is formed which is very unstable.

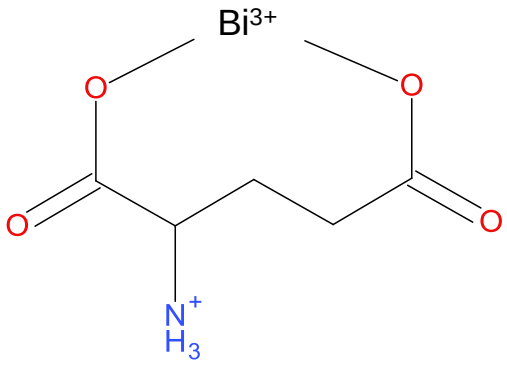

Figure 5.21: An unlikely structure for the Bi-Glu-H complex.

In literature[15] it was shown that chelation via the amide and carboxylate groups is favoured at a neutral pH, however, from the species distribution diagrams it was seen that the Bi-Glu-H species is at its maximum concentration between about pH 2-3. Another consideration is that amino acids form zwitterions which allow an internal transfer of a hydrogen ion from the –COOH group to the $–NH_2$ group to leave an ion with both positive and negative charges.[2a] The zwitterions are in equilibrium with the non-zwitterion form of the molecule. This tells us that even though one site on the amino acid is deprotonated first (i.e. at lower pH), the equilibria for the internal transfer of the hydrogen ion could

afford a complex with alternate donor sites (not only the initial sites of deprotonation). It is therefore also possible that coordination in the Glu complex occurs via the amine group and the adjacent carboxylic acid group thereby forming the structure shown in Figure 5.22. This is the most probable structure because a 5-membered ring structure is formed, the preferred ring size for the large Bi^{3+} ion. [16]

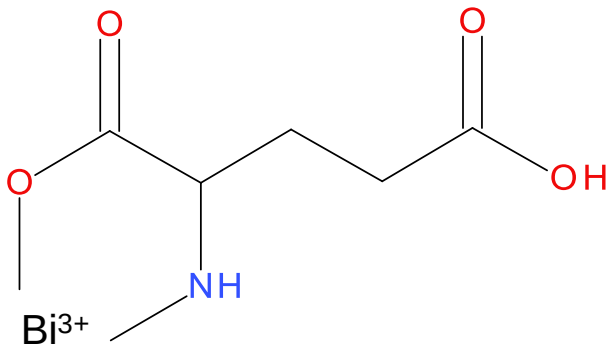

Figure 5.22: Suggested structure for the Bi-Glu-H complex.

5.5 Conclusion

The higher concentration ratios in order to force the complexation is a major determinant to complexing ability in this study. The work presented shows that although previous studies have been able to utilise low [ligand]:[metal], with the case of amino acids, a large differential in the concentration ratios are needed in order to allow complexation to occur. However, the large increase in [amino acid]:[metal] does have limitations, as too large an increase can result in a tendency toward quazi-reversible and irreversible polarographic waves. The predominant complexes found to be forming in solution were Bi-Glu-H_2, Bi-Glu – H and Bi-Glu. As described earlier, the contentious presence of Bi-Glu-H_2 in a region predominantly consisting of nitrates is an interesting complex to be found, and this species was also found in complexation studies of Glu and Ga. It was also found that slope analysis provides an efficient route in order to estimate the types of complexes formed in solution. In the case of amino acids and Bi^{3+}, the slope analysis also showcases the complex formation of different types of complexes, illustrated in Figure 5.12, where the slopes of $E_{1/2}$ were found to be averages of two separate complexation reactions. The structure of the Glu molecule also sheds light on the potential structure formed with Bi^{3+}.

Figure 5.20, Figure 5.21 and Figure 5.22 all show possible sites of coordination between Bi^{3+} and Glu, with the five-membered ring structure present in Figure 5.22 being the most likely candidate.

The successful complexation between Bi^{3+} and Glu provides us an idea as to how the Bi^{3+} ion could behave in a physiological environment rich in glutamic acid. The high concentration of Cl^- present in the body shows that Bi^{3+} will most certainly be complexed by these Cl^- ions and they will actively be in competition with any other type of ligand able to complex with Bi^{3+}. Therefore it is important to note the overall complexation of Bi^{3+} in the body is, in part, largely dependent on the environment it finds itself at different stages in the biological system. As shown earlier, an environment with high concentrations of Glu could result in Bi^{3+} complexation as observed in our study.

5.6 References

[1] Q. R. Smith, *J. Nutr.*, **2000** *130*, 1016.

[2] a) D. Voet and J. G. Voet in *Biochemistry*, *Vol. 3* Wiley, United States of America, **2004**, 736; b) A. E. Martell and R. M. Smith, NIST Standard Reference Database 46 Version 8.0, NIST Critically Selected Stability Constants of Metal Complexes,USA, **2004**

[3] C. Spanaki and A. Plaitakis, *Neurotox. Res.*, **2012** *21*, 117.

[4] M. Liguz-Lecznar and J. Skangiel-Kramska, *Acta. Neurobiol. Exp.*,**2007**, *67*, 207.

[5] L. Pauling in *College Chemistry*, *3* Freeman, San Francisco, CA, **1964**.

[6] I. Cukrowski, H. M. Marques, T. S. Mkwizu, P. P. Magampa and C. Serge, *Anal. Chim. Acta.*,**2007**, *590*, 203.

[7] I. Cukrowski, *Electroanal.*,**1997**, *9*, 699.

[8] P. Franklyn and I. Cukrowski, 3D-CFC software, University of the Witwatersrand, **2003**, *Windows Version 1.2*, (unpublished)

[9] L. D. Petit and K. J. Powell, *Academic Software, IUPAC*,**2002**.

[10] M. K. Singh and M. N. Srivastava, *J. Inorg. Nucl. Chem.*,**1972**, *34*, 2067.

[11] J. Kragten, L. G. Decnop-Weever and P. Gründler, *Talanta*,**(1993)**, *40*, 485.

[12] A. M. Bond, *Electrochim. Acta.* ,**1972**, *17* 76.

[13] a) E. A. Zekharova and V. N. Kumok, *J. Gen. Chem.*,**1968**, *38*, 1868; b) P. Bianco, J. Haladjian and R. Pilard, *J. Chim. Phys.*,**1973**, *73*, 280.

[14] C. Billing, D. C. Levendis and V. L. Vieira, *S. Afr. J. Chem.*,**2011**, *64*, 38.

[15] S. Sajadi, *Natural Science*,**2010**, *2*, 85.

[16] A. E. Martell and R. D. Hancock, *Metal Complexes in Aqueous Solutions*, Plenum Press, New York, **1996**. 46.

Chapter 6: Bi^{3+}-Histidine Complexation

6.1. Introduction

One of the most versatile and important of the amino acids in protein architecture and bioactivities is histidine (His).[1] Due to its unique chemical structure (Figure 6.1) it is able interact in a wide range of vital processes such as growth and repair of the tissues, as well as in maintaining the myelin sheath functional.[1a, 1d] His also plays role in the synthesis of both the red and white blood cells, and is thus important in some immune system responses and helps to protect the body from damage caused by radiation and in removing heavy metals from the body.[1-2]

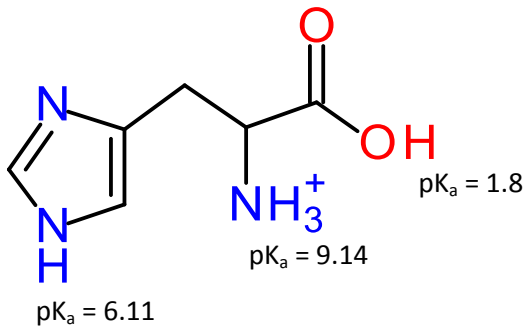

Figure 6.1: Fully protonated Histidine with pK_a^1 = 1.8, pK_a^2 = 6.11 and pK_a^3 = 9.1 at 0.5 M ionic strength and 25°C.[2]

His has been shown in recent studies to be an integral factor in the survival of the ulcer causing bacteria, H. Pylori.[3] The bacteria utilize a histidine-rich cytoplasmic enzyme (Hpn) which is responsible for the uptake and storage of Ni^{2+}, a metal ion vital in the activity of *H. Pylori*. Hpn is thought to play roles in the storage of Ni^{2+}, the donation of Ni^{2+} to other proteins and in detoxification via sequestration of excess Ni^{2+} depending on the exogenous nickel levels.[4].

Histidine contains three possible coordination sites, however, at low pH (pH < 1.8), these sites are mainly protonated. The carboxylic acid moiety, the imidazole group and the amine group have pK_a's of 1.8, 6.11 and 9.14, respectively, at 0.5 M ionic strength and 25°C.[5] In His there are two electronegative groups, the amine group and imidazole ring,

which cause the pK_a of the carboxylic acid to be very acidic. In order to ensure correct pK_a values were assigned to correct sites on His, it was decided to consider related structures or moieties. The pK_a for imidazole (Figure 6.2) is given as 7.15 at 0.5 M ionic strength at 25°C[5] close to the value of 6.11 of the moiety in His. Additionally, the ascribed pK_a's for the carboxylic acid and amine moieties tie in with that seen for Glu in Chapter 5 and glycine (2.39 and 9.54, respectively, also at 0.5 M ionic strength and 25°C[5]). Complexation to a metal ion such as Bi^{3+} would really only be possible if there is sufficient ligand deprotonated at at least one of these sites.

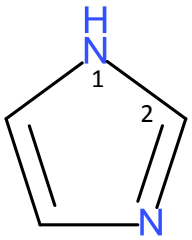

Figure 6.2: Structure of the imidazole ring which forms part of histidine.

One of the most interesting characteristics of the His structure is the imidazole sidechain. The imidazole ring is planar, satisfying the conditions for aromaticity, and is structurally related to the pyridine and pyrrole systems. The lone pair on the nitrogen in position 3 is delocalized round the ring while that on the nitrogen in position 1 is localized in the sp^2 orbital. The interactions of His with other amino acids and metallic cations in proteins can be classified into five types. (1) Cation-π interactions[6] can occur where the imidazole aromatic ring can interact with metallic or organic cations. On the other hand, the fully protonated form of His is an organic cation which can interact with other aromatic amino acids.[7] (2) π-π stacking interactions[7] are possible as the imidazole sidechain is a conjugative π-plane which can form stacking interactions with the aromatic side chains of other amino acids. (3) Hydrogen-π interactions[8] can be formed between the polar hydrogen atom of His and other aromatic amino acids in a 'T'-orientation. (4) Coordinate bond interactions[9] can occur since the basic nitrogen atom in the imidazole sidechain has a lone electron pair which can coordinate to metallic cations, such as Zn^{2+} and Ca^{2+}. (5) Hydrogen bond interactions[10] are possible through the polar hydrogen atom of the imidazole (the hydrogen-bond donor) and the basic nitrogen atom which is a hydrogen-

bond acceptor. The unique behaviour of His has been discussed in literature from different aspects.[6c, 11]

His is also the precursor of the very important amine, histamine, which is formed by its decarboxylation in the presence of the enzyme histidine decarboxylase (see Figure 6.3).[12] Histamine is released by the immune system cells in response to allergic reactions. Many sufferers find it hard to function when high levels of histamine are present, therefore anti-histamines are used to reduce the overall effect that histamines strive toward.

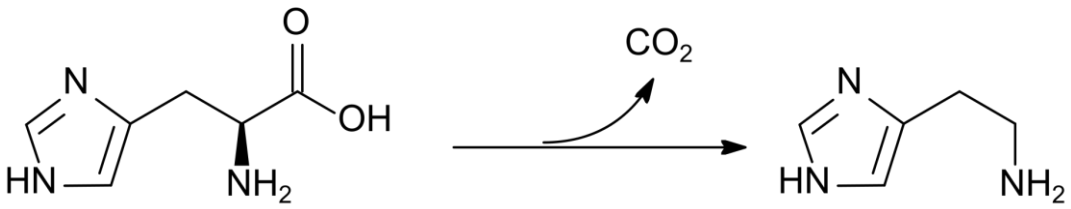

Figure 6.3: The reaction showing the removal of the carboxyl moiety in His to form histamine. [13]

Studies on the coordination of His to various metal ions have been done and the equilibrium constants obtained for metals such as Ni, Cu and Zn[14] using mainly potentiometry. As expected, no previous work was performed where Bi^{3+} was complexed with His. The conflict between the idea that *H. Pylori* uses the histidine-rich Hpn enzyme which acts as a storage for Ni^{2+}, a metal ion also vital in the activity of the bacteria, and the fact that Bi^{3+} acts as an antibacterial to *H. Pylori*,[3] makes this study intriguing and it would be interesting to compare the complexing behaviour of His with Ni^{2+} and Bi^{3+}.

6.2. Aim

The aim of this study was to investigate whether similar conditions to those used in the study of Bi^{3+}-Glu complexation would be sufficient to lead to complex formation before precipitation of Bi^{3+}. His was considered since pK_a^1 = 1.8 for the carboxylic acid moiety, compared to 2.16 for Glu, thus His should be singly deprotonated at a lower pH.

However, pK_a^2 = 6.11 for His, significantly greater than that for Glu (pK_a^2 = 4.07). It would therefore be interesting to see which of these ligands would produce more stable complexes and more successfully prevent precipitation at higher pH.

6.3. Experimental

Experiments were run as for the Bi^{3+}-Glu studies, again at three ligand to metal concentration ratios. In this case, [His]:[Bi^{3+}] of 4000, 5000 and 7005 was used and as before these experiments will be referred to as the rounded values (4000, 5000 and 7000).

6.4. Results and discussion

6.4.1. Initial data inspection

In order to investigate the complexing ability of His with Bi^{3+}, a polarographic-pH titration experiment was initially run at a [His]:[Bi^{3+}] = 2000. However, even at this high ratio, precipitation of Bi^{3+} occurred at a pH ~2. Although an unexpected result, it was decided to increase the [His]:[Bi^{3+}] to 5000. It was hoped that by adding an even larger amount of ligand, the chemical equilibrium would be forced toward complexation, as noted in our Bi^{3+}-Glu studies (Chapter 5).

As can be seen in Figure 6.4, the increase in [His]:[Bi^{3+}] to 5000 extended the solubility range of Bi^{3+} to pH ~3.1, not a very wide range. It must be stated that when the ligand was added to the system, the pH shot up to 1.7. This was due to the basic nature of the amino acid which became protonated itself using the H^+ ions from the nitric acid solution. The increase in pH is not favorable as it prevents data polarographic data being collected in the pH range of pH 1 to pH 1.7. As mentioned in Chapter 5, we should have decreased the pH by adding more HNO_3 and would be suggested as a future betterment to this study.

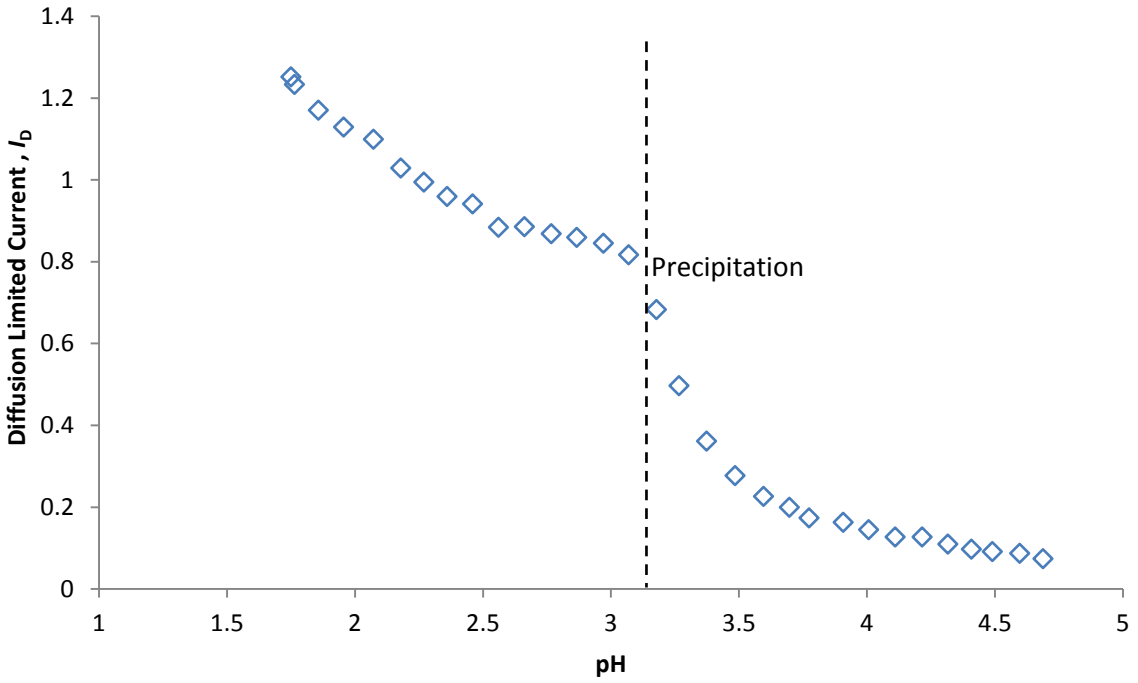

Figure 6.4: Diffusion limited current vs pH for [His]:[Bi^{3+}] = 5000, [Bi^{3+}] = 1 x 10^{-5} M, μ = 0.5 M.

In order to determine whether solubility of the Bi^{3+}-His product could be increased, we decided to increase [His]:[Bi^{3+}] to 7000.Upon adding the higher the [His], the pH of the solution jumped to ~2. Unfortunately we did not readjust it to pH 1 again resulting in about nine data points being lost (in the pH range of 1.0-1.9). Starting at higher pH did mean that the value of E_j was not significant. It can be seen from Figure 6.5 that Bi^{3+} remained soluble until pH ~3.6.

It should be noted that in order to keep the ionic strength constant, very high concentrations of ligand should be avoided. In this work, due to the low Bi^{3+} concentration of 1 x 10^{-5} M, adding 7000 times more ligand to the solution translated to 0.07 M ligand. Given the ionic strength of the solution was 0.5 M, the total ionic strength would be 0.57 M and thus the ligand makes up 12 % of the ionic strength. At higher pH where the ligand is singly deprotonated, the number of ions due to free H^+ is increased. This however is counteracted somewhat by the decrease in H^+ ions from the HNO_3 when it reacts with the OH^- from the titrant to form water (which is not ionic). Any effect on ionic strength due to changes in the extent of metal-ligand complex formation is

negligible since the Bi^{3+} concentration is significantly lower the other components present. Thus a balance had to be reached where the concentration of ligand was high enough for complex formation to occur, but not too high to affect the ionic strength significantly.

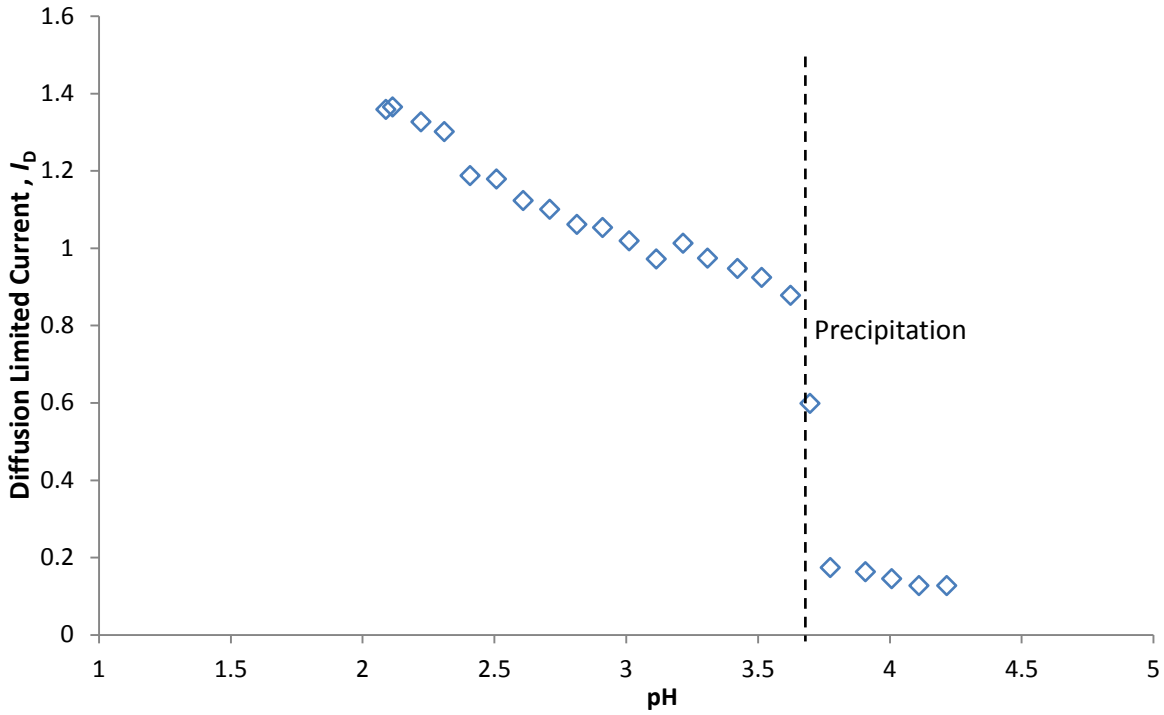

Figure 6.5: Diffusion limited current vs pH for [His]:[Bi^{3+}] = 7000, [Bi^{3+}] = 1 x 10^{-5} M, μ = 0.5 M.

Figure 6.6 shows selected DC polarograms indicating just the Bi^{3+} reduction wave obtained during the polarographic-pH titration where [His]:[Bi^{3+}] = 7000. Starting at the initial polarogram obtained at pH ~2, there is a clear negative shift in the $E_{1/2}(Bi^{3+})$ values as pH is increased which is an indication of complex formation. Figure 6.6 also highlights the current decrease due to increased dilution as more KOH solution is added to raise the pH.

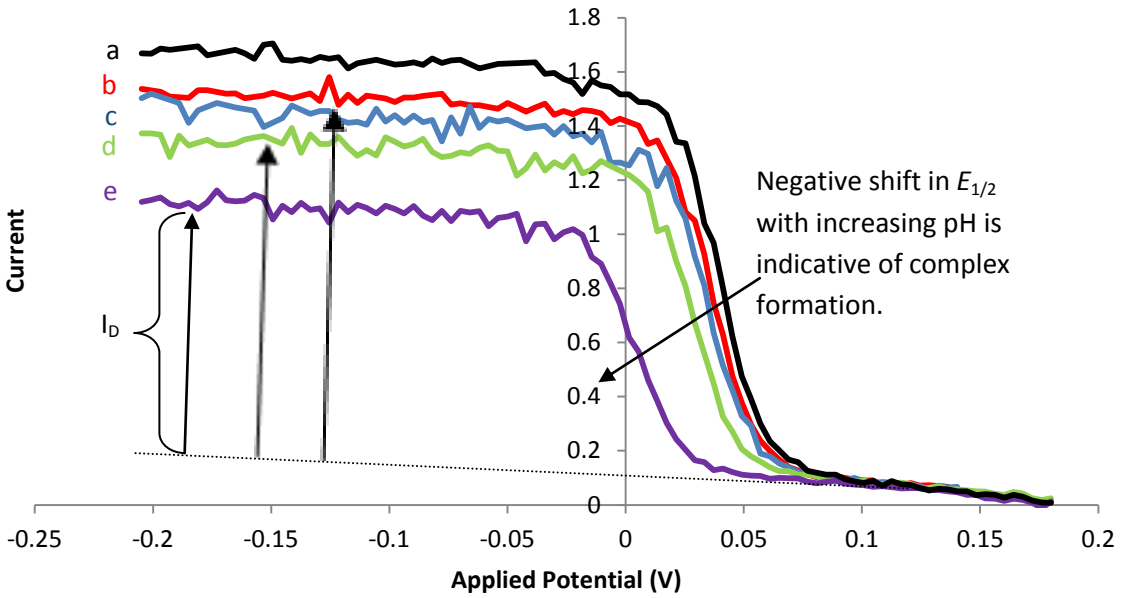

Figure 6.6: Experimental polarograms from the polarographic-pH titration conducted with [His]:[Bi^{3+}] = 7000 at different pHs, namely, a) 2.0, b) 2.3, c) 2.4, d) 2.7 and e) 3.6.

As described in Chapter 5, the $E_{1/2}$ values, obtained from fitting equation 3.4 to the polarograms, must be for reversible reduction waves (i.e. $0.9 < \gamma < 1$) to apply equation 3.1 to determine formation constants. As can be seen from Figure 6.7, the values for γ for the Bi^{3+}-His studies are above 0.9 in all cases, thereby indicating reversible reduction processes. For the two points that lie slightly above $\gamma = 1.00$, the discrepancy is due to fitting errors, but this small error does not affect the $E_{1/2}$ or I_d values significantly.

The E_j corrected $E_{1/2}$ values for Bi^{3+} for the three experiments are shown in Figure 6.8. There is a clear shift of the $E_{1/2}$ values in the negative direction, a strong indication of complex formation. For the experiments where [His]:[Bi^{3+}] = 5000 and only considering the pH range 1.7-3.0, the difference in $E_{1/2}$ values was 22 mV for L = His and 36 mV for L = Glu. This would generally imply greater complex formation for the Bi^{3+}-Glu system than the Bi^{3+}-His system if a similar type of species is formed in that pH range.

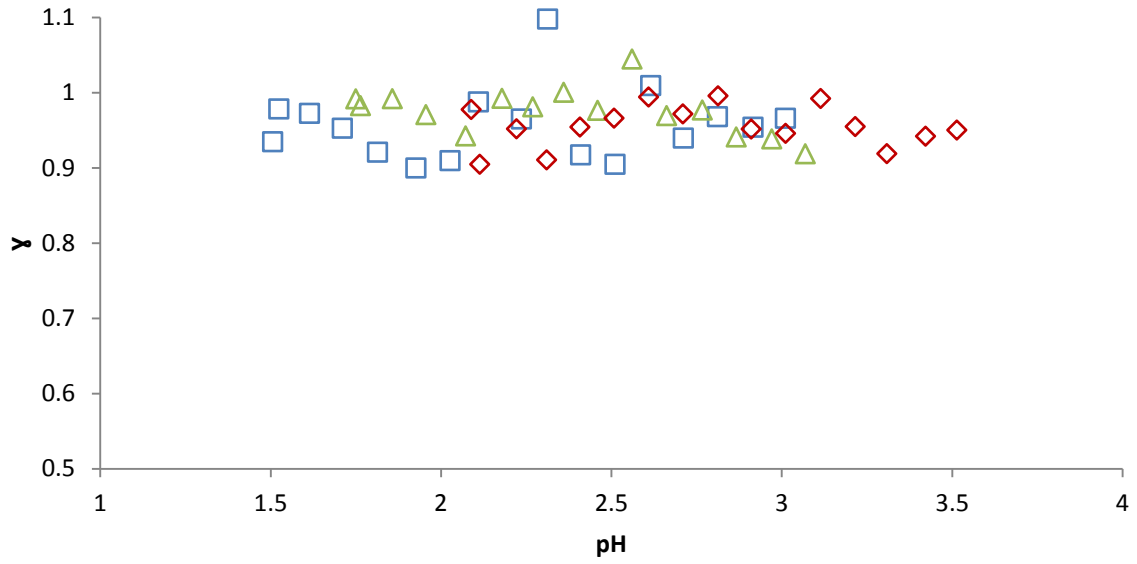

Figure 6.7: *y* vs pH for the Bi^{3+} at the three different [His]:[Bi^{3+}] of (□) 4000, (Δ) 5000 and (◇) 7000.

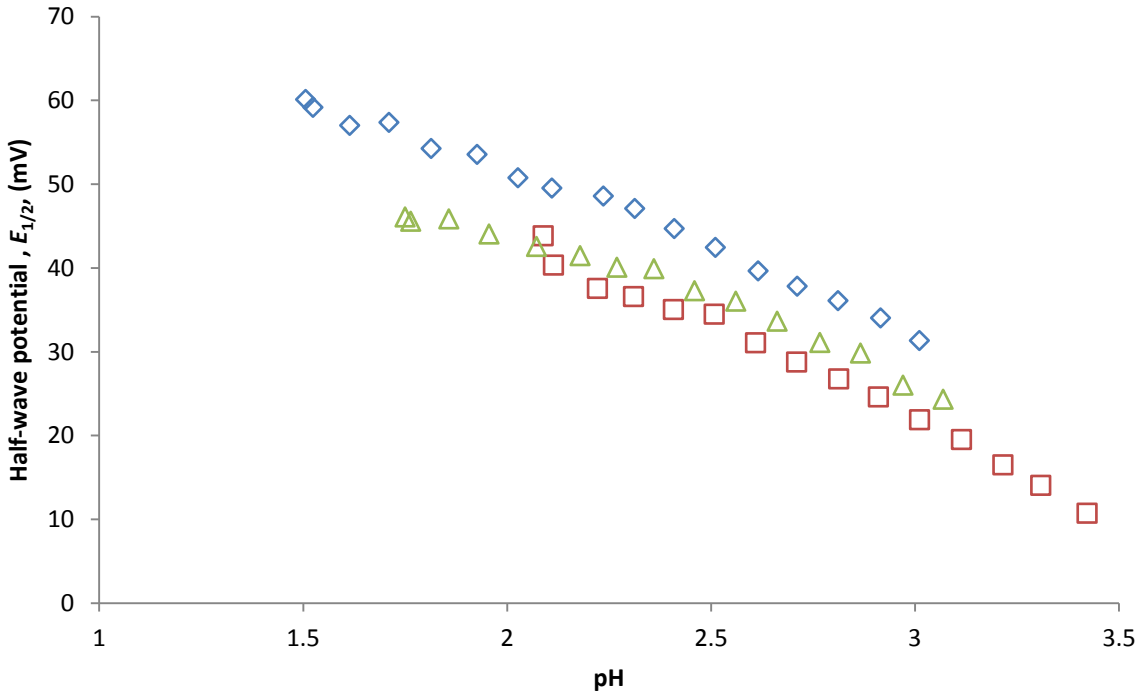

Figure 6.8: E_j corrected $E_{1/2}$ vs pH for Bi^{3+} containing His. [His]:[Bi^{3+}] = (□) 4000, (Δ) 5000 and (◇) 7000.

6.4.2 Slope analysis

Figure 6.9 gives the pictorial representation of the dominant ligand species in solution in specific pH ranges. The calculated theoretical slopes are shown and these are characteristic of the complex that is reduced at the electrode surface in that pH range. Below pH 1.8, the dominant ligand species in solution is the fully protonated His-H_3 and between pH 1.8 – 6.11, the dominant species is His-H_2. There is no need to focus on higher pHs as precipitation in these studies occurred between pH 3 - 3.6.

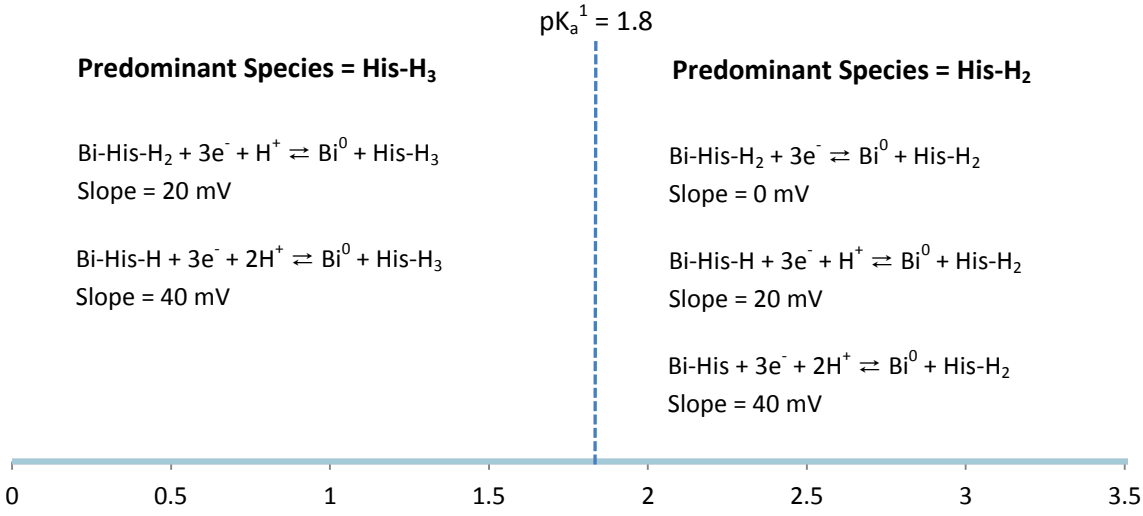

Figure 6.9: Diagram of the predominant ligand species in specific pH ranges and the calculated slopes which indicate the type of complex which could be present in solution.

When considering the E_j corrected $E_{1/2}$ values for Bi^{3+} when [His]:[Bi^{3+}] = 4000 (Figure 6.10), a slope of 16 mV was found for the data between pH 1.5 - 2. This is close to the slope of 20 mV predicted when the species Bi-His-H_2 is reduced. If the Bi-His-H species were in solution in this pH region, the slope would have been closer to 40 mV. A slope of 20 mV between pH 2 – 3 indicates the presence of Bi-His-H. If the Bi-His-H_2 complex is formed in the pH region above pH 1.8, extra protons are not required upon its reduction to form the predominant His species and so its slope is 0 mV is predicted, i.e. it is independent of pH and therefore will not affect the slope of curve.

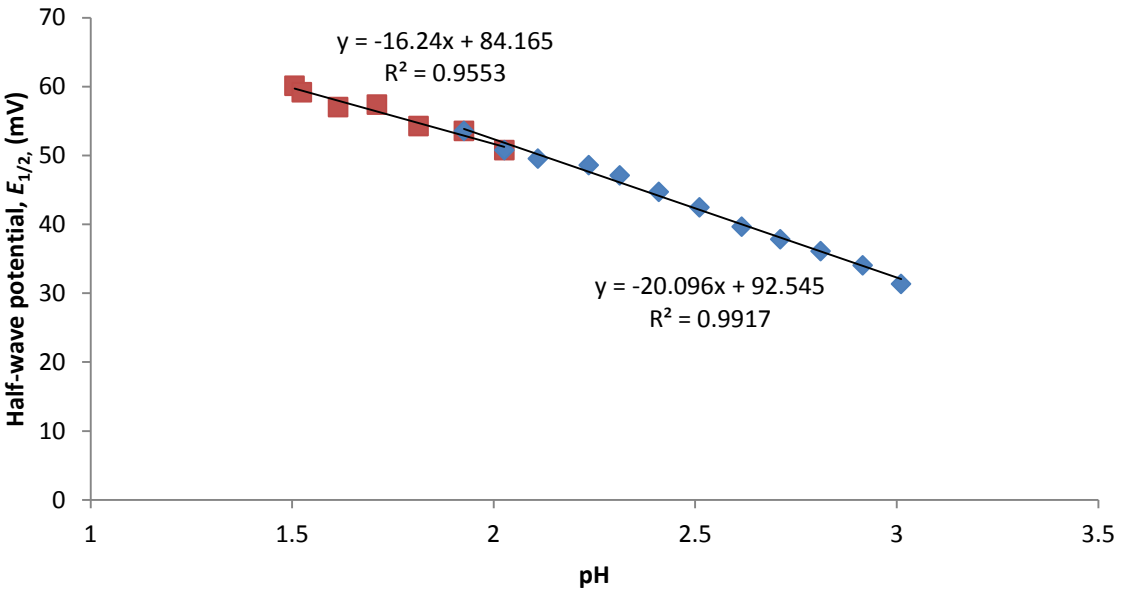

Figure 6.10: Slope analysis on the E_j corrected $E_{1/2}$ for Bi^{3+} vs pH plot with [His]:[Bi^{3+}] = 4000.

It was described earlier that upon addition of the large excess of His, the pH of the solution increased to pH 2. Slope analysis of the E_j corrected $E_{1/2}$ for Bi^{3+} vs pH when [His]:[Bi^{3+}] = 7000 (Figure 6.11) gave a slope of 20 mV between pH 2 - 3, which indicates reduction of the Bi-His-H complex. With this experiment only starting at pH 2 (due to the high concentration of His added), species formed below pH 2 would not be detected, such as the Bi-His-H_2 complex predicted in the [His]:[Bi^{3+}] = 4000 experiment. Above pH 3 the slope increased to 29 mV which could indicate that both the Bi-His-H and the Bi-His complexes were together in solution. The Bi-His was not predicted before as it would only form at the highest pHs where precipitation had already occurred in previous experiments. The Bi-His-OH species was also considered since precipitation occurred straight after the formation of the new species. The reduction reaction that occurs, however, would be expected to be Bi-His-OH + $3e^-$ + $3H^+$ ⇄ Bi^0 + His-H_2 +H_2O in the pH range 3 – 3.6 thereby giving a slope of 60 mV which is significantly greater than that observed

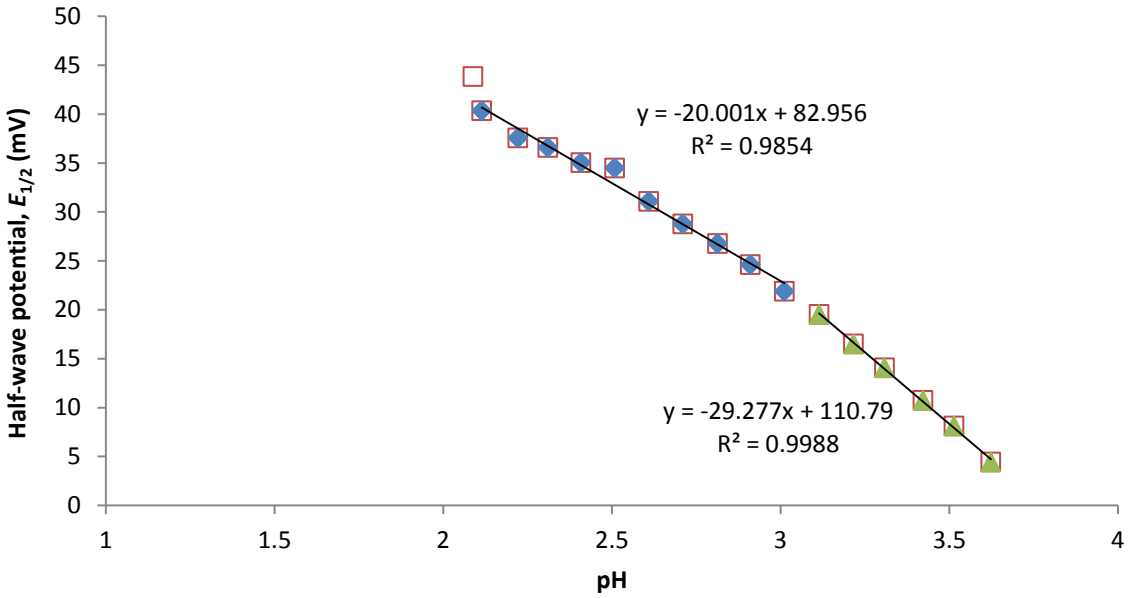

Figure 6.11: Slope analysis on the E_j corrected $E_{1/2}$ for Bi^{3+} vs pH plot with [His]:[Bi^{3+}] = 7000.

6.4.3. Determining Bi-His complexes and respective log β

Figure 6.12 shows the plot of the ECFCs and CCFCs which were calculated for [His]:[Bi^{3+}] = 4000 data using both the $E(Bi_{free})$ and $E(Bi_{free})_{OH}$ values. Since the difference between the values of $E(Bi_{free})$ and $E(Bi_{free})_{OH}$ was 9 mV, the only difference between the two ECFCs is a 9 mV shift for each point in the plot. As predicted from the slope analysis, both the Bi-His-H_2 and Bi-His-H complexes had to be included in the model to provide a good fit. The formation constants determined (see Table 6.1) when calculating the ECFC using $E(Bi_{free})$ are therefore larger than those when using $E(Bi_{free})_{OH}$ due to the larger in the former case. As with complexes formed by Bi^{3+} and Glu, the formation of protonated Bi-His complexes are favoured under these acidic conditions.

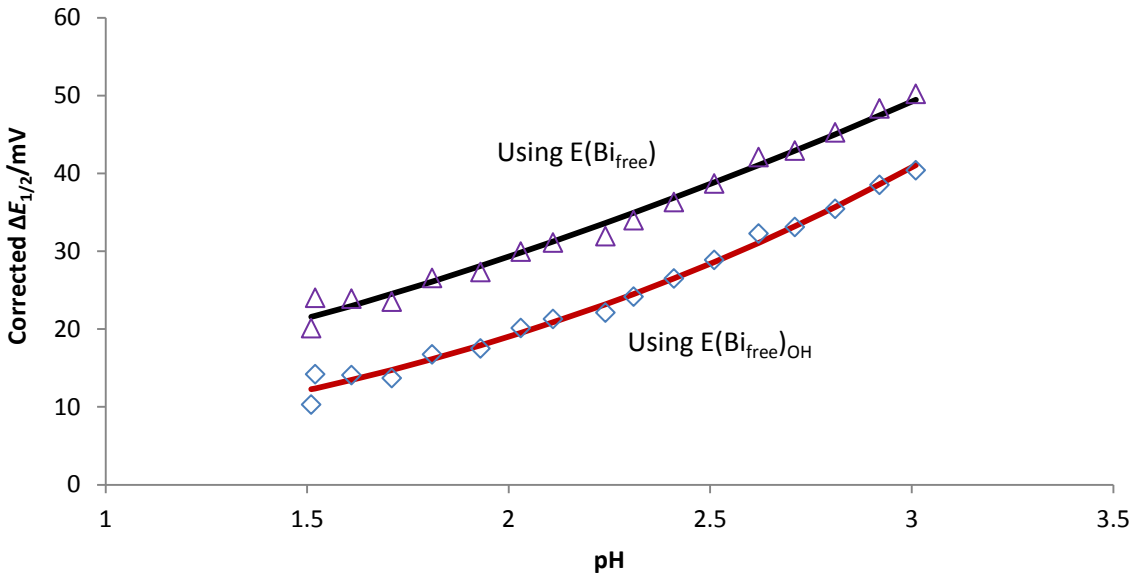

Figure 6.12: The ECFCs calculated using either $E(Bi_{free})$ and $E(Bi_{free})_{OH}$ values and the CCFCs determined by including the Bi-His-H_2 and Bi-His-H complexes in the species model.

In order to fully determine whether the complexes were indeed contributing to the formation of the curves, it was decided to fit the ECFC by either taking only the formation of the Bi-His-H complex or only the Bi-His-H_2 complex into account. As an example, Figure 6.13 shows the ECFC calculated using the $E(Bi_{free})_{OH}$ value and fitted when accounting for only one of the species at a time. The standard deviation of fitting was 2.61 when only Bi-His-H was used, 1.37 when only Bi-His-H_2 was used and 0.82 when both complexes were included. The log β values obtained were 15.36 $\pm$ 0.05 for Bi-His-H and 17.41 $\pm$ 0.05 for Bi-His-H_2, both values being larger than that obtained when both species were incorporated into the model (see Table 6.1). When only a single species is used in calculating the CCFC, an averaging effect occurs throughout the pH range giving CCFCs that do not fit well in the extreme pH regions of the plot.

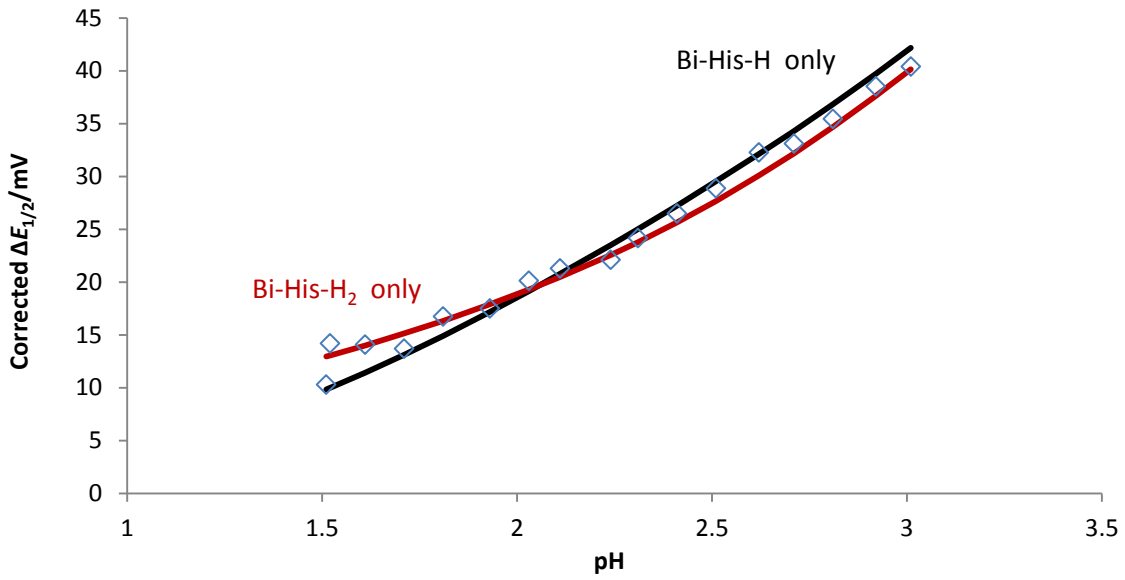

Figure 6.13: The ECFC (points) calculated using $E(Bi_{free})_{OH}$ and the CCFCs (lines) determined taking only the Bi-His-H complex or only the Bi-His-H_2 into account at a time.

To fully understand the implication of using the $E(Bi_{free})$ and $E(Bi_{free})_{OH}$ values to calculate the formation constants, the species distribution diagrams for [His]:[Bi^{3+}]= 4000 were plotted to show the comparison between using the two sets of formation constants (Figure 6.14). The log β values for Bi-His-H_2 and Bi-His-H are larger when $E(Bi_{free})$ is used and the percentage of the species present in solution are predicted to be greater than when using $E(Bi_{free})_{OH}$ to determine the log β values. Of interest are the Bi^{3+} nitrate species which were included in the species distribution diagrams. At pH 1.5 (the starting pH in the experiment), there is a significant amount of the Bi^{3+} nitrates in solution and at pH 3 (just before precipitation) the Bi^{3+} nitrates are almost negligible. Thus in the pH range of the experiment, formation of Bi^{3+} nitrates are definitely in competing equilibria with the formation of the Bi^{3+}-His complexes, but limitations in the 3D-CFC software meant that the nitrate species could not be included in the model when determining the log β values for the Bi^{3+}-His complexes. As discussed in Chapter 5 and seen in Figure 5.14, using the $E(Bi_{free})_{OH}$ value to calculate formation constants for data below pH 1 and using the $E(Bi_{free})$ value to calculate formation constants for data above pH 3 will give the best results. Between pH 1-3, the region in which we were working, the actual log β values will be somewhere between the two sets of results obtained. In the species distribution diagrams it is seen that the Bi-His-H_2 complex forms in solution nearer to pH 1, thus the

log β value found using $E(Bi_{free})_{OH}$ would be closer to the real value and since the Bi-His-H complex it is formed nearer to pH 3, the log β value found using $E(Bi_{free})$ would be more representative in this case. The species distribution diagrams thus showed us which species are present in a solution at a specific pH as well as indicate the other potential complexes which are in competition with the formation of the Bi-His complexes. Therefore allowing us to establish an idea at which the pH our calculated complexes begin to form.

Table 6.1: Calculated log β values for the formation of the Bi^{3+}-His complexes using using both the $E(Bi_{free})$ values and the 3D-CFC software. (Charges were omitted in equilibria reactions.)

[L]:[Bi^{3+}]	**4000**	**5000**	**7000**
(a) using $E(Bi_{Free})$		Log β	
Bi^{3+} + L + H_2 ⇄Bi-LH_2	17.92 ± 0.06	18.01 ± 0.05	-
Bi^{3+} + L + H ⇄ Bi-LH	16.17 ± 0.03	15.88 ± 0.04	16.18 ± 0.02
Bi^{3+} + L ⇄ Bi-L			12.48 ± 0.12
Overall Fit	1.06	0.16	1.67
(b) using $E(Bi_{Free})_{OH}$			
Bi^{3+} + L + H_2 ⇄Bi-LH_2	17.26 ± 0.15	17.50 ± 0.04	-
Bi^{3+} + L + H ⇄ Bi-LH	14.97 ± 0.15	-	15.60 ± 0.03
Bi^{3+} + L ⇄ Bi-L			10.59 ± 0.34
Overall Fit	0.82	0.28	1.45

Figure 6.14 shows the a comparison between the species distribution diagrams for the study where [His]:[Bi^{3+}]= 4000. As can be seen, the formation of the Bi-His-H_2 and Bi-His-H species is more favoured when $E(Bi_{Free})$ was used to calculate the log β values for the respective complexes, with the species percentage of Bi-His-H_2 = 38% and the Bi-His-H =

75%. However, when $E(Bi_{Free})(OH)$ was used, the percentage of species present for the respective complexes drops to below 20 %. This once again illustrates the limitations in software used to calculate log β values. 3DCFC is unable to incorporate the formation of Bi-OH and Bi-NO_3 complexes simultaneously. It is also evident that when $E(Bi_{free})_{OH}$ is used, the log β values are smaller than those calculated when $E(Bi_{free})$ is utilized. The difference between the two is that when $E(Bi_{free})$, the complexation due to NO_3^- complexes is taken into account, hence increasing formation of Bi-His complexes. It must be noted however, that the formation of Bi-NO_3 and Bi-OH complexes begin to form from pH 0 and these actively compete with the formation of our Bi-His complexes.

For the [His]:[Bi^{3+}]= 5000, it can be seen from Table 6.1 that the complexes which have been calculated to have formed are the Bi-His-H_2 and Bi-His-H with log β values of 18.01 and 15.88 respectively for $E(Bi_{Free})$. The Bi-His complex was unable to be calculated possibly due to it forming in such low amounts and unable to overcome the large competition with Bi(OH) species since a [His]:[Bi^{3+}] = 5000. It can be seen in Figure 6.15, that the formation of the insoluble $Bi(OH)_2$ complex from pH ~2 . The result illustrates that even at a [His]:[Bi^{3+}] = 5000, the ratio is not large enough to fully favour the complexation of Bi-His complexes. Using $E(Bi_{Free})_{OH}$, the only complex determined to be forming was that of Bi-His-H_2 and Figure 6.15 b) shows that initially there is a large competition for the Bi^{3+} ion with nitrates. Unfortunately, this has a large effect on the percentage of Bi-His-H_2 species formed, with the percentage of species present at approximately 38% at pH ~1.7. The formation of the insoluble Bi(OH) species once again plays a large role in competing with His for the Bi^{3+} ion leading to less soluble Bi^{3+} complexes forming and precipitating out of solution.

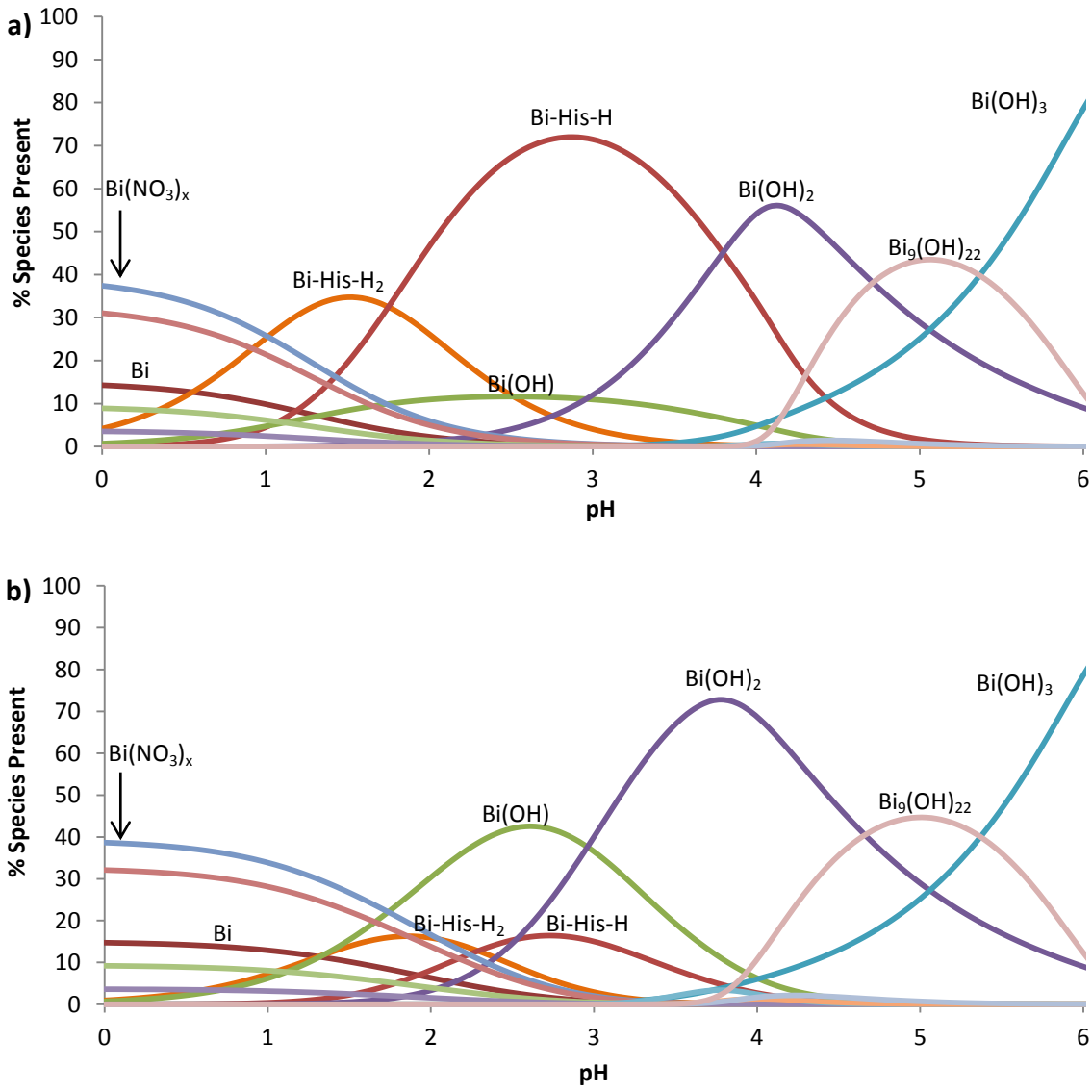

Figure 6.14: Species distribution diagram for [His]:[Bi^{3+}] = 4000, [Bi^{3+}] = 1 x 10^{-5} M and [NO_3^-] =0.5 M. The log β values were calculated using a) $E(Bi_{free})$ and b) $E(Bi_{free})_{OH}$ and the values used are for the 4000 ratio only (Table 6.1).

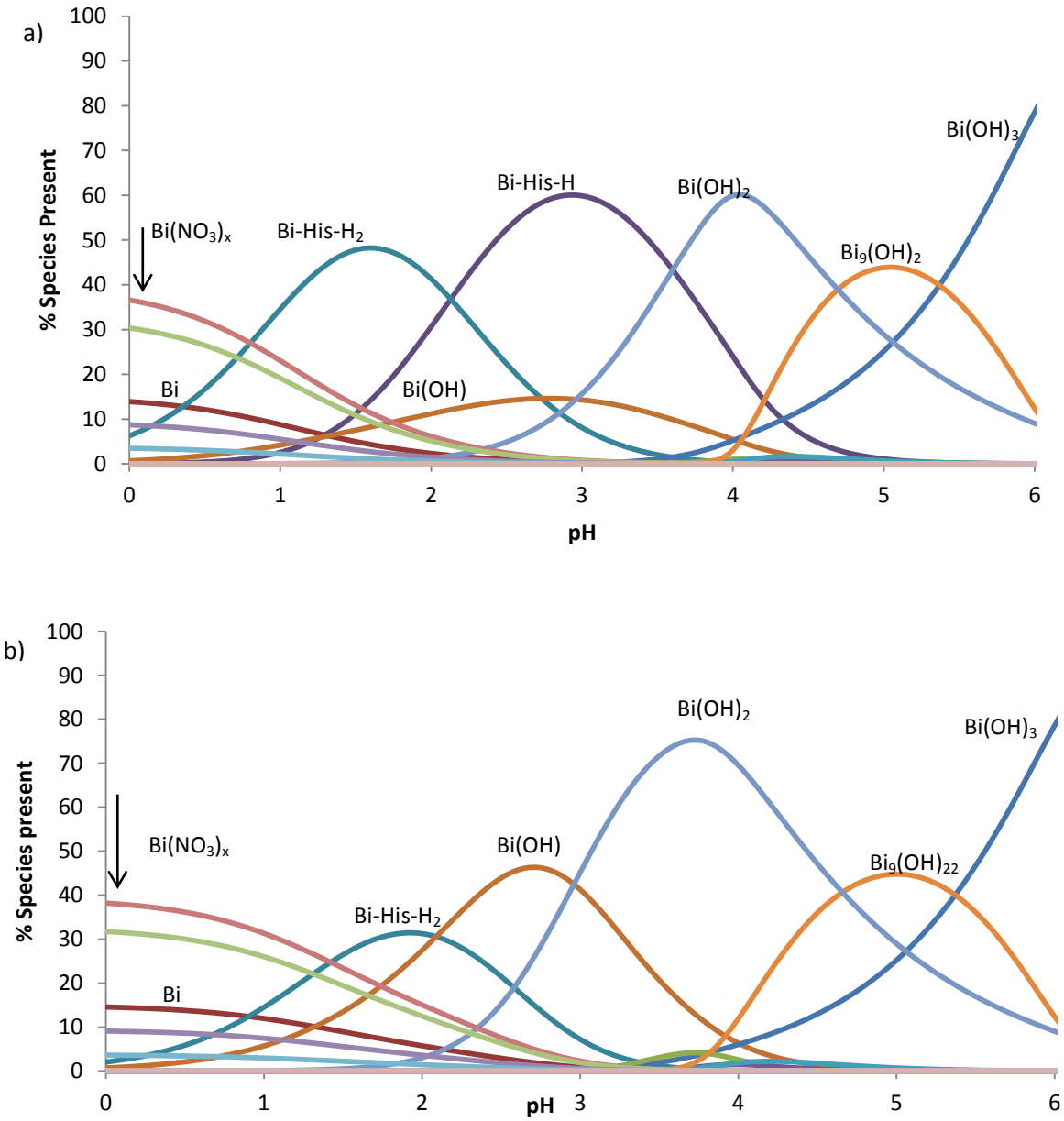

Figure 6.15: Species distribution diagram for [His]:[Bi^{3+}] = 5000, [Bi^{3+}] = 1 x 10^{-5} M and [NO_3^-] =0.5 M. The log β values were calculated using a) $E(Bi_{free})$ and b) $E(Bi_{free})_{OH}$ and the values used are for the 5000 ratio only (Table 6.1).

From the experiment where [His]:[Bi^{3+}] = 7000, the ECFC could be fitted when including the Bi-His-H and Bi-His complexes as predicted by the slope analysis. The Bi-His-H_2 complex could not be included in the model as log β values would not refine, probably since the concentration of Bi-His-H_2 was too low as this experiment was only started at pH ~2. In order to determine this log β value at this ratio the solution will have to be acidified first and data obtained at lower pHs. The ECFC and CCFC are plotted in Figure

6.16 (when using the true $E(Bi_{free})$ value in the calculation) and can be compared to that determined for the [His]:$[Bi^{3+}]$ = 4000 (and 5000) experiment. As expected, larger shifts in the corrected potential are seen for the higher [His]: $[Bi^{3+}]$.

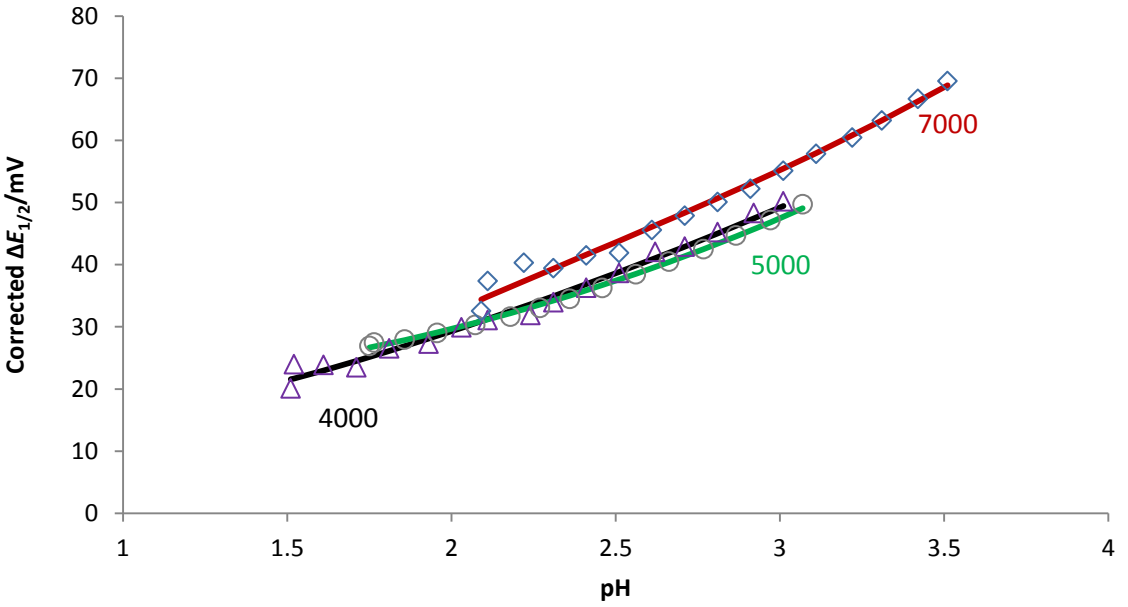

Figure 6.16: The ECFCs calculated using the true $E(Bi_{free})$ value and the corresponding CCFCs (which produced the results in Table 6.1) for the experiments at the [His]:$[Bi^{3+}]$ values indicated.

Plotting a species distribution diagram for [His]:$[Bi^{3+}]$ = 7000 would mean that not only must the formation of Bi-His-H and Bi-His be taken into account, but the Bi-His-H_2 complex must also be included as it is formed at low pH. This is done in Figure 6.17 where results were calculated using both the $E(Bi_{free})$ and $E(Bi_{free})_{OH}$ values. It can be seen that the formation of the Bi-His is only significant for the log β values determined using the true $E(Bi_{free})$ and since it only starts forming to a significant concentration above pH 3, it is expected that this log β value would be more accurate. The log β value for the Bi-His-H_2 complex would be more accurate when using the $E(Bi_{free})_{OH}$ value as discussed before.

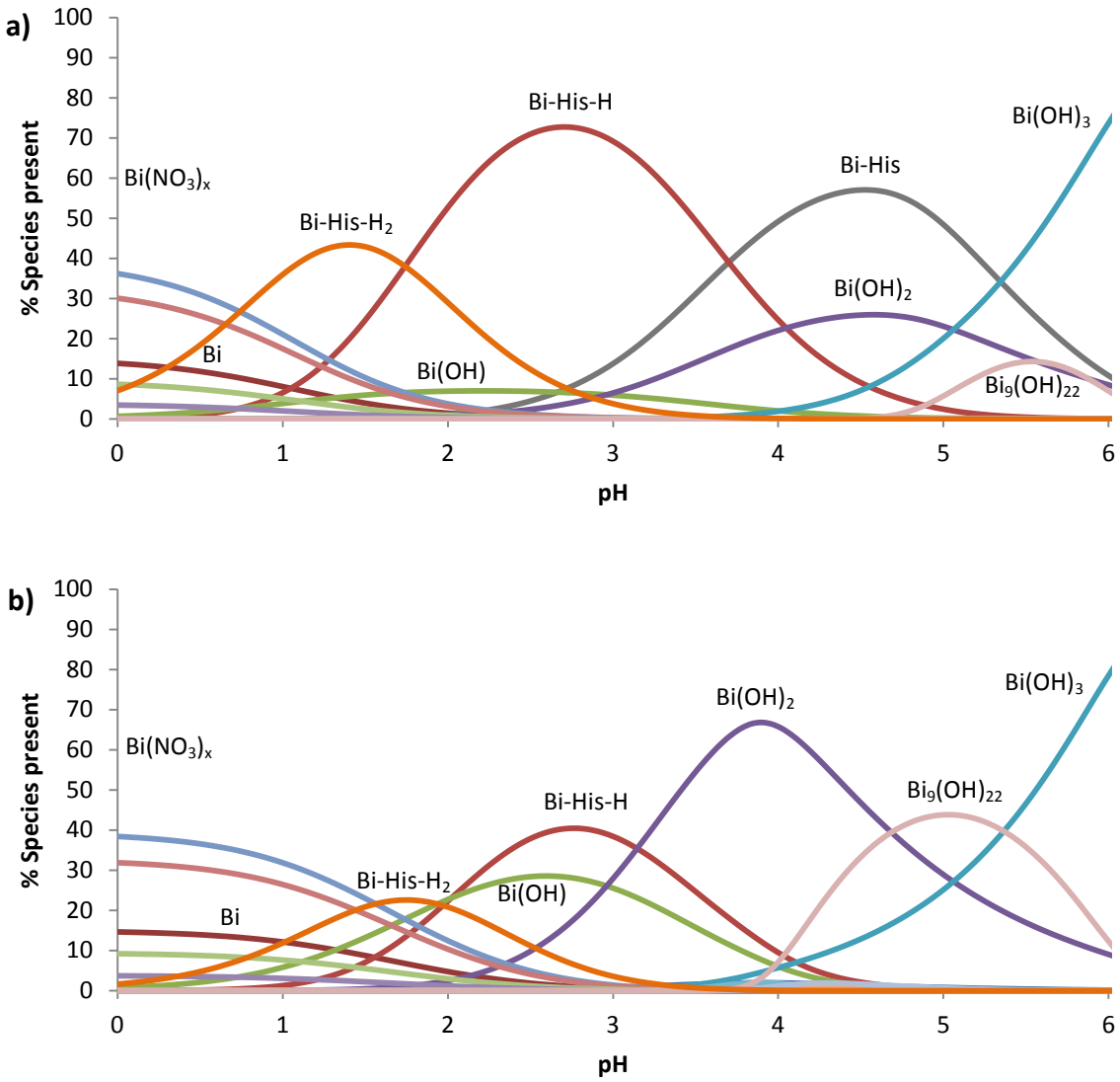

Figure 6.17: Species distribution diagrams for [His]:[Bi^{3+}] = 7000, [Bi^{3+}] = 1 x 10^{-5} M and [NO_3^-] =0.5 M. The log β values were calculated using a) $E(Bi_{free})$ and b) $E(Bi_{free})_{OH}$ and the values used are for the 4000 ratio for MLH_2, the 7000 ratio for ML and the average for the 4000 and 7000 ratios for MLH (Table 6.1).

Since the first pK_a of the His molecule is 1.82, it is likely that the complex formation is occurring via the carboxyl moiety of His. As with the formation of the Bi-Glu complexes, the low pK_a of the amino acid carboxyl groups seems to be most favoured. As described in literature, the pK_a is the point at which 50% of the acid is deprotonated, and so at a pH of 1.82, 50% of the [His] is deprotonated and so results in the higher potential in complexing ability with Bi^{3+}.

Studying the species distribution diagrams of the Bi-His complexes at different [His]:[Bi^{3+}], we are able to see that there are two potential complexes which form due to the deprotonated carboxyl moeity of the His molecule. Due to the high [His]:[Bi^{3+}], more deprotonated molecules of the His are preset, and are thus able to complex with the Bi^{3+}.Due to the structural similarities of His, it is thus proposed that the structure of the Bi-His complexes are similar to those proposed in Chapter 5 for the Bi-Glu complexes. With the pK_a values which were shown earlier, the deprotonation of the carboxlic acid moiety and amine group of the His molecule could allow for coordination to Bi^{3+} via a five-membered ring, a structure which is more stable than other complexes which could form.

Previous studies[5] have been completed where His was complexed metal ions such as Cu(II), Zn(II), Cd(II), Ni(II) and Pb(II). One of the most interesting comparisons would be the complexation of His with the Pb^{2+}, which is isoelectronic to Bi^{3+}. Studies[5] conducted with the Pb^{2+} ion were conducted in ionic strength of 0.1 M and 3.0 M at 25^{o}C. Although it was that the species formed were Pb-His, Pb-$(His)_2$, Pb-$(His\text{-}H)_2$ and Pb-$(His_2\text{-}H)$ with log *K* of 5.94, 10.11, 6.22, and 7.04 respectively[5]. These values are much smaller than those determined for our Bi-His-H_2 and Bi-His-H complexes (Table 6.1). Due to the similarity of the Ga^{3+} ion to Bi^{3+} in terms of Glu, as was seen in Chapter 5, it was also decided to compare the formation constants of Ga^{3+} with His. Interestingly, Ga^{3+} was shown to form Ga-His, Ga-His-H and Ga-His-H_2 complexes[15], the same complexes seen to form in this study with Bi^{3+}. Even more interesting was the fact that the formation constants were calculated to be 12.50, 15.15 and 18.12[15] respectively at 3.0 M NO_3 at 25^{o}C, very similar to the values presented in Table 6.1 (12.48 for ML, 16.07(average) for MLH and 17.97 for the MLH_2 complex). The Ga^{3+} ion seems to behave in a very similar manner to Bi^{3+} when complexed with amino acids as was shown in Chapter 5. One of the most important findings in other metal-ion-His complex studies is that with the varying ionic strength the log *K* values differed and since our studies were conducted at constant ionic strength of 0.5 M, we found different formation constants for our respective complexes. We also found different types of complexes forming than those reported in literature, and the most important reasons for this could be that the pH range in which our study was completed was very low and highly acidic (pH 1-pH 4). At these low pH values, the

carboxyl group of His becomes best suited to form the complex with Bi^{3+} hence leading to the large formation constants which have been determined. Previous studies have been able to complex the His molecule with other metal ions via the imidazole and amine groups via a strong chelation effect, but once again these complexes are favoured at higher pH, and we are unable to reach these pH ranges due to the insolity of Bi^{3+}. No previous Bi-His complex formation studies wherein formation constants are reported were found. The low pH range solubility of Bi^{3+} does prove a huge hurdle to overcome.

6.5 Conclusion

The results presented show that the complexation of an amino acid to Bi^{3+} has complex chemistry associated with it. Initial studies (Chapter 4) have shown that at low [His]:[Bi^{3+}] (=100), complexation is not significant enough to allow the Bi^{3+} to form soluble Bi-His. However, by increasing [His]:[Bi^{3+}] to values greater than 4000 allowed the formation of soluble Bi-His complexes and therefore increasing the pH range of Bi^{3+} to ~3.5. Although the [His]:[Bi^{3+}]= 700 used, the reversibility of the polarographic waves remained within the accepted range of reversibility (0.9-1), indicating that the large His concentration does not affect the reversibility of Bi^{3+}, unlike Glu in Chapter 5 and Glutamine to a larger extent in Chapter 7.

The predominant species determined to be forming in solution are the Bi-His-H_2, Bi-His-H and Bis-H complexes with log β values of 17.97, 16.08 and 12.48 respectively at 0.5M ionic strength at 25^{o}C. Slope analysis of the $E_{1/2}$ values showed that the species forming could be estimated from the slope of the $E_{1/2}$ vs pH (Figure 6.10 and Figure 6.11). The slope analysis also showed the formation of Bi-His-H_2 complex, albeit in small amounts when [His]:[Bi^{3+}] =7000 and it was not possible to calculate the associated log β. The addition of [His]:[Bi^{3+}] = 7000 already showed an increase in the overall ionic strength of the solution so by increasing [His]:[Bi^{3+}] could result affecting this ionic strength even more. One of the major improvements to this work would be to adjust the pH of the solution to pH ~1, thereby allowing more of the Bi-His-H_2 complexes to form in larger quantities for the log β to be determined.

Studies where the complexation of Ga^{3+} with amino acids have once again showed similarities to the results we have obtained in this study with Bi^{3+}. The complexes formed when His complexes with Ga^{3+} are reported to be the same as the complexes we have identified in this study with log β values also corresponding surprisingly well. The results once again show that the Ga^{3+} ion behaves in a very similar manner to Bi^{3+} when placed in a situation where complexation is required with an amino acid, as was seen in Chapter 5. Our studies have therefore shown that Bi^{3+} is able to complex quite strongly with His at low pH levels, however the concentration ratio of [His]:[Bi^{3+}] needs to be significantly high (>4000 times).

6.6. References

[1] a) F. Li, D. Fitz, F. D.G. and B. M. Rode, *Amino Acids*,**2010**, *38*, 287; b) M. Remko, D. Fitz and B. M. Rode, *Amino Acids*,**2010**, *39*, 1309; c) K. Uchida, *Amino Acids*,**2003**, *25*, 249; d) A. Martinez, *Amino Acids*,**1995**, *9*, 285.

[2] A. Reddy and G. N. Sastry, *J. Phys. Chem.*,**2005**, *109*.

[3] R. Ge, X. Sun, D. Wang, Q. Zhou and H. Sun, *Biochim. Biophys. Acta.*,**2011**, *1813*, 1422.

[4] a) G. Ruiguang, S. Xuesong, G. Qing, R. M. Watt, J. A. Tanner, B. C. Y. Wong, H. H. Xia, H. Jian-Dong, H. Qing-Yu and S. Hongzhe, *J. Bio. Inorg. Chem.*,**2007**, *12*, 831; b) H. Li and H. Sun, *Curr. Op. Chem. Bio.*,**2012**, *16*, 74.

[5] A. E. Martell and R. M. Smith, NIST Standard Reference Database 46 Version 8.0, NIST Critically Selected Stability Constants of Metal Complexes,USA, **2004**

[6] a) L. K. Engerer and T. P. Hansua, *J. Org. Chem.*,**2011**, *76*, 42; b) A. Reddy and G. N. Sastry, *J. Phys. Chem.* ,**2005**, *109*; c) U. D. Priyakumar, M. Punnagai, G. P. Krishna Mohan and G. N. Sastry, *Tetrahedron*,**2004**, *60*, 3037.

[7] a) P. Mignon, S. Loverix, J. Steyaert and P. Geerlings, *Nucl. Acid. Res.*,**2005**, *33*, 1779; b) G. Stefan, *Angew. Chem. Int. Ed. (English)*,**2008**, *47*, 3430.

[8] a) R. M. Hughes and M. L. Walters, *J. Am. Chem. Soc.*,**2006**, *128*, 13586; b) E. A. Meyer, R. K. Castellano and F. Diederich, *Angew. Chem. Int. Ed.(English)*,**2003**, *42*, 1210.

[9] S. O. Kang, M. A. Hossain and K. Bowman-James, *Coord. Chem. Rev.*,**2000**, *250*, 3038.

[10] a) M. Henry, *Chem. Phys. Chem.*,**2002**, *3*, 561; b) M. Henry, *Chem. Phys. Chem.*,**2002**, *3*, 607.

[11] L. J. Andrews and R. M. Keefer in *Molecular complexes in organic chemistry.*, *Vol.* Holden-Day, San-Francisco, **1964**.

[12] D. Voet and J. G. Voet in *Biochemistry*, *Vol. 3* Wiley, United States of America, **2004**, 736.

[13] Histamine, http://www.en.wikipedia.org/wiki/Histamine, (Date Accessed: 2014-05-03)

[14] R. Leberman and B. R. Rabin, *Trans. Far. Soc.*,**1959**, *55*, 1660.

[15] P. Bianco, J. Haladjian and R. Pilard, *J. Less-Common Met.*,**1978**, *58*, 58.

Chapter 7: Bi^{3+}-Glutamine Complexation

7.1. Introduction

Glutamine (Gln) is the most abundant free amino acid in the body.[1] Gln is classified as uncharged, since it contains an amide bearing side chain. Gln is synthesized via the amidation of glutamic acid (Chapter 5). The enzyme known as glutamine synthetase catalyses the formation of Gln.[2] Glutamine synthetase allows adenosine triphosphate to be hydrolysed to adenosine diphosphate and the ɣ-glutamylphosphate intermediate is formed. An amino donor group from the synthetase then reacts with the intermediate in order to form Gln (Figure 7.1). Gln contains three electron-donating centres.[3] The value of pK_a^1 for Gln 2.14 at 25°C and 0.5 M ionic strength[4], which is similar to the carboxylic acid moieties present in glutamic acid (Chapter 5) and histidine (Chapter 6) as the carboxylic acid moiety in all amino acids have structural similarities. pK_a^2 = 8.94 (at 25°C and 0.5 M ionic strength)[4] and is associated with the amino group adjacent to the carboxylic acid. The amide group, like that of asparagine, dissociates at a pH near the limit of the ionic product of water and thus the dissociation cannot be detected in aqueous solution.[5]

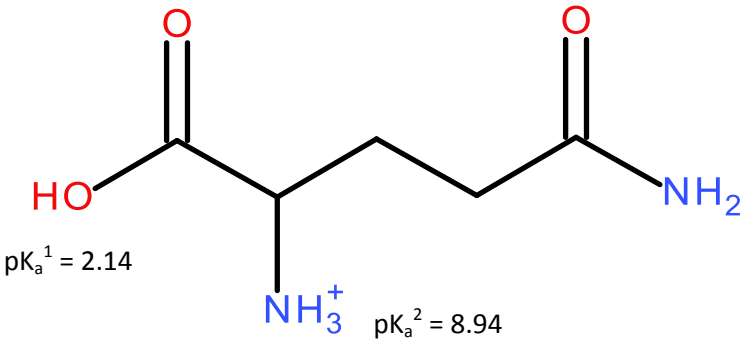

Figure 7.1: Structure of fully protonated Gln.

Gln has been described as the amino-group donor in the formation of many biosynthetic products, as well as being the storage form of ammonia. Gln also serves as a vehicle for transporting ammonia in a nontoxic form from peripheral tissues to visceral organs where

the ammonia can be excreted as ammonium ions in the kidneys or converted to urea in the liver. The importance of Gln within the biological system is thus paramount to the functioning and survival of an organism. Gln is produced in the muscles and is distributed by the blood to the organs that need it. It has also shown to be a helpful agent in the gut function, the immune system and other essential processes in the body, especially in times of stress. It is also important for providing "fuel" (nitrogen and carbon) to many different cells in the body.[5b]

One of the most important aspects of Gln in the human body is that it performs a central role in nitrogen metabolism. After surgery or traumatic injury, nitrogen is necessary to repair the wounds and keep the vital organs functioning. About one third of this nitrogen comes from Gln.[5b] If the body uses more Gln than the muscles can make (i.e. during times of stress), muscle wasting can occur. [5b] This often occurs in people suffering from HIV and in cancer patients, so Gln is used as a supplement to prevent weight loss due to muscle wasting.[6]

Gln is also used to protect the immune system and digestive system in people undergoing radio-chemotherapy for cancer of the oesophagus. Recent studies[7] have shown that L-Gln may help prevent toxic side effects of chemotherapy and radiation therapy (by preventing of damage to normal tissue, including peripheral nerves) and possibly also increase the effectiveness of some chemotherapy drugs.

The complexing ability of Gln has been studied previously with various metal ions,[8] and studies have shown that the complexation, although difficult, is possible and thus it was decided to study its complexation with Bi^{3+}. One of the important factors contributing to the complexation of amino acids with metal ions is the size of the ring formed due to complex formation. In amino acids, bonding through the carboxylic acid and adjacent amine groups results in 5-membered rings being formed, which is what was proposed for the Glu molecule in Chapter 5 and His molecule in Chapter 6. It is the polar side chains that need consideration to see whether tridentate chelates can form. Berthon[8] describes the formation of the chelate rings as highly dependent on the type of side chain present on the respective amino acid. Both asparagine and Gln contain an amide functional group

which is at the β and ɣ-positions respectively. Thus if these amino acids behave as tridentate ligands, asparagine will form 6-membered rings and Gln 7-membered rings when chelated through the amide group.[8] Previous studies have attempted to characterise a possible participation of the amide group in the coordination of several metal ions.[9] Given the unfavourable size of the chelate rings potentially involved, Gln displays only a very weak tridentate capability with Co^{2+} and Ni^{2+} and exclusively behaves as a bidentate ligand with Cu^{2+}.[10] This is in line with the fact that the formation of Cu-Gln complexes is not accompanied by any stereoselective effect.[11] Since Bi^{3+} is a large metal ion, formation of small rings are preferred, thus it would be expected that coordination through the amide group not occur significantly. It is important to understand these characteristics as they influence whether Bi^{3+}-Gln complexes would form and if so, how stable the complex would be.

7.2. Aim

Since it is not expected that Gln form strong complexes with Bi^{3+}, it was decided to investigate whether complexes could be formed under acidic conditions by adding the large excess of Gln in solution (as in our previous studies). Polarography was again employed and data used determine the log β values if complexes were formed.

7.3. Experimental

Initial findings in Chapter 4, where experiments were run with relatively low [Gln]:[Bi^{3+}] of 100, showed that precipitation occurred at pH ~2 thus indicating that complex formation was most likely not taking place. Experiments were therefore run as before at a higher [Gln]:[Bi^{3+}] of 2000, 3076, 4081 and 5075 and these experiments will be referred to as the rounded values (2000, 3000, 4000 and 5000).

An additional complication was found in the study of Bi^{3+}-Gln complexation. The polarographic waves became increasingly less reversible at higher pH (as the titration proceeded) and also as the [Gln]:[Bi^{3+}] was increased. This was problematic because in order to use equation 3.1 to determine the formation constants all the values for $E(M_{free})$ and $E(M_{comp})$ must be for reversible electron transfer processes. As discussed in section 3.3.3, a value of γ between 0.9-1 (obtained when fitting a polarogram using equation 3.4)

indicates a reversible process. Values of y between 0.5-0.9 indicate quasi-reversible electron transfer. Thus it was necessary to determine the reversible $E_{1/2}$ values from the quasi-reversible waves. A more detailed explanation will be made in the discussion. In order to determine the effect of accounting for the non-reversibility of the reduction of the Bi-Gln complexes, the formation constants will be reported when analysing data both before and after correction for non-reversibility was made.

7.4. Results and discussion

7.4.1. Initial data inspection

As seen in Figure 4.8, when [Gln]:[Bi^{3+}] = 100 precipitation started occurring at pH= ~2.3. It was expected that by increasing the [Gln]:[Bi^{3+}] ratio, precipitation would be postponed to high pH's due to complex formation as seen with the previous experiments conducted with Glu and His in Chapters 5 and 6 respectively.

Figure 7.2 shows the I_d vs pH plot for the experiment where [Gln]:[Bi^{3+}] = 2000, 3000, 4000 and 5000 which shows that precipitation had only been delayed by about 0.5 pH units in this case signifying that only weak Bi^{3+}-Gln complexes were formed. The increase in solubility of the experiment where [Gln]:[Bi^{3+}] = 3000 is an anomalous result and is not part of the trend seen with the other [Gln]:[Bi^{3+}] ratios. Gln with its lack of an extra complexing site seems to not greatly favour the complexation with Bi^{3+}. Although we expected the complexation to increase as more Gln was added, it was seen that precipitation of the Bi^{3+} occurred at approximately the same pH for all [Gln]:[Bi^{3+}] ratios.

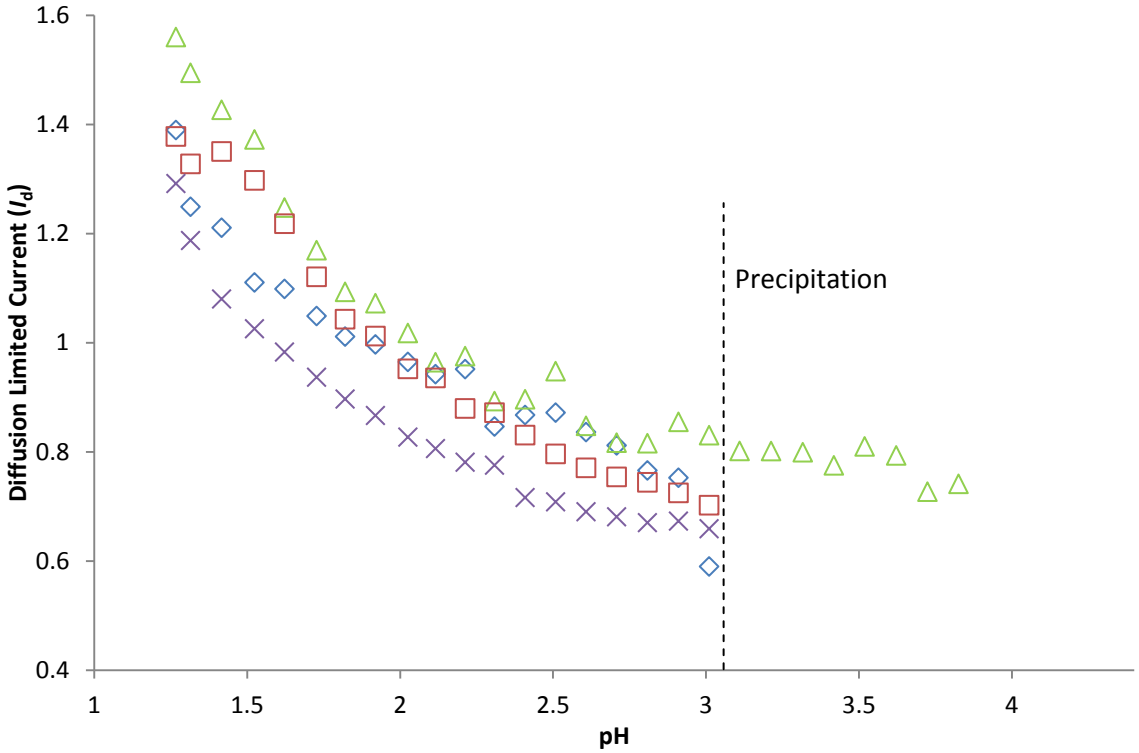

Figure 7.2: I_d vs pH for Bi^{3+} with Gln added Where [Gln]:[Bi^{3+}] = (X) 2000, (Δ) 3000 (□) 4000 and (◇) 5000. Only data before precipitation is shown.

Figure 7.3 shows the $E_{1/2}$ values of Bi^{3+} (plotted vs pH) and as obtained directly from fitting equation 3.4 to the polarograms and then corrected for E_j. In order to use the $E_{1/2}$ values in determining formation constants, corrections for quasi-reversibility still have to be made.

The formation of complexes of the Bi^{3+} has been clearly shown to be indicated by the negative shift in $E_{1/2}$ for the Bi^{3+} ion. Figure 7.4 shows these negative shifts as pH increases for Bi^{3+} vs pH (corrections for E_j were taken into account). It should still be borne in mind that the formation of Bi^{3+} nitrate and hydroxide species are still competing processes.

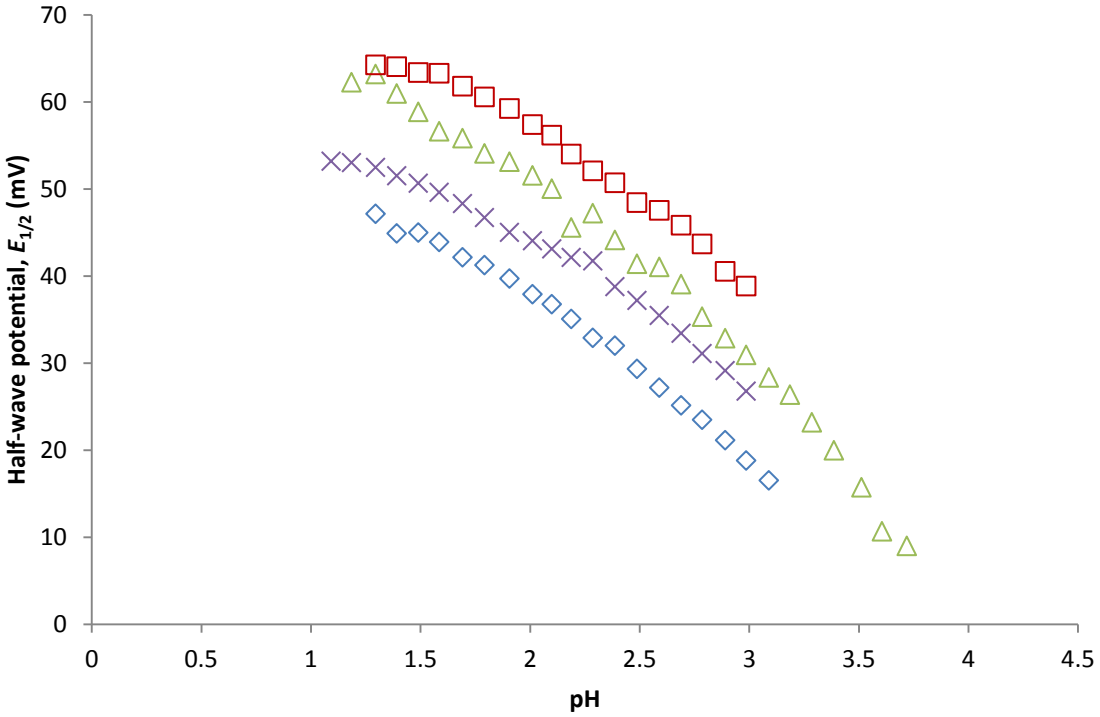

Figure 7.3: E_j corrected $E_{1/2}$ of Bi^{3+} vs pH with Gln added. [Gln]:[Bi^{3+}] = (×) 2000, (Δ) 3000, (□) 4000 and (◇) 5000.

In order to show that complex formation was occurring, the $E_{1/2}$ values for [Gln]:[Bi^{3+}]= 3000 and 5000 were compared to an experiment conducted when no ligand was added, and only Bi^{3+} was present (Figure 7.4). Comparing the $E_{1/2}$ values directly is not possible as the actual values differ slightly from experiment to experiment as was noted from the $E(Tl_{free})$ values (and hence the $E(Bi_{free})$ values) which also differed slightly between experiments. Of interest though is the trend in the $E_{1/2}$ values with an increase in pH. It appears that the trends with and without the ligand present are very similar, except that precipitation occurs at higher pH in the presence of Gln thus clearly indicating complex formation had taken place. However, the similar trends and the only slight increase in the pH at which precipitation occurs shows that these complexes are in strong competition with hydrolysis and nitrate complexation. For [Gln]:[Bi^{3+}] = 5000 data, the negative slope is however steeper, signifying that the large excess of ligand promotes complex formation.

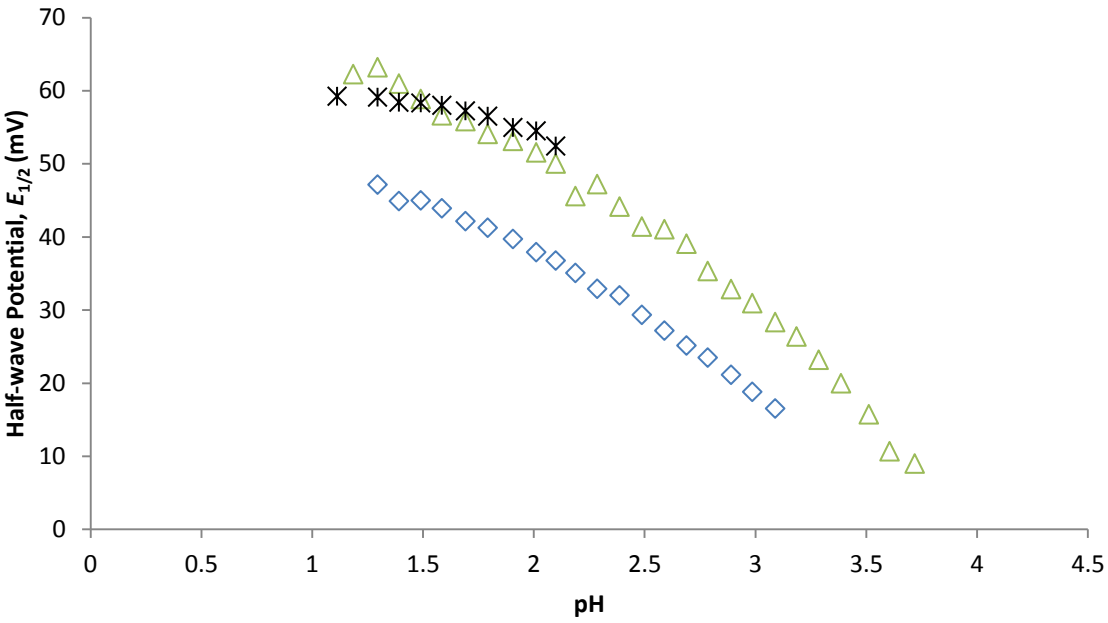

Figure 7.4: E_j corrected $E_{1/2}$ of Bi^{3+} vs pH with [Gln]:[Bi^{3+}] = (Δ) 3000 and (◇) 5000 and also in the absence of Gln (✳).

Figure 7.5 shows the values of *y* obtained from fitting the polarograms using equation 3.4. It was observed that although the *y* values were initially between at 0.9 – 1, as the pH increased *y* dropped below 0.9. Also, as the [Gln]:[Bi^{3+}] increased, the reversibility of the polarograms decreased substantially, with the *y* values dropping below 0.9 at lower pH's. The reason for the lack of reversibility in this case is not understood. It could be due to the increase of free Gln in solution inhibiting the electron transfer (as is observed when too much gelatine is added to the solution), but this was not observed in the high concentrations of His and Glu. In the case of [Gln]:[Bi^{3+}] = 2000 and 3000, the process was considered reversible throughout the pH range.

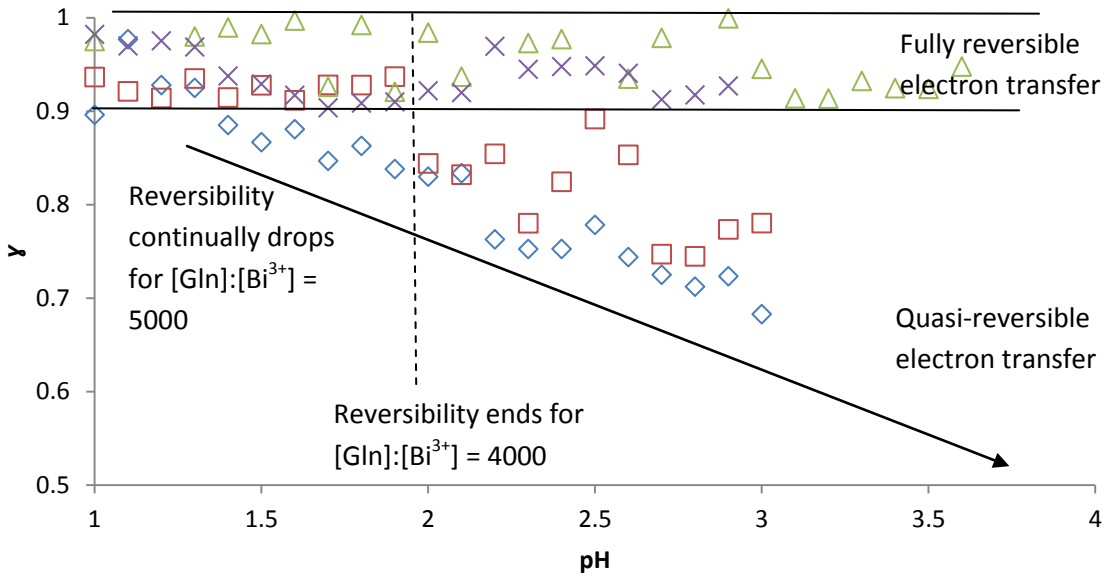

Figure 7.5: *V*alues of *γ* indicating reversibility vs pH for [Gln]:[Bi^{3+}] = (×) 2000, (Δ) 3000, (□) 4000 and (◇) 5000.

As can be seen in Figure 7.6, the reversibility of the wave affects the overall shape of the polarogram. For slower electron transfer reductions (quasi-reversible processes), there is a delay in the current reaching the diffusion limited current and the slope of the wave is flatter (it is no longer Nernstian as for a reversible process). The lower slope results in the polarogram becoming drawn out and hence the value of $E_{1/2}$ is also affected.

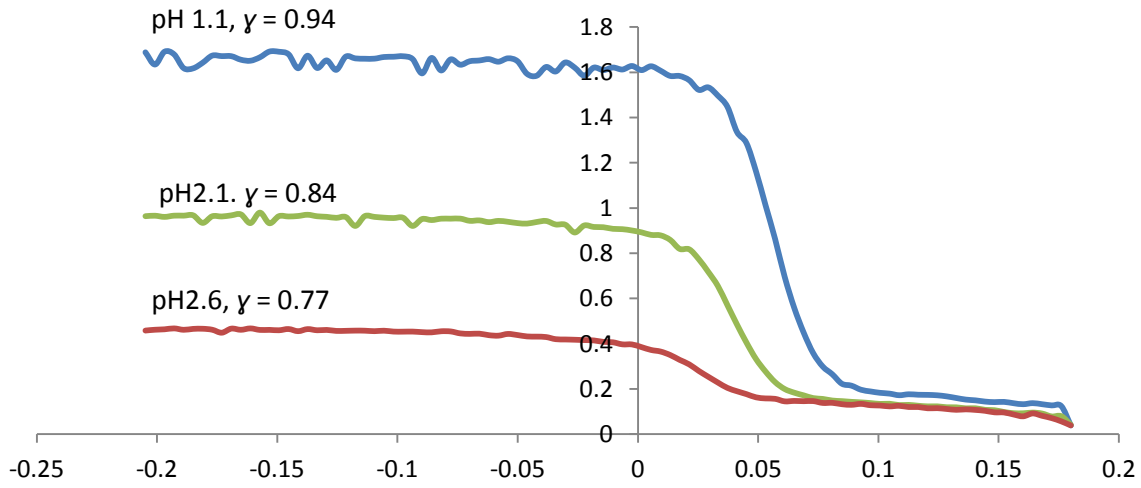

Figure 7.6: DC polarograms for [Gln]:[Bi^{3+}] = 4000 indicating the decrease in reversibility of electron transfer illustrated by the drawn out reduction wave.

As there is no other means of determining the complexing ability when quasi-reversible waves are produced, a method to determine the reversible potentials from these waves had to be used. A non-linear least squares fitting program called Precision Curve Fitter[12] was used to fit a single polarographic wave at a time using a process that will be described shortly.

One of the ways in which we were able to compensate for the change in reversibility of the Bi-Gln complex was to fix the γ value to the reversible value of 1. This was done by firstly fitting the Bi^{3+} polarogram using Precision Curve Fitter where all parameters (I_d, $E_{1/2}$, γ and the capacitance current (a, b c, d) were solved for using equations 3.4 and 3.5. Quasi-reversible electron transfer processes results in a delay of the current in reaching the diffusion limited value, but value of I_d is independent of the electron transfer kinetics. As a result, the I_d calculated initially using Precision Curve Fitter will remain the same and can therefore be fixed. The capacitance current or background can also be fixed as no electron transfer process is occurring at this point, therefore it will not be affected by the quasi-reversibility. To force a reversible process, γ was fixed to 1 and the points along the slope of the polarogram that deviated from the Nernstian behavior and lead to the drawn out polarogram were deleted. The Precision Curve Fitter[12] allows the parameters mentioned to be fixed and therefore the only parameter to be refined was $E_{1/2}$. Figure 7.7 gives an example of how a quasi-reversible polarographic wave was fitted to obtain the reversible $E_{1/2}$ value.

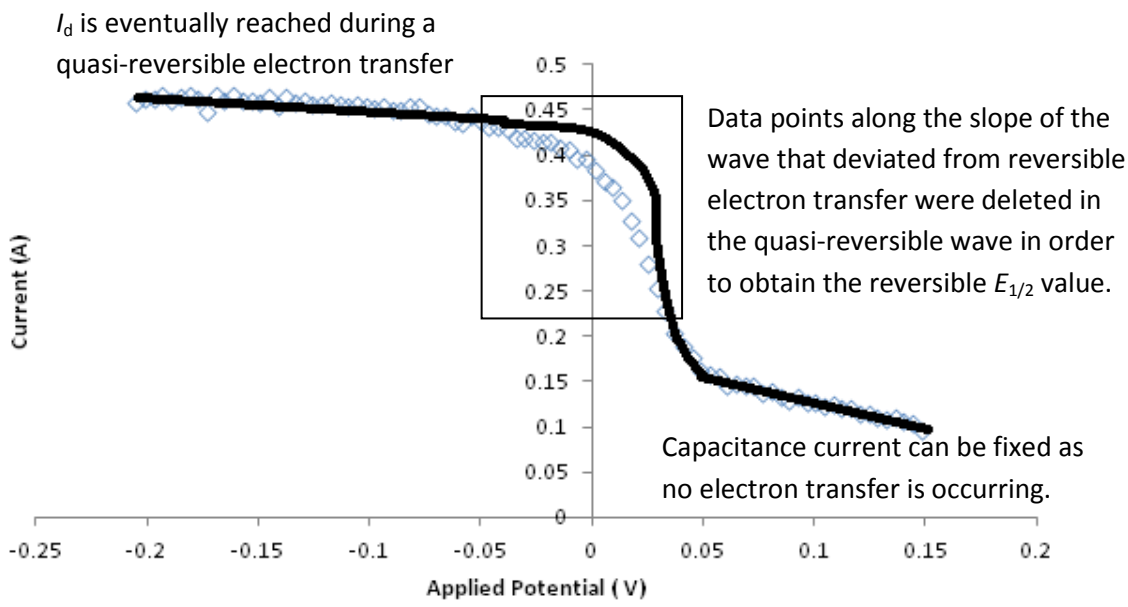

Figure 7.7: A quasi-reversible polarogram where the slow electron transfer region is highlighted and reversible fit is superimposed where I_d and capacitance was fixed and ɣ set equal to 1.

The removal of data points as a result of decreasing reversibility resulted in the reversible $E_{1/2}$ being more positive than the quasi-reversible $E_{1/2}$, with the difference between these two values ranging between 0.4 – 1.5 mV for the quasi-reversible polarograms measured. The small differences in this study was due to the *ɣ* value not falling below 0.7, therefore not affecting the $E_{1/2}$ to a large extent, thus the quasi-reversibility would not heavily impact the overall study of the formation constants of the Bi-Gln complexes. Also, since these deviations are small, the method used to obtain the reversible $E_{1/2}$ for a quasi-reversible process could be completed successfully.

Figure 7.8 compares the the quasi-reversible $E_{1/2}$ for Bi^{3+} (where *ɣ* was allowed to vary) and the reversible $E_{1/2}$ (where *ɣ* was fixed to 1 after removing some data points on the polarogram) for the experiment where [Gln]:[Bi^3+] = 4000. As can be seen, in the pH range 1 – 2, the $E_{1/2}$ values are similar because the electron transfer process was reversible. However, above pH 2 and up to the point of precipitation, the reversibility decreased.

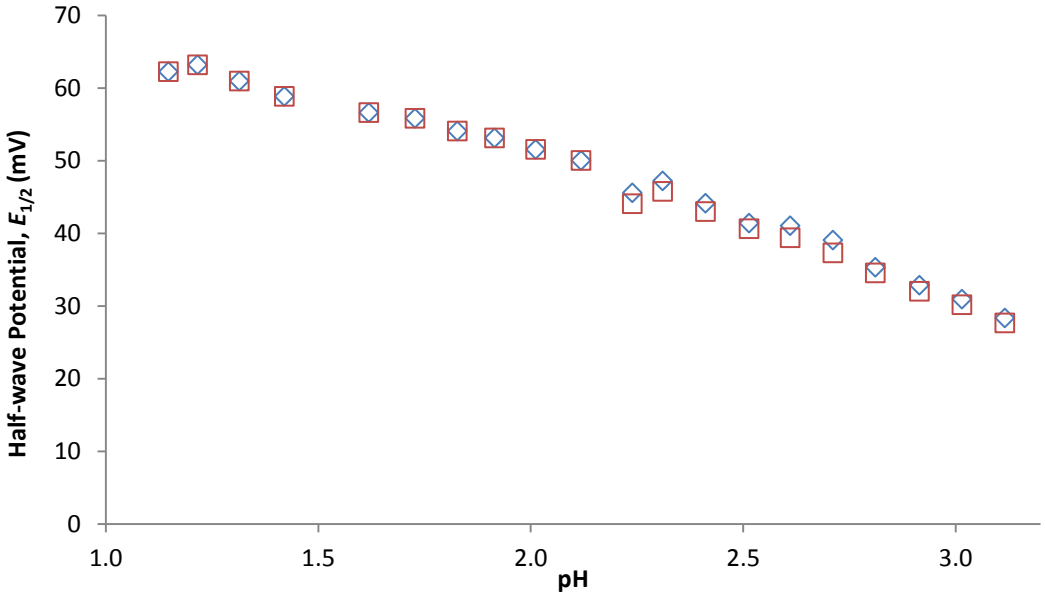

Figure 7.8: Graph showing that the (□) quasi-reversible $E_{1/2}$ and (◇) reversible $E_{1/2}$ values for Bi^{3+} for [Gln]:[Bi^{3}+] = 4000 do not differ greatly.

7.4.2 Slope analysis

Figure 7.9 indicates the dominant species of Gln in the system in various pH ranges. Gln contains only two proton donor sites with pK_a values of 2.14 and 8.94,[4] thus both sites are mainly protonated below pH 2.14. Since precipitation occurs at pH ~3, it was expected that only two dominant ligand species, Gln-H_2 and Gln-H, could form. In the studies with Glu and His (Chapters 5 and 6) we found that precipitation occurred at a pH of approximately 4.5 and 3.5 respectively. These amino acids have a greater ability to stabilise complex formation due to their extra donor site. Complexation with Gln could be inhibited due to the lack of the additional binding site and due to minimal complex formation we would expect precipitation to occur at a lower pH than Glu and His.

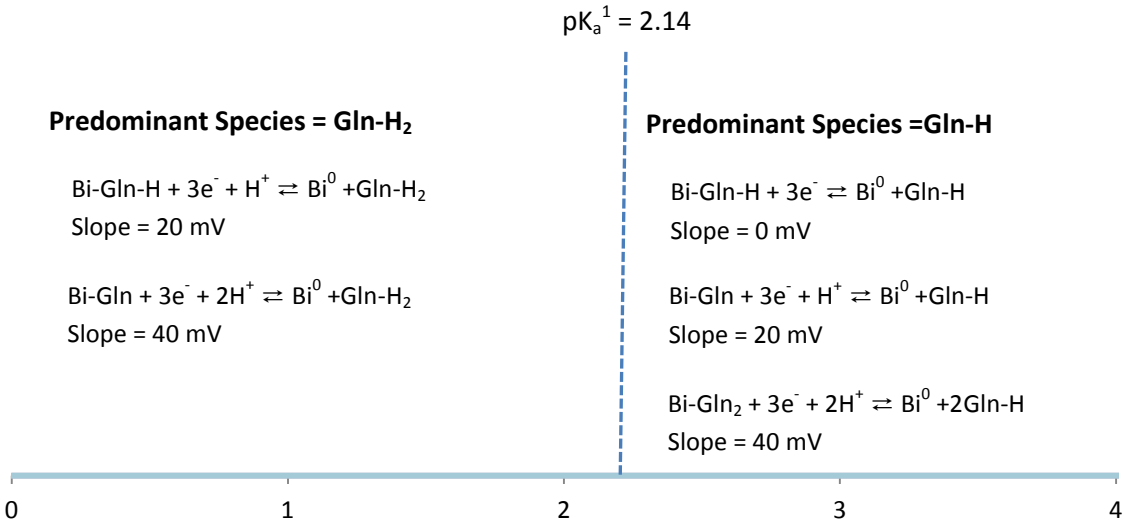

Figure 7.9: Diagram of the predominant ligand species in a specific pH range and the calculated slopes which indicate the type of complex which could be present in solution.

For the region before pH 2.14, we have suggested the Bi-Gln and Bi-Gln-H species to form. During the polarographic measurement, the Bi-Gln-H complex will be reduced, affording Bi^0 at the electrode and Gln-H in solution which immediately gains a proton to form the predominant species Bi-Gln-H_2. Since only one H^+ is needed to form the predominant species, we use equation 3.6 to calculate the expected slope of the $E_{1/2}$ vs pH plot. The same process is used to calculate the slope for the Bi-Gln complex, where we find that if the Bi-Gln complex is present, the slope of our plot should be approximately 40 mV. For the region above pH 2.14, the new predominant form of the Gln species in solution is Gln-H. Using the same methods explained above, we are able to calculate an expected slope of 0 mV for the reduction of the Bi-Gln-H complex and 20 mV for the Bi-Gln complex. Reduction of the Bi-Gln-H complex gives a slope of 0mV, indicating that the reduction of the Bi-Gln-H complex is independent of pH in this region.

Figure 7.10 shows the plot of the E_j corrected reversible $E_{1/2}$ values for Bi^{3+} vs pH where [Glu]:[Bi^{3+}] = 5000 which was used in the slope analysis. In the region below pH 2.14 the slope was 14 mV indicting that some complex formation was taking place. Since the formation of the Bi-Gln-H complex is expected to produce a slope of 20 mV it was suggested that some Bi-Gln-H was formed in this pH region. In the higher pH range above 2.14, a slope close to 20 mV was again found, thus predicting the formation of the Bi-Gln

complex. The Bi-Gln-H complex formation in this region is considered to be independent of pH due to the reduction of the complex resulting in the formation the predominant ligand species in solution, Gln-H at this pH, along with Bi^0.

The complex formation studies between Bi^{3+} and Glu (Chapter 5) and His (Chapter 6) showed similarities with Gln in that all three results showed the formation of a protonated Bi^{3+}-amino acid complexes at low pH. Whereas Bi-Glu-H_2 and Bi-His-H_2 were found in the pH range 1 to approximately 2, Bi-Gln-H was instead found. This is due to Gln only having two protonation sites and the amide group does not really take part in complexation.

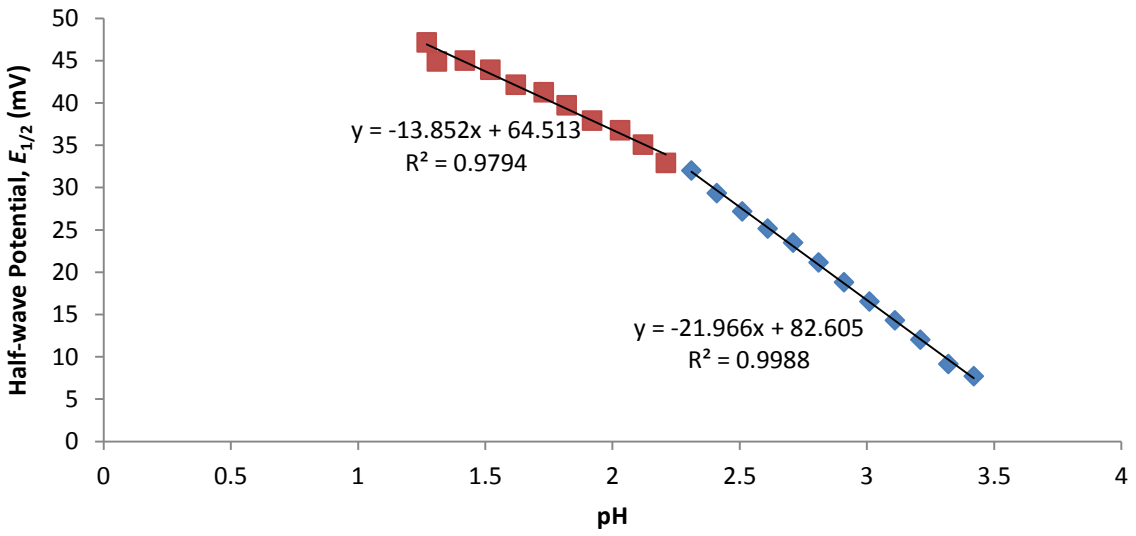

Figure 7.10: Slope analysis of the E_j corrected reversible $E_{1/2}$ of Bi^{3+} where [Glu]:[Bi^{3+}] = 5000 which indicates the formation of two types of complexes, Bi-Gln-H and Bi-Gln.

Slope analysis allows us to predict the species which could possibly be forming in solution in different pH ranges during the pH-polarographic titration.[13] The predicted species can then be included in the 3D-CFC programme[9] to see if it fits the experimental data and to refine the respective formation constants.

7.4.3 Determining Bi-Gln complexes and respective log β

As described in Chapter 3, the 3D-CFC programme[14] is used to calculate the formation constants for the species predicted to have formed in solution. Figure 7.11 shows the ECFCs calculated using the true E(Bi_{free}) value and the corresponding CCFCs for all four experiments, and indicates that the calculated curves correlate well to the experimental values.

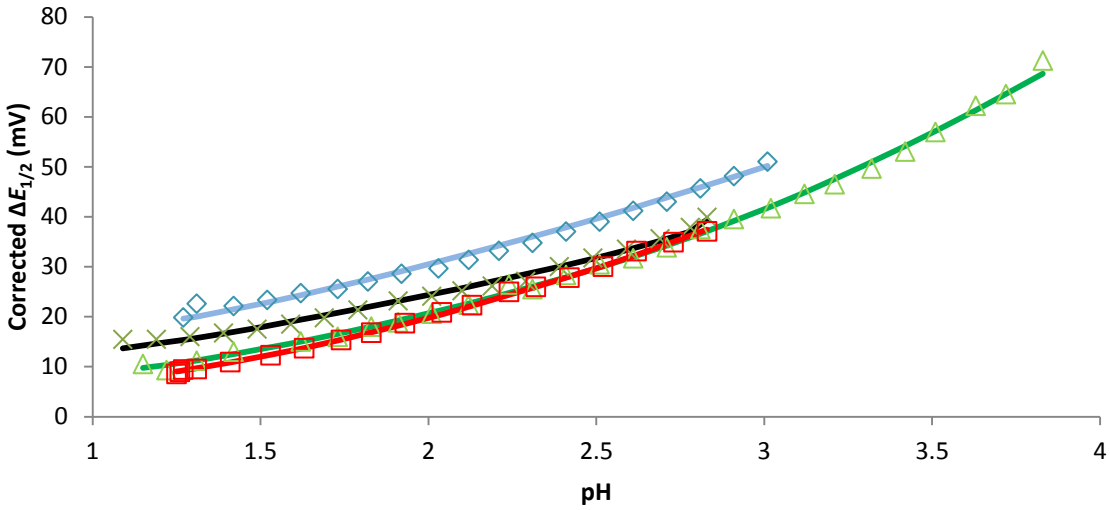

Figure 7.11: Shift in $E_{1/2}$ of Bi^{3+} vs pH for [Gln]:[Bi^{3+}] = (×) 2000, (Δ) 3000, (□) 4000 and (◇) 5000.

Table 7.1 shows the log *β* constants calculated at each [Gln]:[Bi^{3+}] using both *E*(Bi_{free}) and E(Bi_{free})$_{OH}$ as before. Additionally the log *β* constants were calculated using the quasi-reversible $E_{1/2}$ values directly for the [Gln]:[Bi^{3+}] = 4000 and 5000 experiments simply for comparison purposes.

The log *β* values calculated using *E*(Bi_{free}) will be discussed first. In all cases the Bi-Gln-H and Bi-Gln species were required in the species model to fit the experimental data across the pH range. It can be seen that the reproducibility of log *β* in all cases was difficult to achieve. From the relative positioning of the ECFCs in Figure 7.11 it was expected that the results from the [Gln]:[Bi^{3+}] = 2000 and 5000 experiments would be greater than the other two experiments. It would be expected that the most accurate values would be produced by the [Gln]:[Bi^{3+}] = 5000 due to the largest shifts being observed and since

such a high concentrations of ligand was used successfully in the cases of Glu (Chapter 5) and His (Chapter 6).

When the quasi-reversible $E_{1/2}$ values were used to calculate the log β values, for the [Gln]:[Bi^{3+}] = 4000 experiment the values were very similar due to only slight deviation from reversibility. For the [Gln]:[Bi^{3+}] = 5000 experiment larger differences between the log β values were seen, especially for the Bi-Gln complex which forms at higher pH where there was more deviation from reversibility.

Table 7.1: Table showing the log β values for the respective Bi-Gln complexes (at 0.5 M ionic strength and 25°C) using 3D-CFC[14]. "Rev" was calculated using the reversible $E_{1/2}$ values and "Quasi" the quasi-reversible $E_{1/2}$ values.

[L]:[Bi^{3+}]	**2000**	**3000**	**4000**		**5000**	
Equilibrium	**log β**					
(a) using E(Bi_{Free})	**Rev**	**Rev**	**Rev**	**Quasi**	**Rev**	**Quasi**
Bi^{3+} + L + H^+ ⇄ Bi-LH	12.26 ± 0.02	11.65 ± 0.04	11.23 ± 0.06	11.25 ± 0.06	12.01 ± 0.03	12.05 ± 0.03
Bi^{3+} + L ⇄ Bi-L	9.17 ± 0.02	9.19 ± 0.08	9.08 ± 0.06	9.10± 0.08	9.90 ± 0.03	9.77 ± 0.03
(b) using $E(Bi_{Free})_{OH}$						
Bi^{3+} + L + H^+ ⇄ Bi-LH	11.79 ± 0.03	-	-	-	11.45 ± 0.04	11.48 ± 0.04
Bi^{3+} + L ⇄ Bi-L	8.90 ± 0.16	-	-	-	8.77 ± 0.13	7.46 ± 0.13

When $E(Bi_{Free})_{OH}$ was used to calculate the log β for the complexes believed to be forming in solution (as determined from slope analysis conducted earlier) it was found that the 3D-CFC programme[14] would not refine the formation constants for the [Gln]:[Bi^{3+}] = 3000 and 4000 experiments. This was probably due to the Bi-Gln complex formation having significant competition with Bi^{3+} nitrate complexation in pH range up until a pH ~2.5, where after significant competition will take place with Bi^{3+} hydrolysis. This was already expected when considering Figure 7.4 which did not show much of a difference between the $E_{1/2}$ values in the absence and presence of Gln up to about pH 2.

Interestingly, log β values could be calculate for both the [Gln]:[Bi^{3+}] = 2000 and 5000 data when using $E(Bi_{Free})_{OH}$. Figure 7.12 shows the ECFCs (calculated using $E(Bi_{Free})_{OH}$) and CCFCs used to calculate the log β values for [Gln]:[Bi^{3+}]= 2000 and 5000. The shifts in $E_{1/2}$ are greater for [Gln]:[Bi^{3+}] = 5000 compared to that of 2000, showing a greater extent of complex formation when [Gln]:[Bi^{3+}] = 5000. It is thus expected that the values for [Gln]:[Bi^{3+}] = 5000 would produce more accurate results

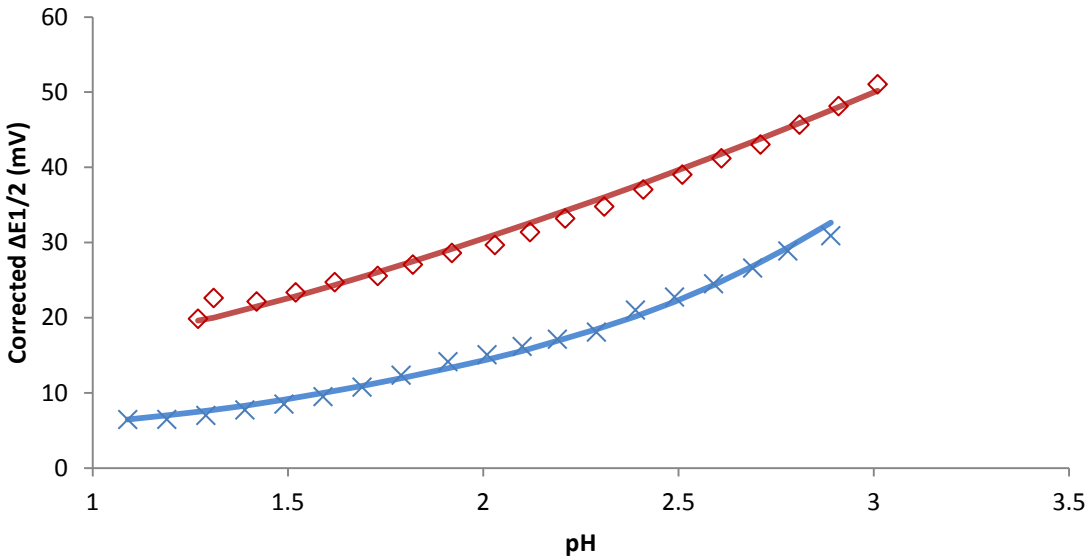

Figure 7.12: The ECFCs (points) (calculated using the true $E(Bi_{free})_{OH}$ and the corresponding CCFCs (lines) for [Gln]:[Bi^{3+}] = (×) 2000 and (◇) 5000.

Figure 7.13 shows the species distribution diagram for [Gln]:[Bi^{3+}] = (a) 3000 and (b) 5000. The log β values used for the Bi^{3+}-Gln complexes are those in Table 7.1 when using the true $E(Bi_{free})$ and reversible $E_{1/2}$ values. For [Gln]:[Bi^{3+}] = 3000 the Bi-Gln-H complex begins to form at slightly lower pH than $Bi(OH)^{2+}$, but is shown to always be present in solution together with the Bi^{3+} nitrate species and Bi(OH) and is never really dominant in solution at any pH. The formation of the $Bi(OH)^{2+}$ also completely swamps the Bi-Gln complex which is only able to reach approximately 20% (and only begins to form at pH ~1). It is therefore not surprising that the log β values could not be refined for this data set when using the $E(Bi_{free})_{OH}$ value. When the log β values for [Gln]:[Bi^{3+}] = 5000 was used and with the larger excess of ligand, the formation of the Bi-Gln-H complex (~50%) and the Bi-Gln complex (70%) occurred to a much greater extent, again indicating the benefit of using

high [Gln]:[Bi^{3+}]. The species distribution diagram again indicate that the log β value for Bi-Gln-H calculate using the $E(Bi_{free})_{OH}$ value and that for Bi-Gln calculate using the true $E(Bi_{free})$ value would give the most representative results.

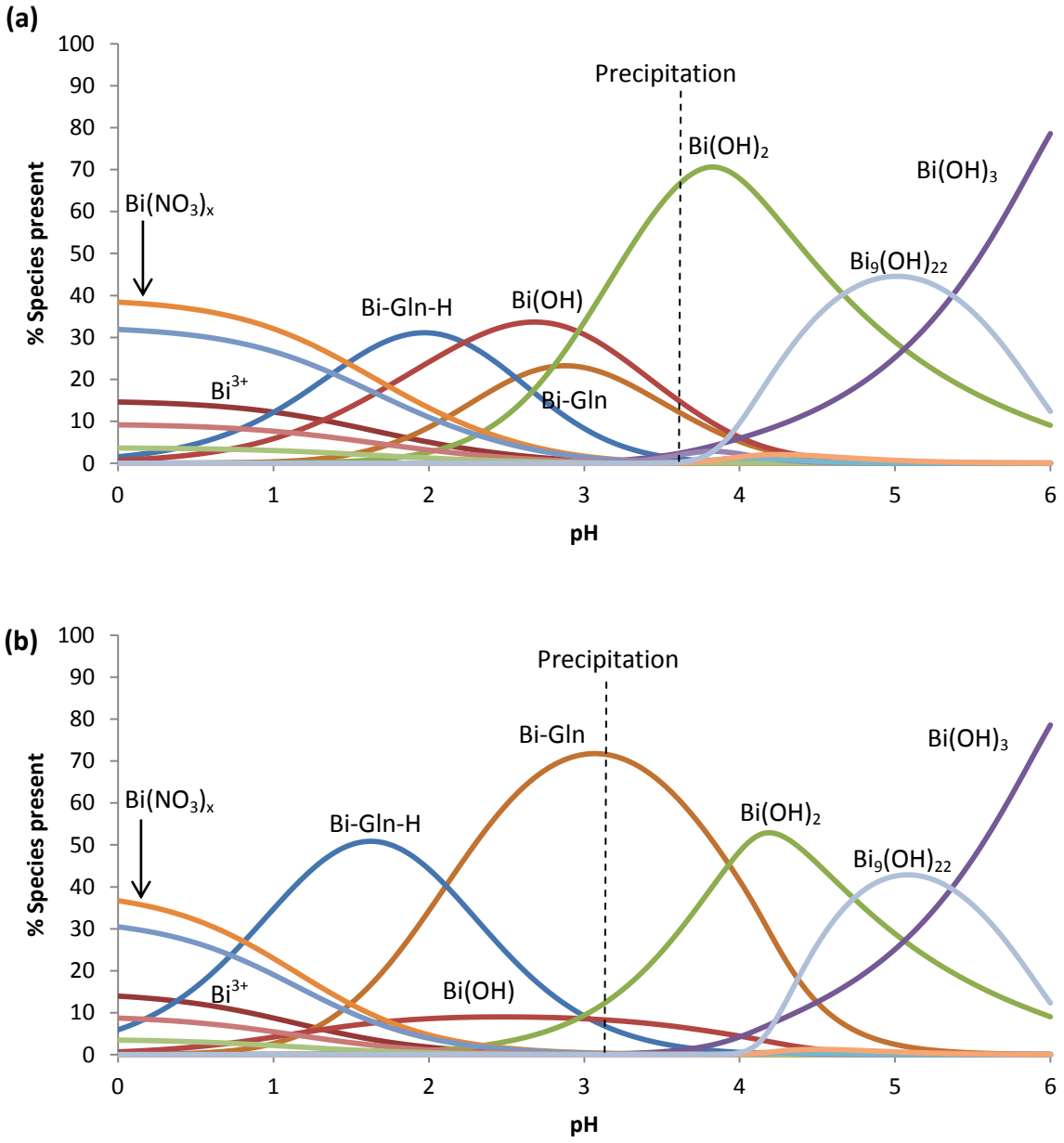

Figure 7.13: Species distribution diagrams for [Gln]:[Bi^{3+}] = (a) 3000 and (b) 5000, where log β values were calculated using the true $E(Bi_{Free})$ as given in Table 7.1.

Although literature on Bi-Gln complexes is extremely limited, formation constants of 9.81 and 17.25 were determined for the ML and ML_2 species for Bi-Gln complexes, respectively.[15] These studies were conducted in perchlorate solutions and began above

pH 2. It was interesting to note that the log β of 9.90 ± 0.03 for the Bi-Gln complex where [Gln]:[Bi^{3+}] = 5000 calculated using the true $E(Bi_{free})$ and which has been indicated as the value for which we consider to have the greatest confidence in, compared to that in literature. No Bi-Gln-H complex was reported in literature as these studies were stared above pH 2. An additional experiment should be run at around [Gln]:[Bi^{3+}] = 7000 to allow the determination of more accurate log β values as the higher [Gln]:[Bi^{3+}] results in complex formation to a greater extent.

Studies[8] involving the complexation of Gln with a variety of other metal ions have been done, however as described by Berthon[8], the comparison to each other is difficult due to studies being conducted under completely different experimental conditions. For Pb^{2+}, a metal ion which is isoelectronic with Bi^{3+}, the complexation with Gln has been performed in two different media, and the study in the $NaNO_3$ electrolyte gave information about Pb-(Gln)-OH_2,[8, 16] and the study in the $NaClO_4$ electrolyte gave information about Pb-Gln, Pb-$(Gln)_2$ and Pb-$(Gln)_3$ complexes. The NIST[4] database unfortunately does not contain formation constants for Ga^{3+} with glutamine, however, recent studies conducted by Sharma[17] did produce results when working in 0.1 M KNO_3 solutions. They showed that the complexes formed were Ga-Glu, Ga-Glu_2 and Ga-Glu_3 with stability constants of 1.35, 6.5 and what is assumed to be 13.50 (quoted as 1.350 in the publication but which cannot be correct), respectively at 30°C. The polarographic waves in this study also showed non-reversibility, as was seen in our studies with [Gln]:[Bi^{3+}] > 3000. It is not sure how accurate these values are because when using their experimental conditions ([Ga^{3+}] = 1 mM, [Gln]:[Ga^{3+}] = 10 – 30 and solution pH = 3.5) to plot a species distribution diagram, it was indicated that no complexation with Gln occurred and precipitation took place before pH 3.5.

7.5 Conclusion

The complexation between Bi^{3+} and Gln, although difficult to achieve in nitrate solutions, produced two complexation products, Bi-Gln-H and Bi-Gln. This however requires large [Gln]:[Bi^{3+}] ratios.

The complexation of Gln with Bi^{3+} has shown that when polarographic techniques are used, the transfer of electrons tends to be quasi-reversible as [Gln]:[Bi^{3+}] increases (>3000). Since fully reversible waves are required for the calculation of log β values, the reversible $E_{1/2}$ values had to first be determined from the quasi-reversible waves. However, the differences between the two $E_{1/2}$ values were not great due to only small deviations from reversibility indicated by γ values not dropping below about 0.7.

Gln complexation with Bi^{3+} appears to need a large [Gln]:[Bi^{3+}] ratio in order for complexation sufficient to occur and to override competition with the formation of hydroxide and nitrates. This was only really seen where [Gln]:[Bi^{3+}] = 5000 and further experiments should be run at ratios higher than this. Thus as shown in Table 7.1, the reproducibility of the log β was not ideal due to insufficient complex formation at the lower [Gln]:[Bi^{3+}] ratios. However, the quasi-reversibility would increase with further addition of Gln in solution and possibly even result in irreversible electron transfer taking place.

Although the results presented in this study do differ, it must be taken into account that Berthon[8] has described the complexation of Gln with metal ions as being tentative at best, with only a few metal complexes, such as Cu^{2+} (Cu-Gln and Cu-Gln_2),[18] being recommended as a true representation of the complex formation. The intricate chemistry which governs the formation of Gln complexes with metal ions is still in the process of being understood. In future the actual Bi^{3+}-Gln complexes formed in solution could be investigated using electrospray ionisation-mass spectrometry.

7. 6 References

[1] a) J. T. Brosnan, *J. Nutr.*,**2013**, *133*, 2068; b) W. J. Lee, R. A. Hawkins, J. R. Vina and D. R. Peterson, *Am. J. Phys.*,**1998**, *274*, 1101.

[2] R. Minet, F. Villie, M. Marcollet, D. Meynial-Denis and L. Cynober, *Clinica. Chimica. Acta.*,**1997**, *268*, 121.

[3] C. K. Mathews, K. E. van Holde and K. Ahern, *Biochemistry*, Addison Wesley Publishing Company, New York, **2002**.

[4] A. E. Martell and R. M. Smith, NIST Standard Reference Database 46 Version 8.0, NIST Critically Selected Stability Constants of Metal Complexes,USA, **2004**

[5] a) A. C. Baxter and D. R. Williams, *J. Chem. Soc. Dalton Trans.*,**1974**, 1117; b) P. Newsholme, M. M. R. Lima, T. C. Pithon and R. B. Bazottes, *Braz. J. Med. Biol. Res.*,**2011**, *36*, 153.

[6] a) C. M. Noyer, D. Simon, D. Borczuk, A. Branst, M. J. Lee and V. Nehra, *Am. J. Gastroenterol.*,**1998**, *93*, 972; b) K. J. Shabert, C. Winslow, J. M. Lacey and D. W. Wilmore, *Nutrition*,**1999**, *11*, 860; c) C. Kulkarni, K. S. Kulkarni and B. R. Hamsa, *Indian. J. Pharmacol.*,**2005**, *36*, 148.

[7] Y. Xiayo, C. Bi, Y. Fan, C. Cui, X. Zang and D. Q. Ping, *Int. J. Oncol.*,**2008**, *33*.

[8] G. Berthon, *Pure. Appl. Chem.*,**1995**, *67*.

[9] R. B. Martin, 'Metal Ions in Biological Systems', *20*, M. Dekker, **1986**, 21

[10] A. Gergely, I. Nagypal and E. Farkas, *J. Inorg. Nucl. Chem.*,**1975**, *37*, 551.

[11] J.H. Ritsma, G. A. Wiegers and F. Jellinek, *Recl. Truv. Chim.* ,**1965**, *84*, 1577.

[12] G. Brink, Precision Curve Fitter, University of the Witwatersrand, **1995**, (unpublished)

[13] I. Cukrowski, *Electroanal.*,**1997**, *9*, 699.

[14] P. Franklyn and I. Cukrowski, 3D-CFC software, University of the Witwatersrand, **2003**, *Windows Version 1.2*, (unpublished)

[15] M. K. Singh and M. N. Srivastava, *J. Inorg. Nucl. Chem.*,**1972**, *34*, 2067.

[16] a) T. T. Lai and M. C. Chen, *Talanta*,**1969**, *16*, 544; b) A.M. Corrie, M. L. D. Touche and D. R. Williams, *J. Am. Chem. Soc.*,**1973**, 2561.

[17] V. Sharma and K. D. Gupta, *Monat. Fur. Chem.*,**2011**, *142*, 481.

[18] a) A. Kayali and G. Berthon, *Polyhedron*,**1982**, *1*, 371; b) A. Cole, C. Furnival, Z. X. Huang, D. Ceri Jones, P. M. May, G. L. Smith, J. Whittaker and D. R. Williams, *Inorg. Chim. Acta.*,**1965**, *108*, 165.

Chapter 8: Final Conclusion

The procedures developed using the NOVA software (as discussed in Chapter 2) allowed for the automation of the entire polarographic-pH titration method and proved to be a major success. Initial development of the software showed some limitations in the NOVA[1] software when carrying out the many functions needed for the polarographic studies completed in this work. However, with the support from EcoChemie (the suppliers of NOVA[1]) who wrote new commands that were needed, the development of the automated procedures began taking shape. Validation of the NOVA procedures for GE calibrations and polarographic studies were carried out as described in Chapter 4. Once the methodology was robust and reproducible, the amino acid complexation studies with Bi^{3+} were initiated. The NOVA[1] software replaced the older LABVIEW[2] software which was previously used and more costly to develop further. Due to its successful use in monitoring complex formation in this study, it can be a concluded that the NOVA[1] software will be used in many other polarographic-pH titrations and the backbone of the procedures developed can be used to extend this application to incorporate other electrochemical measurements.

The study of Bi^{3+} and its complexing ability by different ligands is not straight-forward. Previous work[3] had shown that precipitation of Bi^{3+} occurs due to the formation of Bi-hydroxy-nitrate complexes and this happened around pH 2-2.5 under the conditions used in this work. The first major breakthrough to the success of this study was the realization that previous work using relatively low [ligand]:[metal] (of around 100-200) would not suffice when investigating complexation of Bi^{3+} with amino acids. Le Chateliers' principle provided the answer to ensuring that Bi^{3+} complexation with amino acids could be achieved. By increasing [ligand]:[metal] to magnitudes of greater than 2000, Bi^{3+} remained soluble to higher pHs due to complexation taking place with the amino acid ligands (as shown in Chapters 5-7).

The use of polarography, and by extension the pH titration associated with increasing the pH of the solution to promote complex formation, proved to be successful in these studies. Table 8.1 summarises the results and is given in terms of log *K* values for complex formation between Bi^{3+} and the amino acid in the given protonated form, rather than in terms of log *β* values as quoted in each chapter. These clearly show the small extent of complex formation with the protonated forms of the ligand. This implies that there certainly are Bi^{3+} nitrate species present below pH 2 and that the stability constants calculated using the $E(Bi_{free})_{OH}$ values would give more accurate results. For the Bi-L species which form at higher pH, the stability constants calculated using the true $E(Bi_{free})$ values would provide the more accurate results. Due to the strong competition between nitrate and amino acid species at low pH, it highlights the importance of developing software that takes competition with nitrates into account, something the 3D-CFC software[4] does not do.

Table 8.1: Log *K* values for the formation of Bi^{3+}amino acid complexes in solution at 25 °C and μ = 0.5 M (KNO_3). The values in italics indicate which constants give the more representative values for the particular species when using the two $E(Bi_{Free})$ values in the calculations.

Ligand (L)	**Glu**	**His**	**Gln**
Equilibrium		**log *K***	
(a) using $E(Bi_{Free})$			
$Bi^{3+} + LH_2 \rightleftarrows Bi\text{-}LH_2$	3.4	2.7	
$Bi^{3+} + LH^{+} \rightleftarrows Bi\text{-}LH$	5.3	7.0	3.1
$Bi^{3+} + L \rightleftarrows Bi\text{-}L$	*12.3*	*12.5*	*9.8*
(b) using $E(Bi_{Free})_{OH}$			
$Bi^{3+} + LH_2 \rightleftarrows Bi\text{-}LH_2$	*2.6*	*2.0*	
$Bi^{3+} + LH^{+} \rightleftarrows Bi\text{-}LH$	4.7	6.2	*2.5*
$Bi^{3+} + L \rightleftarrows Bi\text{-}L$	11.6	10.6	7.5

From the results in Table 8.1, the complexing ability of Glu and His was fairly comparable with the Bi-L-H_2 complex being more stable with Glu and the Bi-L-H complex being more

stable with His. The stability of the Bi-L complexes was comparable. The addition of a large excess of His in particular (as compared to Bi^{3+} concentration) lead to a significant increase in the pH of the initial solution. For future work the pH should be adjusted to about pH ~1 before the titration experiment in initiated to obtain data across a wider pH range.

The study with Gln was interesting in itself since, by maintaining a high [ligand]:[metal] ratio (>3000), the polarographic reduction waves became quasi-reversible. The reversible $E_{1/2}$ values had to be obtained from these quasi-reversible waves before the data could be used to determine stability constants. The difference between the reversible and quasi-reversible $E_{1/2}$ values was at most 1.5 mV since values of y only went down to about 0.7. Only the Bi-L-H and Bi-L complexes were formed with Gln and their stability was significantly lower than that for Glu and His.

One of the most interesting observations in this study is the similarity in both the types of species formed and the actual formation constants between Ga^{3+} and Bi^{3+} with Glu and His.[5] Unfortunately the NIST database[6] did not contain information about Ga^{3+} with glutamine, and those found in literature did not appear to be reliable[7]. The fact that Ga^{3+} also readily hydrolyses and precipitates from solution at fairly low pH confirms what we have found in our studies with Bi^{3+}.

This study has shown that Bi^{3+} can be complexed by Glu, His and Gln, all amino acids which are integral building blocks for proteins, provided the amino acid is in large excess. However, to extrapolate these results to predict how Bi^{3+} could behave in the body would be premature. Proteins are large molecules with a unique chemistry, however, by isolating its building blocks (i.e. amino acids), an insight of how Bi^{3+} could interact in the body was achieved. This could prove extremely beneficial in the design of new and effective bismuth drugs, which could potentially increase the efficacy of its action.

8.1 References

[1] Metrohm-Autolab, NOVA, **2012**, (Utrecht, Netherlands)

[2] Chance E, Vipin V, Wesley Z and H. Richard, *J. Lab. Auto.*,**2007**, *12*, 17.

[3] M. V.A. and T. G. Spiro, *J. Am. Chem. Soc.*,**1966**, *88*, 1410.

[4] P. Franklyn and I. Cukrowski, 3D-CFC software, University of the Witwatersrand, **2003**, *Windows Version 1.2*, (unpublished)

[5] a) P. Bianco, J. Haladjian and R. Pilard, *J. Chim. Phys.*,**1973**, *73*, 280; b) P. Bianco, J. Haladjian and R. Pilard, *J. Less-Common Met.*,**1978**, *58*, 58; c) E. A. Zekharova and V. N. Kumok, *J. Gen. Chem.*,**1968**, *38*, 1868.

[6] A. E. Martell and R. M. Smith, NIST Standard Reference Database 46 Version 8.0, NIST Critically Selected Stability Constants of Metal Complexes,USA, **2004**

[7] V. Sharma and K. D. Gupta, *Monat. Fur. Chem.*,**2011**, *142*, 481.

Appendices

Appendices

Appendix 1

Supplementary information for Chapter 3 –PXRD

Table A 1.1: Experimental parameters used in NOVA for the polarographic- pH titrations.

Potentiometric Parameters	
Initial pause	20 s
Sample rate	2 s
Dose	0.300 mL up to pH 2.3, thereafter 0.025 mL
pH step	0.1
Polarographic Parameters	
Purge	400 s
Initial potential	0.180 V
Final potential	0.700 V
Step potential	-4 mV
Interval time (drop life)	1 s
Rest time	5 s
Stop Condition	
Stop pH	8

Table A 1.2: Initial parameter estimates for the fitting of Bi^{3+} and Tl^{+} DC polarograms

Parameters	**Estimates for Bi^{3+}**	**Estimates for Tl^{+}**
I_d	1.5 x 10^{-8}A	4.5 x 10^{-8}A
$E_{1/2}$	0.05 V	-0.45 V
γ	1	1
a	1	1
b	1	1
c	-0.001	0.001
d	1	-1

Table A 1.3: Instrument settings for the Bruker D2 Phaser

X-ray source	Co-Xray source (1.78897 Å)
Goniometer	Primary radius (70.7 mm) Secondary radius (70.7 mm)
Detector	Bruker Lynxeye PSD
Slits	Primary Soller Slits (2.5°) Secondary Soller Slits (2.5°)
Temperature	294 K
Start 2θ	10.000°
End 2 θ	90.006°
Step	0.026°
Step Time	185s

Appendix 2

Supplementary information for Chapter 5

Pb^{2+} is isoelectronic with Bi^{3+}. The complexation of Pb^{2+} with amino acids thus had the potential to show comparisons to Bi^{3+}. Bi^{3+} also has the ability to form hydroxide products from pH as pH ~2. The Pb^{2+} hydroxide log β were thus used to compare Bi^{3+} and Pb^{2+} complexation with Glu.

Table A2.1: Pb hydroxide species log β for species distribution diagrams plotted in Chapter 5 as a comparison to Bi^{3+}-Glu.[1]

Pb-hydroxide species	**Log β**
Pb OH	6.3
$Pb(OH)_2$	10.9
$Pb(OH)_3$	13.7
$Pb_2(OH)$	7.7
$Pb_3(OH)_4$	34
$Pb_4(OH)_4$	37.6
$Pb_6(OH)_8$	71.5

Ga^{3+} has been shown to exhibit complex formation with Glu and His with log β values which are comparable (see Chapter 5 and Chapter 6). Table A2.2 shows the Ga^{3+} - hydroxide complexes which are found to be in solution and the subsequent species distribution diagram plotted with Glu as the ligand, where [Glu]:[Ga^{3+}] = 100 and 5000. It is interesting to note that species are able to form at low [Glu]:[Ga^{3+}], whereas our study has shown that a large excess in ligand is required in order to achieve complex formation. More interestingly, is the formation of the Ga-Glu-H_2 complex at both [Glu]:[Ga^{3+}], indicating that it is indeed a complex which could be forming.

Table A2.2: Ga^{3+} log *β* for complexation with hydroxide in 0.3M NO_3 solutions at 25°C.[1]

Ga^{3+} hydrolysis complexes	Log *β*
Ga(OH)	-3.74
$Ga(OH)_2$	-7.68
$Ga(OH)_4$	-17.36
$Ga_2(OH)_2$	-1.68

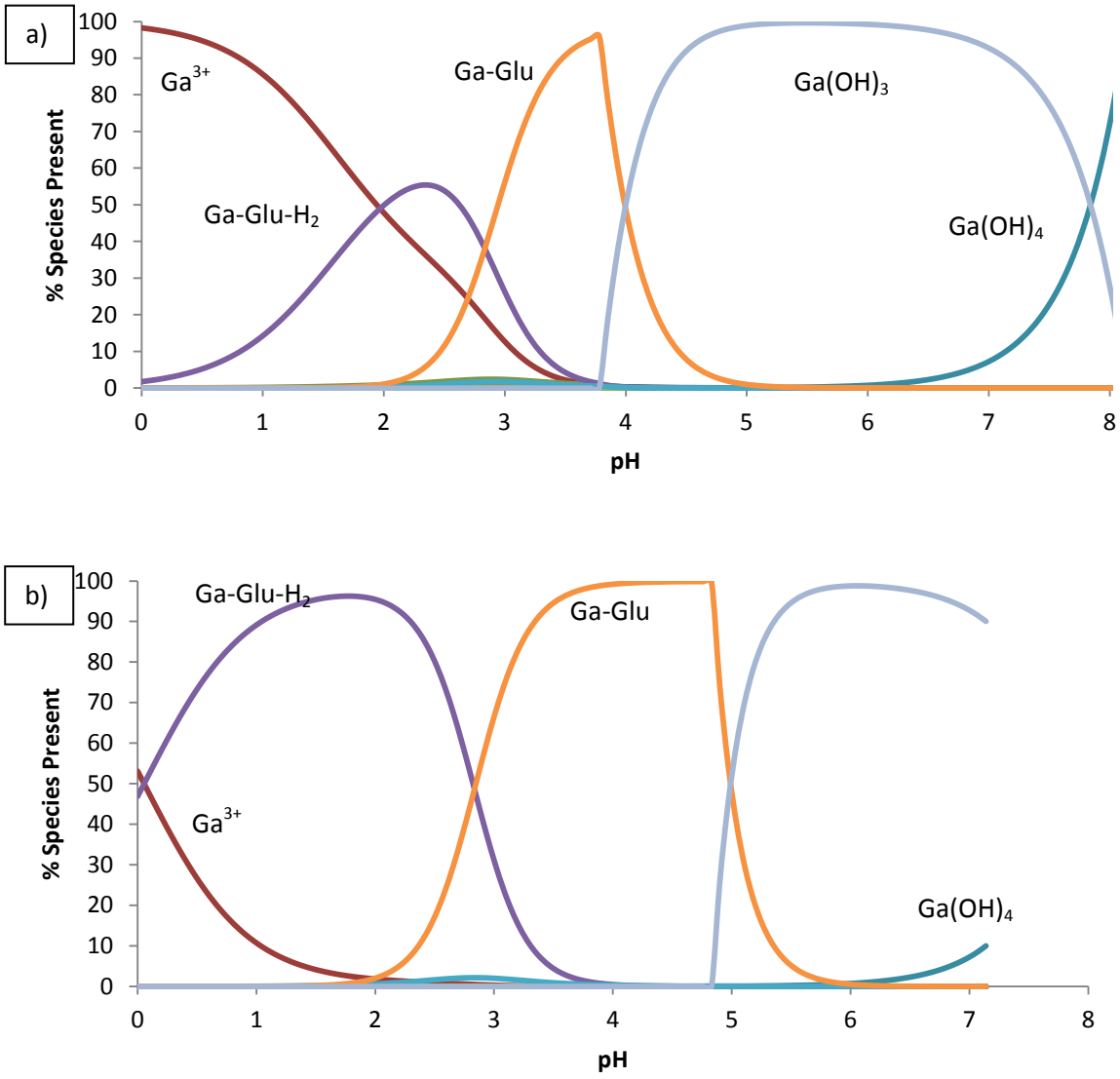

Figure A2.1: Species distribution diagram of Ga-Gln complexes formed where [Glu]:[Ga^{3+}]= a) 100 and b)5000 at 25°C.

Appendix 3

Supplementary information for Chapter 6

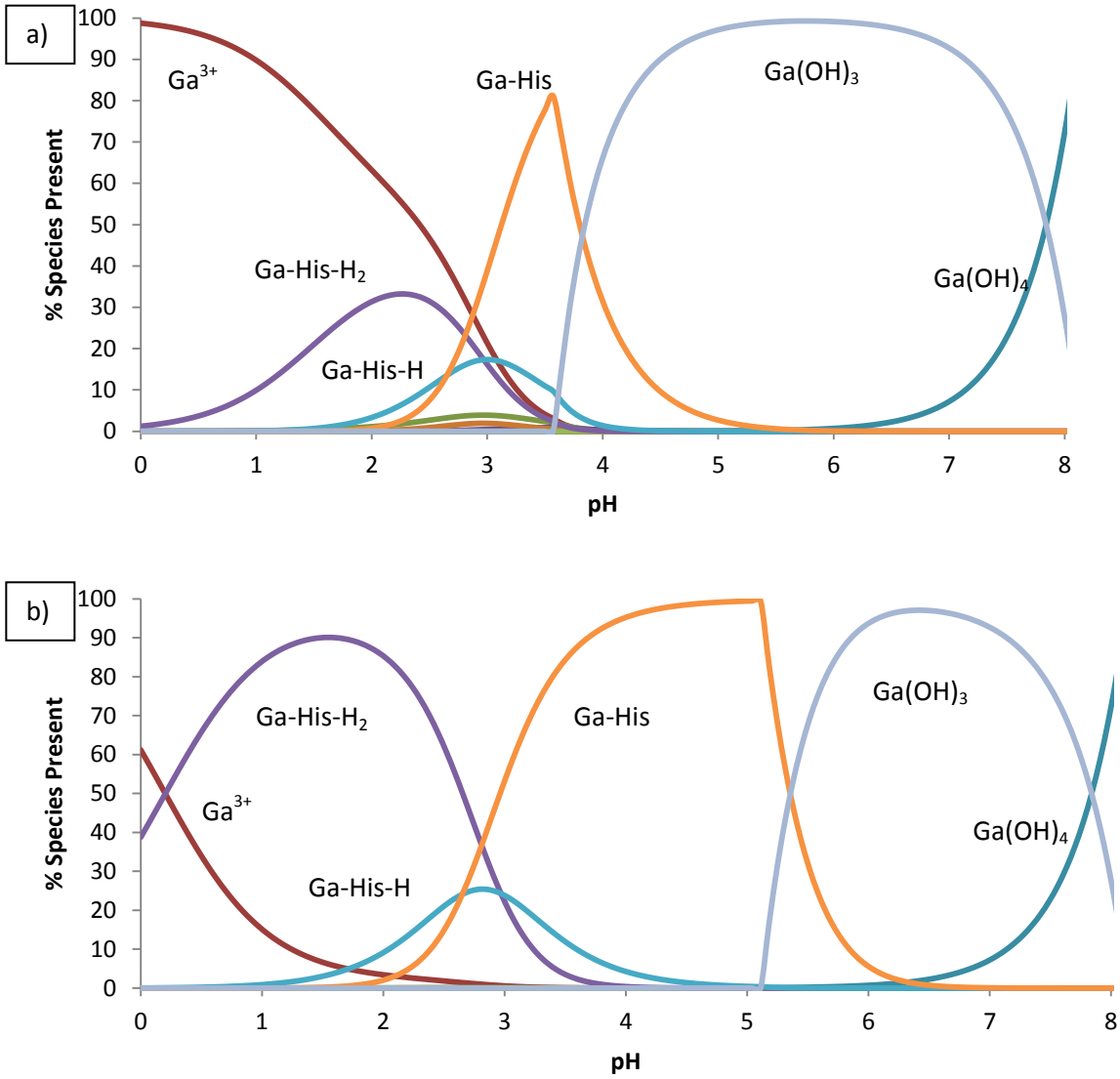

Figure A3.1: Species distribution diagram of Ga-His complexes formed where [Glu]:[Ga^{3+}] = a) 100 and b)5000 at 3.0 M NO_3 at 25°C

Species distribution diagram of Ga^{3+} with His at [His]:[Ga^{3+}] = 100 and 5000. It can be seen that the formation of Ga-His-H_2, Ga-His-H and Ga-His are formed in high percentages, a possible reason as to why the three complexes were found in literature.

References

[1] A. E. Martell and R. M. Smith, NIST Standard Reference Database 46 Version 8.0, NIST Critically Selected Stability Constants of Metal Complexes,USA, **2004**